ABSTRACT

MCWILLIAMS, ANTHONY JOSEPH. Characterization of Atmospheric Pressure Plasma Torch and the Surface Interaction for Material Removal. (Under the direction of Dr. Jerome J. Cuomo).

An atmospheric pressure plasma torch has been developed and characterized for removal of organic based coatings. The focus of the Strategic Environmental Research & Development Program (SERDP) project WP-1762, that funded the bulk of this dissertation work, is removal of paint from US Navy vessels. The goal is to develop a novel technology for coating removal that is capable of reducing the amount of environmental waste produced during the commonly used grit blasting process. The atmospheric pressure air plasma torch was identified as having the capacity to remove the paint systems while using only compressed air and electricity as a media-less removal system with drastically reduced waste generation. Any improvements to the existing technology need to be based on scientific knowledge and thus the plasma removal mechanisms or material warranted investigation. The removal of material does not show a strong relation to the plasma parameters of power, frequency, and gas flow, nor is there a strong relation to the presences of inorganic fillers impeding or altering the removal rates. The underlying removal mechanisms also do not show a strong correlation to the rotational temperature of the plasma but do show a strong correlation to the optical emission intensity. Primarily, the emission from atomic oxygen and molecular nitrogen were identified significant contributors and were investigated further. The plasma feed gas was then varied from the nitrogen and oxygen ratio present in ambient air to pure nitrogen to identify the effect of oxygen on the removal mechanism. From these experiments it was concluded that the oxygen present in air does contribute to the overall

removal mechanism; however, it is not the sole contributing factor with the other major factor being nitrogen.

Characterization of Atmospheric Pressure Plasma Torch and the Surface Interaction for Material Removal

by
Anthony Joseph McWilliams

A dissertation submitted to the Graduate Faculty of
North Carolina State University
in partial fulfillment of the
requirements for the degree of
Doctor of Philosophy

Materials Science and Engineering

Raleigh, North Carolina

2012

APPROVED BY:

_____	_____
Dr. Jerome J. Cuomo Committee Chair	Dr. Steven C. Shannon
_____	_____
Dr. Dick Guarnieri	Dr. James M. Rigsbee

DEDICATION

This dissertation is dedicated to my parents, David and Sue McWilliams, who were instrumental in forming my interest in science and appetite for learning.

Also, this dissertation is dedicated to my wife, Heather Regina McWilliams, for the support and encouragement you gave me since the day we met. Thank you for your love and friendship.

Non scholae, sed vitae discimus

(We do not learn for school, but for life)

BIOGRAPHY

Anthony McWilliams knew from an early age that his academic career would be centered on the physical sciences. College at the undergraduate level started at NCSU majoring in Civil Engineering with an interest in the large scale interaction and eventually switched to Chemistry as it resonated with the intrigue of how things work at the elemental levels. During the last semester of senior year, a chemistry lab-project required use of an instrument located in the Materials Science & Engineering (MSE) Department. After exhausting the MSE website and exploring related information, it was apparent that this field had it all. It encompassed the macroscopic interactions of materials right down to the interplay of individual atoms. An opportunity was presented that allowed Anthony to join the group under the direction of Dr. Cuomo and explore a research field that was truly of interest and not just available. It was here that he was introduced to the exotic state of matter, plasma, and the litany of possible applications. The research was initially focused on plasma processing and then transitioned to concentrate on plasma torches, which are the basis of this dissertation.

ACKNOWLEDGMENTS

I would like to acknowledge several people whose help has been indispensable throughout my time in graduate school.

First and foremost, recognition is due to Dr. Cuomo, for providing me an unparalleled opportunity to learn and develop.

Dr. Shannon, for not only supporting and advising on my research projects but also being a mentor, guide, and friend.

Edna Deas, for the incredible amount of compassion, assistance, and guidance you gave me and many other graduate students who walked through your office. You were the one who started the dominoes falling by helping with applications, introducing me to the graduate students which resulted in meeting Dr. Cuomo, and the guidance to navigate the final forms. Thank you.

TABLE OF CONTENTS

LIST OF TABLES

LIST OF FIGURES

1 Introduction

The need for an efficient environmentally benign method of coating removal for marine applications prompted research into the novel application of an atmospheric plasma torch to meet that demand. Basic ambiguities developed centered around the effect of inorganic fillers and plasma parameters on the overall removal rate and effect of plasma treatment on the underlying steel substrate. Upon refinement the central issues became focused on the underlying removal mechanism(s) and the interaction between the plasma and the substrate.

Plasma, the 4th state of matter comprising the vast majority of all matter in the known universe, has been the subject of study and investigation for generations. While the majority of plasmas are cosmic in nature, this dissertation focuses on laboratory plasmas. Of these plasmas the preponderance is at vacuum pressures used for semiconductor related processes, lighting, tribological coatings and a recently exiguous type of higher pressure discharge, the atmospheric pressure plasma (APP), has begun to emerge. Even as APPs are being applied to scientific and industrial applications, there remains a dearth of knowledge of the fundamental processes as compared to vacuum plasma in part due to the length of time that vacuum plasma have been researched and implemented compared to the relatively short time that APP have begun to emerge. Also, challenges with diagnostic and characterization techniques can often hinder the investigation of these types of plasma. A comparison of the number of journal articles for the different types of plasmas is shown in Table 1-1.

Table 1-1: Comparison of vacuum and APP search terms using Google Scholar- excluding patents, over 'anytime', search performed on 1/3/12

Search Terms	Results
Vacuum Plasma	1,290,000
Atmospheric Pressure Plasma	368,000
"Atmospheric Pressure Plasma"	6,650
"Atmospheric Pressure Plasma" etch	439
"Atmospheric Pressure Air Plasma" etch	12

The evolution of semiconductor plasma processing, from experiments of curiosity to a $144 billion in sales industry as of 2010[1], was possible through the development of vacuum plasma fundamentals. Additionally, plasma is instrumental in the production of LEDs[2] and OLEDs [3] that are contributing to high efficiency lighting and flat panel displays. Traditional vacuum plasma processing is also used to produce thin film solar panels,[4,5] deposit diamond-like carbon films for enhanced tribological properties on both hard and on soft substrates [6] [7] and surface treatment for improving biocompatibility for medical implants[8]. APP processing is well poised for a similar growth possibility through a revolution in the understanding of the fundamental underpinnings for applications such as plasma-assisted chemical vapor deposition, etching, polymerization, gas-phase synthesis, protective coating deposition, toxic and harmful gas decomposition, destruction of warfare agents, electromagnetic wave shielding, polymer surface modifications, and gas laser excitation[9]. Energy and chemical processes are possible with the unique plasma chemistry and used to form higher order hydrocarbons and syngas. [10,11] [12] Novel work by Ady Hershcovitch, out of Brookhaven

National Laboratory, has developed a 'plasma window' that is able to maintain a pressure difference between a vacuum environment and ambient atmosphere. This device utilizes a stabilized plasma arc forming the window for non-vacuum electron beam welding. Additionally, the arc beneficially acts as a lens to compress the electron beam giving a higher precision compared to vacuum electron beam welding.[13-15] The plasma window is even capable of replacing solid windows for X-ray transmission purposes as demonstrated as a port window for the National Synchrotron Light Source on beamline X6A offering low attenuation and no damage to a material window.[16] Another area of considerable interest for APP is the application of non-thermal plasma for medical uses such as wound care and sterilization.[17-19]

As the overseeing entity of the US Navy, the Department of Defense (DOD) partnered with the Strategic Environmental Research and Development Program (SERDP) to investigate the development and application of technologies that reduce environmental risks while reducing costs and enhancing military readiness. SERDP recognized that the coating removal process was not the most environmentally benign and seeing that it had room for improvement developed a project to address the matter. Project WP-1762 "Atmospheric Plasma Depainting" is a collaboration between North Carolina State University (NCSU), Atmospheric Plasma Solutions, Inc. and several government and military groups focused on researching the feasibility of employing atmospheric pressure air plasma to the coating removal process.

2 Paint and Methods for Paint Removal

This chapter focuses on the various aspects of coatings. The vast scale of painting removal and a brief history of the development of protective naval coatings are introduced. Then a synopsis of coating removal follows covering current methods and technologies employed, and new removal technologies including APP plasma removal systems.

2.1 Scope of Problem

Humans have been using various forms of paint for at least 100,000 years.[20] One of the main applications of paint, aside from aesthetics, is providing a protective layer over the substrate. The US Navy has over 2.1 million m^2 of painted surface area due to exterior hulls accounting for less than 36% of Deployable Battle Force Ships as of January 3rd, 2012.[†] This estimate is a significant underestimate as it does not include the interior structure containing floors, ceilings, walls, ballast and fuel tanks, piping, sealants, and specialty coatings that would drastically increase the total painted surface area. Additionally there are other sectors that must be considered including the other branches of the Armed Forces, commercial shipping, aviation, infrastructure, industrial, and countless others that would contribute to the scale of painted surfaces that at some point will likely need to have the coatings removed. With respect to the US Navy paint removal often occurs for materials inspection and regularly scheduled maintenance intervals. Given the vast scope of painted surfaces the cost and time associated with paint removal can become a significant factor. For example it costs

[†] Surface area estimates are derived from correspondence with NAVSEA that provided rough surface areas for the vessels and number of ships at 285 from the 'Status of the Navy'

approximately $6,800-$24,000 per day to maintain a ship in dry dock (from tour of BAE on 12/1/11).[21]

The commercial industry also faces considerable challenges with coating removal, a typical super tanker has over 30,000 m^2 (~323,000 ft^2) of exterior hull surface.[22] There are also demanding non-naval coating removal applications including aircraft, building, bridges, and ground vehicles.

For antifouling and protective applications, painted surfaces typically consist of several different layers to maximize lifetime, surface protection, and aesthetics. The "paint stack" refers to this compilation of the different layers of paint and paint system refers to the different types of paints employed. The work presented in this dissertation is part of a larger program that focuses on two main Navy paint systems: the underwater anti-fouling and the above-water haze-grey or freeboard as indicated in Figure 2-1. The freeboard paint stack is shown in Figure 2-2.

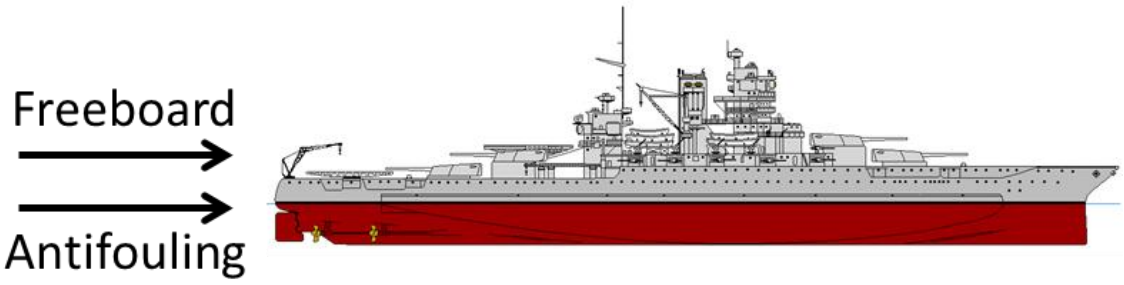

Figure 2-1: The indicative locations of the freeboard and antifouling paint systems as shown on the USS Mississippi (http://www.kitsune.addr.com/Naval_Vessels/Naval_Ships.htm)

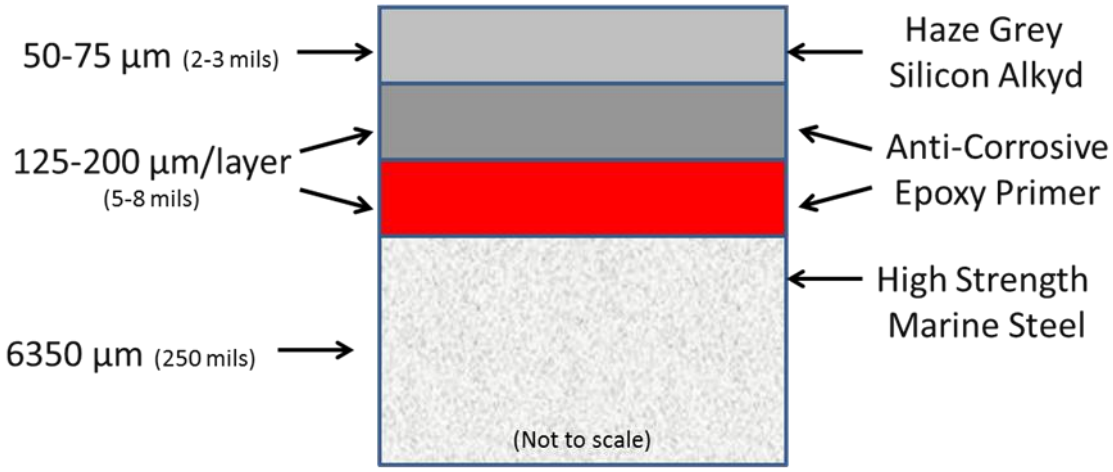

Figure 2-2: A typical freeboard paint stack (Image Source: SERDP WP-1762 In-Progress Review)

2.2 Paint Background

Aside from aesthetic reasons, paint is primarily used as a protective coating to avert corrosion or degradation of the coated material. This type of protection requires that the coating remain adhered to the surface and any adhesion failure must be avoided. While coating failure can occur in the bulk of the material, the failure mode critical to plasma removal is interfacial failure which involves the adhesion of the paint to the surface when painted following plasma paint removal.

Adhesion can be enhanced through mechanical bonding by increasing the surface roughness thereby increasing the effective bonding area, assuming that the coating is able to penetrate the surface irregularities.[23] The surface condition can also detrimentally affect the coating adhesion if it is contaminated with particulates or water soluble material as these can

lead to osmotic blistering and adhesion loss.[23] Osmotic blistering, as inferred from the name, is a result of the basic physical process, osmosis, which describes the net movement of a solvent through a semipermeable membrane in order to equalize the solute concentration. With respect to osmotic blistering of ship hulls, the paint is the semipermeable membrane as nearly all polymeric materials experience some degree of water permeation.[24] As the water permeates to the hull surface, any water soluble material forms a solution that is separated from the surrounding water by the semipermeable coating that allows water molecules to pass through but not the solubilized materials. This process continues as the dilute surrounding water enters the region with the concentrated solution minimizing the concentration gradient and as a result the pressure of the water increases until it exceeds the strength of the coating and ruptures. [24]

Grit blast treatment of surfaces presents pathways that are both beneficial and detrimental with respect to the adhesion of coatings after treatment. The process is advantageous two fold; by roughening the surface and providing more surface area for bonding with the coating and by physically removing large amounts of contamination. However, it has also known that grit blasting will always leave grit residue on the blasted surface, affecting the low cycle fatigue properties, diffusion between the substrate and coatings, wetting properties, and thermal stress due to mismatched thermal expansion coefficient between grit and matrix.[25]

Even if the coating remains adherent to the surface protecting it from corrosion, it can still be plagued by the problem of fouling. Microscopic fouling is primarily a result of

bacteria and diatoms that produce slime films on submerged surfaces that can incorporate particulate matter suspended in the water. Macroscopic fouling includes the individual and colonial masses observable by the unaided eye, common forms include 'grass' and 'moss' which are usually stringy growths of algae, hydroids or bryozoa, barnacles an arthropod species, and 'clams' which are generally goose barnacles.[26]

Of interest to the US Navy and the SERDP project is the implementation of paint systems to combat biofouling. Biofouling is the accumulation of biological samples to the ship hull underneath the water line. This accumulation of biomass can reduce speed by several knots and increase cost of operation. The increased costs are due to the effect of increased drag on fuel consumption as well as wear and tear on machinery and expense for remediation measures that must be taken to ensure efficient operation of these vessels. This corresponds to a ¼ % and ½ % increase in friction per day in temperate and tropical waters resulting in reduction of tops speed by 2 knots at the expense of increasing fuel consumption by 50% to maintain a speed of only 10 knots based on 1950's era US Naval vessels.[27] The Office of Naval Research and The Naval Surface Warfare Center, Carderock indicate the detrimental effects of biofouling include the addition of 150 kg/m^2 in barnacle weight in as little as 6 months reducing speed by up to 10% and 40% increase in fuel consumption.[28] A recent report puts the cost of cleaning the US Navy Arleigh Burke-class destroyer DDG-51 fleet at $56 million per year and additional fuel costs of $2.3 million per ship per year equating to over $140 million per year only for the fleet of 61 destroyers.[29] Commercial shipping is also seriously affected as fuel constitutes about 50% of the operational costs which at a 40% increase in consumption results in 120 million tonnes of fuel costing $7.5

billion in 2000 and a more recent estimate of $30 billion per year, for a large container vessel this equates to $250,000 per year in additional fuel costs.[30] Another biofouling induced problem is accelerated corrosion caused by interruption of the flow of ions and water creating a differential aeration concentration cell and creating a more corrosive environment or microbially induced corrosion by the production of sulphides from sulphate reducing bacteria resulting in pitting corrosion of steel surfaces.[31]

Antifouling efforts have been around as long as seafaring, starting with known efforts by the Ancient Greeks to coat vessels with wax and lead sheathing due respectively to the hydrophobic nature preventing adhesion of organisms and toxicity but with an environmental contamination caveat. The next major development of these efforts occurred in the 18th century when the H.M.S Alarm made use of copper antifouling capabilities by copper sheathing the exterior hull. However, when iron hulled ship came in service copper cladding could no longer be used due to the electrolytic corrosion of iron. By mid-19th century a variety of antifouling paints had been patented with the first practical composition being 'McIness' a copper sulfate based coating.[32] The antifouling properties of copper stem from the long known biocidal properties that have been employed for thousands of years from the Ancient Egyptians using copper to sterilize water and wounds, the Roman Empire made use of copper cooking utensils to prevent the spread of disease, Aztecs used copper oxide for treating skin conditions, and even early American pioneers put copper coins in water casks to provide safe drinking water and in WWII Japanese soldiers put pieces of copper in their water bottles to prevent dysentery.[33] The biocidal and even antiviral properties are the result of several parallel mechanisms such as induced damage to the microorganism's plasma

membrane via the electrostatic forces exerted by Cu^{2+} causing the membrane to collapse, damage to the function of proteins by conformational changes in the protein structure or the protein active sites, damage to nucleic acids by crosslinking within and between DNA strands by copper ions, and the redox cycling between Cu^{2+} and Cu^{1+} can catalyze the production of highly hydroxyl radicals that are damaging to lipids, proteins, DNA and other biomolecules.[33]

The next major advancement in antifouling technology was the implementation of biocides such as tributyltin $(C_4H_9)_3Sn$, tributyltin hydride shown in Figure 2-3, incorporated into the paint coating the vessel hull. Introduced in the 1960's, it is toxic to microorganisms and can deter or kill the organisms before significant biofouling occurs; however, it is toxic to larger marine organisms through bioaccumulation and can harm oysters and mollusks with a low toxicity level on the order of 1 ng/L.[34] A common issue is imposex when male sex characteristics are superimposed on female gastropods and is of concern since the compounds are retained in the sediments, thus the use of this material on certain craft has been banned in several countries.[35]

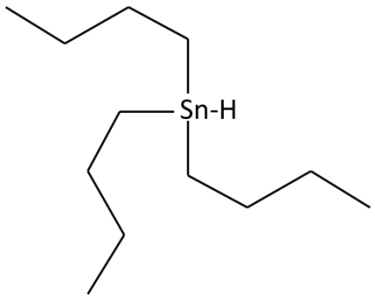

Figure 2-3: Tributyltin hydride structure where the straight lines represent bonds and the 'corners' and 'ends' represent carbon atoms.

The use of chemical methods for antifouling might have limited use with the development of modified surface features by the Genzer group at NCSU, where hierarchically wrinkled surface topographies remain relatively biofouling free after 18 months of marine exposure.[36] The process involves uniaxially stretching a silicone elastomer followed with ultraviolet light exposure and then coating the surface with a silane deposition treatment. It was determined that the physical surface profile, as opposed to a chemical alteration of the surface, that was responsible for impeding the biofouling process.

2.3 Primer on SERDP WP-1762 Paint Systems

Freeboard paint is the protective coating that not only provides protection against the harsh elements of a marine environment, but also provides naval ships with the distinctive haze gray color that has become almost synonymous with naval warfare vessels, sometimes being referred to as 'battleship gray', as such the freeboard coatings are typically referred to as "Haze Gray" paint. A freeboard paint system consists of two coats a primer and tie-coat of anticorrosive epoxy polyamide MIL-DTL-24441 [37] consisting primarily of polyamide +

polyamide adduct, magnesium silicate, titanium dioxide, butyl alcohol epoxy resin, and naphtha. Type III Formula F150 (green) followed by a topcoat of silicon alkyd MIL-PRF-24635 [38] Type II, Class 2, Grade B semi-gloss low solar absorbent (Interlac 665).

Antifouling systems are designed to minimize surface corrosion due to marine micro-organisms. It is designed to wear away over time, taking parasitic organisms with it and leaving behind a pristine surface. Antifouling systems consist of two coats of an anticorrosive epoxy primer and tie-coat MIL-PRF-24647, Type II (Interguard 264) and followed by three coats of a copper biocide self-polishing ablative antifouling paint MIL-PRF-24647, Type II (Interspeed 640).[39]

There is a plurality of coating layers that are employed in both of these coatings, and define the mechanisms by which anti-fouling is accomplished during service. For two component epoxy-polyamide paint systems Type III is a three coat system and Type IV is a two coat system both used where air pollution regulations restrict volatile organic content to 340 g/L. For anticorrosive and antifouling paint systems as defined in MIL-PRF-24647C [39] Type I have topcoats that contain biocide(s) other than copper which ablate or self-polish when in contact with a flow of seawater, Type II have topcoats that contain a variety of possible biocides and ablate or self-polish, Type III have topcoats that are foul-release and contain no biocide, and Type IV have topcoats that contain biocides that are copper or other and do not ablate or self-polish.

2.4 Paint Removal

Once the paint or coating is applied it has a service life on the order of 1-10 years depending on the coating, application, and environment before the efficacy of the coating to prevent corrosion or fouling is lost. While it is possible to simply apply the new coating atop the old, it would likely lead to coating failure. The best adhesion performance is generally obtained when the coating is applied to a clean substrate. Although the coatings, having been designed for rigorous performance specifications and remain adhered to the substrate under conditions that are often extreme, must now be removed for successful reapplication and in some cases the coatings must be removed even for maintenance or inspection.

2.4.1 Current Methods & History of Paint Removal

Some of the common current methods employed in paint removal include the established abrasive media blasting and ultra-high pressure water jetting (UHPWJ) and the emergent laser, induction, and plasma methods.

Removal of coatings with grit blasting first requires a source of abrasive material that is introduced to a high pressure gas stream and ejected at high velocities at the coated surface subsequently abrading away the softer material. The choice of abrasive material depends on the type of coating and surface being treated. Sensitive substrates such as fiber-composites, aluminum, or aerospace surfaces a starch media can be used as it will do little damage to the underlying surfaces,[40] another example is the use of plastics such as polyester and urea formaldehyde on the removal of coatings on graphite epoxy composites.[41] More durable

surfaces and tenacious coatings can more abrasive materials such as sand can be employed.[42] Additionally coal slag, copper slag, garnet, hematite, and steel shot can be used.[43]

Grit blasting brings with it a host of logistical and environmental issues that the military seeks to minimize or eliminate. For instance at the BAE† shipyard in Norfolk, VA the grit blasting work is generally performed at night to minimize negative public opinion of dust clouds in the case of containment failure. Given that each of the hoppers can hold 28 tons of grit it is no small matter.[21] Additionally, according to one of the grit blast operators [21] the hoppers have problems associated with valve blowouts which is not only a safety issue to the operators but any passersby. The operator also conveyed that 850 CFM is delivered to each blast hose and 8 hoses can be operated simultaneously with a nozzle pressure of 110 psi with each compressor delivering up to 1600 CFM. This correlates to an operator experiencing approximately 86-194 pounds of force for a hose diameter of 1-1.5" which in some cases can approach or exceed the weight of the operator requiring a starting or effective stance leaning heavily into the direction of spray to oppose the recoil force. Another issue that grit blasting faces is that the hoses experience roughly a 4 psi drop every 50 feet that can cumulate to considerable pressure losses over the ranges that must be considered when dealing with the size of vessels being serviced. Additionally, abrasive blasting with silica sand as the abrasive media been associated with detrimental health effects such as silicosis, also known as 'Potter's Rot', which is an occupational lung disease caused by the inhalation of crystalline silica dust.[44]

† BAE Systems is resulting company from the purchase by British Aerospace (BAe) of Marconi Electronic Systems, which was the defense arm of The General Electrical Company (GEC)

Grit blasting is significantly labor intensive and can require over 5,000 man-hrs to strip a typical super tanker with an exterior hull surface area of 30,000 m^2. Operational drawbacks include the large amount of airborne grit produced that can preclude most other concurrent maintenance work, require substantial clean up while posing a hazard to sensitive equipment and machinery, the setup, teardown, and space associated with the required scaffolding and tenting of the work areas and occasionally the entire vessel, and with regard to the physical nature of grit blasting paint adhesion can be compromised as the process can drive salts and other debris into the micro-textured surface increasing the likelihood of corrosion and other detrimental forms of paint adhesion failure.[22]

There is the issue of airborne particulates associated with grit blasting as the toxic hull coatings are pulverized into fine airborne particulate dust that, even despite extensive tenting and other recapture methods, can still settle in workers lungs, surrounding communities, and local water ways.[22] Then there is the issue of disposal, as the stripping of a large ship can generate in excess of 3,000 tons of contaminated grit that represents a serious environmental issue.[22,45†] Another estimate conservatively puts the US Navy, while performing corrosion control, at generating more than 9 million pounds of mixed abrasive and paint waste a year on the 750,000 ft^2 of steel that comprises just the ships tanks and voids and does not include additional corrosion control and maintenance painting and could be estimated to be at least equal to that for ship maintenance.[46] A heavily estimated value for the total waste stream from grit blasting an entire ship can be achieved using the following

† This reference does state implicitly that the 3,000 tons of contaminated grit is generated solely from the hull and specifies that it is an aircraft carrier.

several assumptions. A) The removal of coatings from the hull of an aircraft carrier results in $3{,}000(Tons) = 2.72 \times 10^6 kg$ of waste. B) That there are approximately 280 capital ships excluding 10 aircraft carriers that must be serviced every 10 years for a yearly rate of 28 capital ships and 1 aircraft carrier. C) The entire fleet generates $9 \times 10^6 lbs = 4.08 \times 10^6 kg$ waste in corrosion control efforts and $2 \times \left(4.08 \times 10^6\right) kg = 8.16 \times 10^6 kg$ for the combined equivalent estimated value for general ship maintenance. D) The average hull surface area is 36,000 ft^2,[47] extrapolated across 28 ships is 1,008,000 ft^2 and an aircraft carrier has 797,500 ft^2 resulting in 79.1% of the total hull surface area that need to be serviced per year coming from aircraft carriers. D) That the combined value from corrosion control efforts and general ship maintenance is proportional to the surface area of the ship. Finally, f) using this proportionality a total of $8.16 \times 10^6 kg * 79.1\% = 6.46 \times 10^6 kg$. This estimated total value for waste generated by the removal of 'all' paint from an aircraft carrier is as follows: $2.72 \times 10^6 kg + 6.46 \times 10^6 kg = \underline{9.18 \times 10^6 kg}$.

The other common method employed in the coating removal industry is water jetting, sometimes referred to as 'hydroblasting'.[22] The general operating premise is similar to grit blasting where a fluid, water instead of air, is pressurized and shot out a nozzle at the surface imparting kinetic energy to the coating breaking it off of the substrate. Water jetting is generally classified in two categories based on the water delivery pressure: high pressure water jetting HPWJ is generally on the order of several thousand psi, and ultra-high pressure water jetting UHPWJ can range from 40,000-100,000 psi. Water jetting has both advantages and disadvantage compared to dry grit blasting. Advantages include that the dust exposure is

greatly reduced although it is possible that the dust particles are aerosolized in the water droplets and still represent an inhalation hazard. Noise exposure is reduced for the worker in a comparison to steel shot water jetting resulted in 106.6 dB and steel shot resulted in 109.5 dB at a distance of 6' and 122.7 dB and 125.6 dB respectively when normalized to a distance of 0'.[44] The surface contaminant issue [22] is reduced and waste reduction from 3,000 tons to 50 tons is achievable.[45] According to the Navy, for automated water jetting, other benefits include the elimination of personal protective equipment, reduced waste disposal costs, producing a cleaner surface, allow concurrent maintenance, reduced time in dry-dock, and reduced man-hour requirements.[45] Disadvantages include the likelihood of the operators getting wet and even though the water is hot as it exits the nozzle due to the compression the splash back can cool quickly and in cold weather coat the operator in a layer of ice. While water jetting reduces the visible dust increasing overall visibility, it also impairs worker visibility by obfuscating the facemask with water. Additionally, the excess water presents an electrical hazard, and there is a pressure hazard as the water lines are under high pressures and could undergo catastrophic failure.[44] The removal rates for hand-held UHP are typically less than grit blasting and the automated vacuum-attached robots have seen limited implementation in shipyards as the machines have failed to live up to performance expectations and have a high cost per area stripped.[22] The waste streams can be reclaimed and reused as describe in a case study by Spray Technique Analysis and Research for Defense at Camp Dodge National Guard base in Johnston, Iowa,[48] but can be an issue with hand held devices.[22]

A major drawback to water jetting is the subsequent flash rusting on the steel surface. Flash rusting is, simply, the formation of corrosion products over a rather short period of time following treatment as defined by ISO 12944-4,[49†] and generally requires the presence of water soluble salts and either liquid water, water vapor, or relative humidity.[50] The progression of flash rust is described as:

$Fe(OH)_x\,(ferrihydrite) \rightarrow FeOOH \rightarrow \gamma \cdot FeOOH(lepidocrocite) \rightarrow \alpha \cdot FeOOH(geothite) \rightarrow Fe_3O_4\,(magnetite)$ and the existence of akaganeite $Fe^{3+}O(OH,Cl)$ $e.g.: \beta - FeO(OH)$ if there is chlorine present.[50,51] It was also noted that under certain conditions such as high water temperature and low oxygen content in the water the flash rusting is effectively 'blocked' due to the formation of magnetite acting as a passivation layer.[50†] As most paint specifications require the surface to be reworked to bare steel and most paint manufacturers will not accept liability if their coatings are applied on flash rusted surfaces since adhesion failure is likely to occur.[52]

Laser paint removal is an emerging technique that offers a dry process resulting in lower waste volume than other chemical or mechanical processes.[53] Parameters affecting paint removal include wavelength, fluence, pulse duration and repetition rate. CO_2 lasers at 10.6 μm are used as the ablation threshold for the metallic substrate is higher than that of the paint, and excimer lasers in the UV wavelengths enable photochemical ablation decreasing the thermal effects.[53] Parameters affecting paint removal include wavelength, fluence, pulse duration and repetition rate. A wavelength of 523 nm from a Nd:YAG laser results in

† International Organization for Standardization (ISO)
† References: P. LeCalve, *J. Prot. Coat. Lin.* 2007, 24, 13.

thermal ablation as it is below the electronic transition energy that would result in direct bond breaking.[53] One limitation is at high powers a decrease in ablation can be observed due to plasma formation and vapor or fragments that absorb the laser energy before it is able to reach the surface.[53]

Substantial research into pulsed laser coating removal began in the 1980's for the Air Force using CO_2 lasers while excimer lasers were demonstrated to remove coatings in the early 1990's.[54] The reasoning for CO_2 lasers is that most organic material including the paint resins strongly absorb the 10.6 μm photons.[54] There are various mechanisms by which the coatings are removed. One mechanism is ablation by a thermo-chemical or pyrolysis where the organic material is essentially burned or decomposed but remain relatively clean because there is not enough time to produce char at peak irrandiance levels of 300 kW/cm^2.[54] Limitations of the pulsed CO_2 lasers (as of 2000) is the limited availability of commercial devices at a competitive cost compared to continuous CO_2 laser devices, and both systems share the lack of cost-effective fiber optics in the 10.6 μm wavelength range and thereby limit the applicability to remote paint removal. However, the advancement of solid-state pulsed lasers operating at 1064 nm such, as the Nd:YAG, could be a contender with reduced maintenance and remote paint removal through flexible fiber optic cable.[54] This type of laser generation introduces a second removal mechanism that is observed for pulses <30 ns. When the material fluence threshold is exceeded, instead of just vaporizing or burning the material, the rate of vaporization sends a shockwave through the coating which combine with reflected waves to fracture and break up more of the coating resulting in a lower energy cost per unit mass removed compared to the thermo-chemical ablation by a factor of 5 down to 4 kJ/g. [54]

For comparison if a laser system requires 15 kJ/g it should result in a removal rate of 2.5s ft^2-mils/(kW-min) or 1.0 ft^2/min per kW for a 2.5 mil coating which might be sufficient for thin aviation coatings but for marine coatings that can exceed 50 mils the effective removal rate would drop to ~ 7 in^2/min/kW[54] and to match a grit blasting rate of 250 ft^2/hr would require 555 kW for a 15% efficient laser system.

Some laser removal systems include a jet of oxygen gas impinging at the laser-surface interaction to support combustion.[55] Another limitation to laser paint removal is the coupling efficiency of the optical energy to the material which can vary significantly between materials such as chlorinated rubber paints commonly used in corrosion resistant applications has a very high reflectivity over 600-1100 nm compared to 40-60 % for epoxy coatings.[55] Other generic issues include fire risk, the release of hazardous gases, particulates, combustion products, general laser safety concerns, and the cost of equipment and maintenance.

While the technology behind heat induction is not new, it is the novel application to coating removal that is of interest. The process makes use of a relatively high frequency alternating current passed through an antenna in close proximity with the surface that induces eddy currents in the steel substrate. As these induced currents pass through the electrically resistive substrate the energy is dissipated as ohmic heat resulting in the surface reaching hundreds of degrees in seconds resulting in failure of the coating-substrate interface.[46] Lifting of the coating can occur due to the increased temperature and the differences in thermal expansion coefficients.[56] The equipment consists of four main components: the

induction generator, a capacitor, cable, and induction head and often a supplemental cooling system. The electrical demands require approximately 460 V, 3-phase power pulling 125 amps for roughly 50 kW.[46] Another device requires 480 V, 150 amp 75 kW power supply driving capacitors at a frequency of 10 kHz.[57] Given the size and power of the technology it has a limited application to tight geometries or operating spaces and the difficulty in controlling heat input limits application to thin substrates. Removal rates for a nonskid epoxy coating using a 10" wide coil was on the order of 120 ft^2/hr; however in the test the coil and protective components were heavily worn. Substrate alterations include the infrequent discoloration as a result of thermal oxide formation and temperature effects. The peak temperature in excess of 547 K (274 ^oC) was achieved with in seconds of exposure and lasted for under 2 seconds while the bulk temperature remained below 394 K (121 ^oC) on the order of minutes. Under normal operating parameters there was no significant change in the macrostructure or the microstructure as well as no discernible increase in magnetism.[46] Any changes in the macrostructure and microstructures are primarily driven by thermal effects; the concern about residual magnetism is a function of the applied magnetic field from the inductor. As indicated by a magnetic hysteresis loop in Figure 2-4, when a magnetic field is applied across a ferromagnetic material such as steel the atomic dipoles align with the magnetic field and even when the field is removed some of the alignment remains and the material is 'magnetized'.

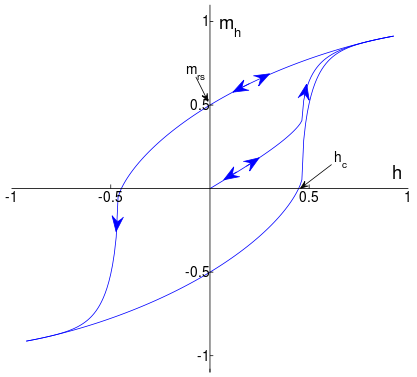

Figure 2-4: A representative magnetic hysteresis loop showing magnetization (m) plotted against the magnetic field (h). Starting at the origin the upward curve is the initial magnetization curve and the downward curve after saturation and the lower return curve have intercepts h_c and m_{rs} which are the coercivity and saturation remanence.[58]

While these coating removal techniques may be effective, there remain serious issues with the environmental impact caused by waste products, surface condition after treatment, and overall efficiency. A new methodology is needed that is capable of addressing these concerns and plasma based coating removal stands as a leading prospect.

2.4.2 Review of Plasma Paint Removal Technology

An effective plasma based coating removal system will need to meet several design criteria to be competitive against the legacy removal platforms. Firstly, a plasma based system will produce far less particulate waste than grit blasting or water jetting since it is essentially a 'media-less' removal technique using only compressed air as the removal media. The next issue is the plasma system must not damage or detrimentally alter the surface during the coating removal process. Also, the plasma system must be capable of

removing thick and tenacious coatings at an equivalent or excessive rate compared to current methods. Finally, the plasma technology system needs to address the ease of use and accessibility of hard to reach areas in comparison to other alternative coating removal techniques. These evaluation merits require a plasma system designed to produce either copious amounts of active species for a chemical reaction based etching, high temperatures and large heat fluxes for thermal ablation, or some species capable of transferring energy to the coating. Generally, the easiest method for generating some combination of these products in a substantial amount is through torch based plasma systems. There is however at least one caveat that the removal rate may not be the deciding merit for a successful technology as the economics associated with waste management, operation, setup and take down time, interference with other maintenance activities, and certainly a host of other criteria not listed.

Utron Inc. is a research and development corporation headquartered in Manassas, Virginia that is primarily centered around high-energy and hyper velocity gun-launchers. They also have a patent for an arrayed system of overlapping pulsed plasma jets that is capable of ablating paint and coatings while the exhaust is mitigated by a reduced pressure enclosure.[59] The device uses inert gases such as argon to form a small pulsed arc capillary discharge initiated between a high voltage electrode and a ground electrode separated by an insulating ceramic liner such as boron nitride, silicon nitride, or silicon carbide as shown in Figure 2-5. The ceramic liners offer increased resistance to temperature and chemical erosion but are limited by low tensile strength and ductility which were addressed by using a heat shrunk steel jacket assembly. The jet is pulsed at 1 kHz with a duty cycle of 2% and a

delivered power of roughly 10 kW/cm^2 and the discharge current is on the order of a few kilo-amps and several hundred volts supplied by a conventional high voltage capacitor network. The patent indicates that an average operating power of 50 kW is capable of removing a 0.007" thick paint coating at a rate of 140 ft^2/hr using a single pulse proof-of-principle device and alludes that it can attain rates that are 5-18 times larger, than the previously listed rate, under optimized conditions. Scaling the initial removal rates to a comparable rate for grit blasting, ~250 ft^2/hr, the power consumption approaches 100 kW and extrapolating the power consumption to match the theoretical scaled-up version it would approach a megawatt of power. Additionally, the device would consume significant amount of inert gases adding to the cost and complexity of requiring the delivery and positioning of large tanks on site at the maintenance docks. The removal rates from the Utron Inc. device normalized to the required power input are comparable to the plasma device used in conjunction with the SERDP project WP-1762. However it should be noted that the removal rates of the former device are achieved with a supply of inert gas whereas the removal rates of the plasma device used for SERDP project WP-1762 are achieved solely with a feed gas of compressed air.

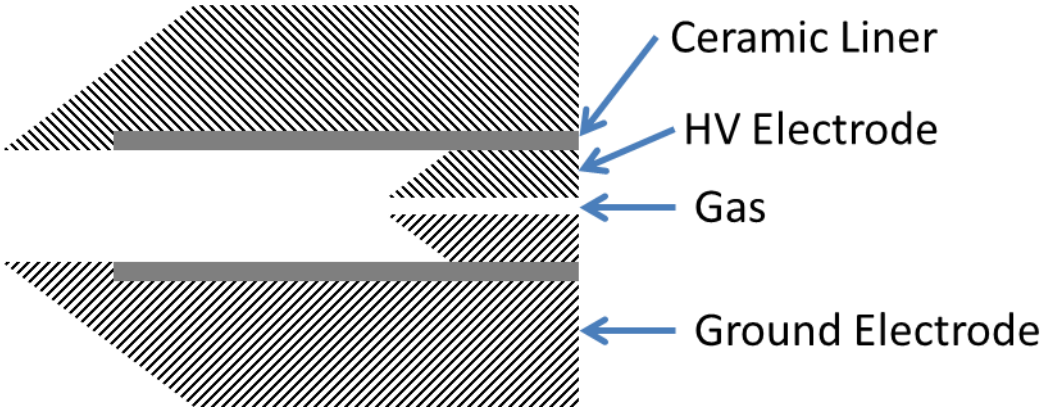

Figure 2-5: Utron Inc., pulsed plasma jet adapted from Patent # 5,970,993

NASA produced multiple patents describing the use of atomic and ionic oxygen for the removal of organic material although it seems to be directed more towards delicate substrates such as historical paintings and delicate equipment as depicted in Figure 2-6. [60,61] It makes use of a 3-30 kV DC arc using an inert carrier gas such as helium, neon, and argon mixed with oxygen. The size was configured such that the applicator could be hand held. The plasma is generated between two high voltage electrodes forming a weak plasma or arc that the patent refers to as a glow discharge that generates the atomic and ionic oxygen and are then accelerated out of the device toward the substrate.[60] This device has considerable limitations based on the scale of removal needed for naval vessels and the requirement for costly inert carrier gas.

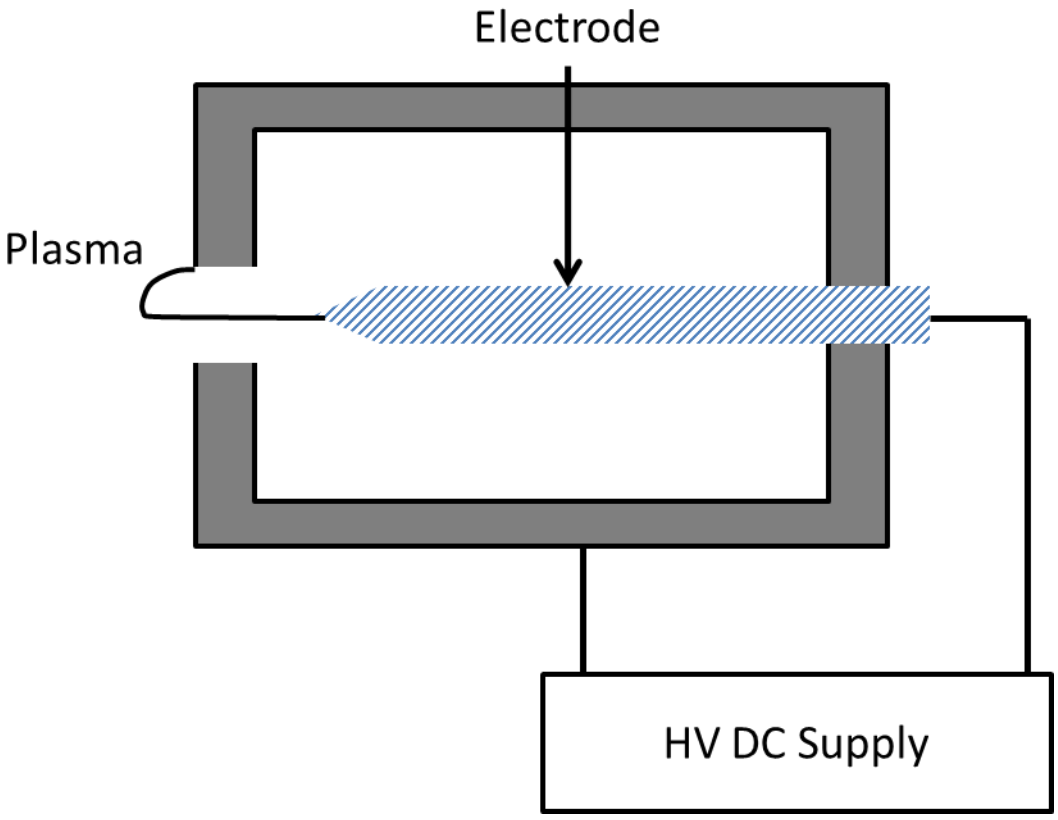

Figure 2-6: Depiction of NASA plasma device

Gary Selwyn produced a patent through Los Alamos and with similar technology Robert Hicks from UCLA founded a company in 1999 that became Surfx Technologies LLC. The plasma device described in the patent is an atmospheric pressure plasma jet that is a resonant-cavity discharge formed between two concentric electrodes operated using a 13.56 MHz rf power supply with a gas-phase effluent of no hotter than 250 ^{o}C of helium used to prevent arcing as depicted in Figure 2-7.[62] It also indicates the etch rate of Kapton to be just under 14 microns/minute. While this device maintains a lower operating gas temperature than some torches which is beneficial to limiting substrate damage it does so at the cost of

using an increasingly expensive feed gas (He). Additional work has been performed in using atmospheric pressure plasma operating at 27.12 MHz by Dr. Hicks for plasma-enhanced chemical vapor deposition of silicon nitride and the deposition of glass coatings on aluminum.[63,64]

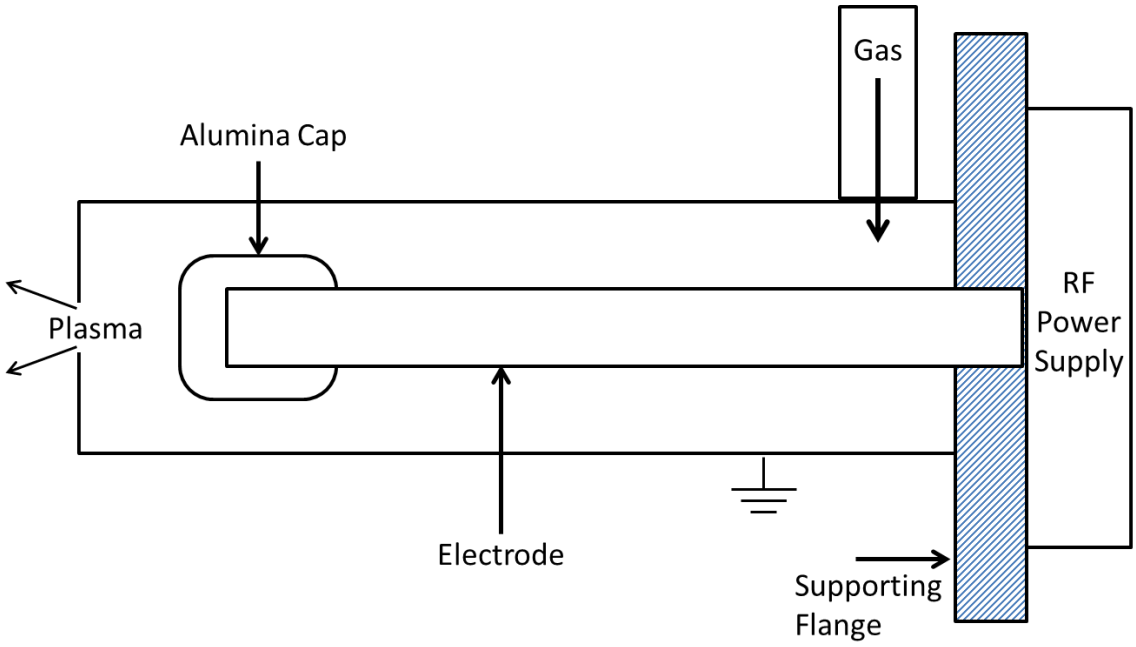

Figure 2-7: Depiction of the plasma device invented by Selwyn

John Roth *et al.* from the University of Tennessee developed a plasma device with a pair of parallel insulated metal plates operating as a uniform glow discharge powered with an RMS potential of 1-5 kV at 1-100 kHz using air, nitrous oxide, noble gases etc, or mixtures thereof.[65] A similar patent by John Roth *et al.* is used to treat polymer materials primarily to increase the wettability of nylon, poly(ethylene terephthalate), polypropylene, and polyethylene.[66] These devices show an improvement in technology through the utilization of

non-noble gases, especially air; however, the plasma generated remains limited to surface modification and is not aggressive enough for coating removal.

Boeing generated a patent based on a handheld atmospheric pressure capacitive glow discharge powered by an LC resonator at 13.56 MHz using Ar, He, and O_2 mixtures for low powered, <100 W, removal of organic material such as oil and grease.[67] The tuning network, actuator, and electrodes are housed in a gun type device with the discharge formed between a rod electrode and a ground electrode chamber at the nozzle. The handheld design appears to be strongly based on an earlier patent that was focused on the applications of paint removal, surface modification, microelectronic fabrication, and medical sterilization as depicted in Figure 2-8. [68] The patent also mentions removing charred flux from circuit boards, striping paint off metal surfaces, high etch rate of about 1 μm/min of photoresist in He/O_2, a significant etch rate of Kapton in Ar/O_2, and an etch rate of epoxy paint in both He/O_2 and Ar/O_2 with no numbers given for the last two capabilities. While an etch rate of 1 μm/min for photoresist might be sufficient, this equates to over 2 hrs to etch through a 0.005" (0.127 mm) thick coating which is approximately the thickness of one layer in a typical marine paint stack.

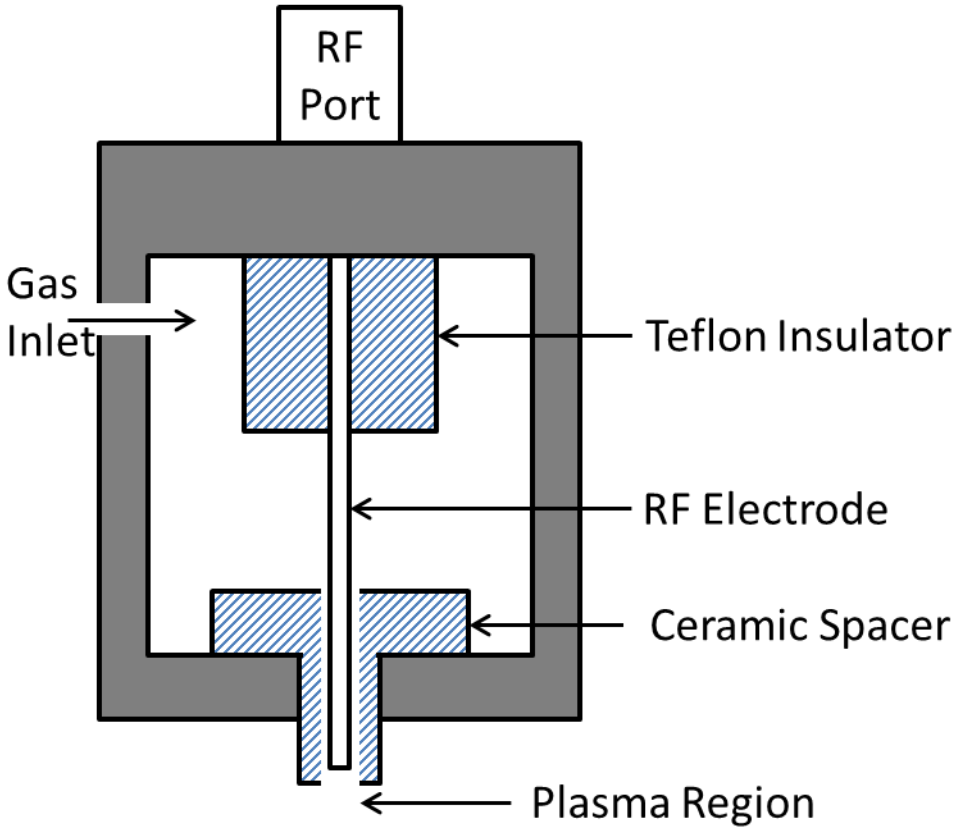

Figure 2-8: Schematic of initial Boeing plasma device

Additionally, there is the plasma device used for the material removal experiments in support of the SERDP WP-1762 project and the plasma characterization experiments presented within this dissertation. The plasma system comprising of the torch and power supply were manufactured by Atmospheric Plasma Solutions Inc. with a model name PlasmaFlux™ 5000 (referred to as PF5K in this dissertation). The advantages of this system are that the primary plasma feed gas is compressed air and it is capable of relatively high

removal rates of high density polyethylene and a variety of paint systems in comparison to other atmospheric pressure plasma systems.

All of these developments and devices have critical limitations of either having to use a noble or otherwise costly operating gas or have minimal interaction with the substrate only altering the surface chemistry or minimal removal rates that would be unrealistic on the scale of large marine vessels. There is thus a need for a plasma device that is capable of operating with a widely abundant feed gas, air, and with removal rates that can address the capital vessels of the US Navy.

3 DH36 Steel

While it is important to investigate the interaction between the plasma and the organic based coatings in order to achieve maximal removal it is also imperative that the underlying support substrate, in this case the outer hull of a ship, is not compromised. For the SERDP WP-1762 project DH36 steel was used as test substrates as it is indicative of material used in the US Navy.

Naval and structural applications make use of DH36 steel as it has high strength, high toughness, and good weldability with the chemical composition is shown in Table 3-1.[69] Specifically, DH36 is a hypo-eutectoid alloy with ferrite and pearlite as the prime constituents with volume fractions of 82.5% and 17.5%, respectively, with the relative low amount of pearlite making it more rust resistant than other carbon steel alloys.[70] The ferrite (α-Fe) has a body centered cubic (BCC) crystal structure and lower strength and hardness but higher plasticity and toughness relative to pearlite. Pearlite is an alternating two-phase lamellar structure of α-Fe and cementite or iron carbide at 88% and 12% by weight respectively accounting for the higher strength and hardness and lower plasticity and toughness.[70]

Table 3-1: Chemical composition in wt. % of DH36 steel for components >0.01[69]

C	Mn	Cu	Si	Cr	Mo	Nb
0.14	1.37	0.14	0.22	0.08	0.03	0.03

Steel that is produced with a hot rolling method can develop a surface coating, or mill scale, which is composed of iron oxides and metallic iron steeped with oil and grease contents.[71] One problem with mill scale is the electrochemical potential is more positive relative to bare steel allowing the formation of a galvanic cell. The ensuing electrochemical reactions result in corrosion products being formed that can lead to the removal of the mill scale from the substrate. This causes additional problems if the mill scale is painted over, leading to cracking or loss of paint protection.[72]

An area of concern with the removal of protective coatings and subsequently exposing native iron is the generation of flash rust, which is the formation of corrosion products on steel due to atmospheric corrosion over a rather short time. For this process to occur necessary parameters include the amount of water soluble salts as stimulators, the relative humidity as an electrolyte, wetting cycles, surface temperature and surface cleanliness.[50] The concern with flash rust as well as mill scale is that both can cause complications with coatings through loss of adhesion or other detrimental effects.

There are approximately 16 iron oxides of which three are of significance to paint adhesion and plasma treatment: the iron-hydroxides that comprise rust, hematite, and magnetite. Iron-hydroxides include $Fe_2O_3*H_2O$ and $FeO(OH)*Fe(OH)_3$ are loosely bound to the iron substrate and can be easily removed thereby exposing more iron to corrosion. It is also possible to form hematite (Fe_2O_3) and magnetite (Fe_3O_4) through oxidation of iron.

4 Plasma

This chapter focuses on the various aspects of plasma processing that tie into removing coatings and plasma devices similar to the plasma torch used for the coating removal experiments.

Plasma is often referred to as the 4th state of matter since it has properties that are not found in the other three states: solid, liquid, and gas. Naturally occurring terrestrial plasmas include the Aurora Borealis (and Australis), lightning, ball lightning, St. Elmo's fire, SPRITES, ELVES, and even conventional combustion flames. Industrially plasma has been used as a critical component in IC fabrication, deposition, thermal spray, arc welding, arc lamps, fluorescent lighting, TVs, and even space propulsion.

4.1 Plasma History & Development

The concept of plasma is often attributed to Sir William Crookes in 1879 as he described "a fourth or ultra-gaseous state of matter"[73] and the development of the Crookes tube; however in his publication of "*On Radiant Matter*"[74] he credits, in the opening paragraph, Michael Faraday for delivering a lecture titled "On Radiant Matter" in 1816. The term *plasma* was first coined by Irving Langmuir in 1928 to "describe a region containing balanced charges of ions and electrons"[75].

Early research explored the role of plasma in the ionosphere with the development of the radio, astronomy and astrophysics recognized the influence of plasma in the universe and more locally with solar flares. One of the first industrial applications of plasma was the

carbon-arc for lighting purposes. This application was demonstrated by Sir Humphry Davy in 1810 using electrodes made out of light wood charcoal and powered by a 2,000 cell battery. The initial experiments used horizontal electrodes where the resulting plasma 'arched' upward due to the heated air rising, this resulted in the device being coined as an 'arch lamp' and the term later abbreviated to 'arc' retaining the name of the luminous space between the electrodes.[76] While T.A. Edison is credited with inventing the first commercialized incandescent light bulb,[77] that largely replaced the arc-lamp he also was awarded a patent for a fluorescent lamp[78] that was later commercialized by General Electric Co. Ltd. Mid-century research began to investigate plasma for thermonuclear fusion reactions for both weaponized and energy means. Additionally, significant research focused on using plasma for industrial applications most notably for IC fabrication beginning in the later portions of the past century. It should also be noted in a somewhat ironic passage of events that the plasma based vacuum tubes were replaced by solid state semiconductors, which are produced using plasma processing. Current research trends include plasma based thrusters[79], microplasma devices[80], and medical applications[81].

4.2 Plasma Properties and Physics

Plasma is comprised of charged particles generally in a quasineutral assembly of electrons and ions whereby there exists a global charge balance where, the number density of electrons and ions ($n_e \approx n_i$), respectively. It exists over a wide range of pressures, temperatures, and densities as shown in Figure 4-1. The size can range from $10^{-6} m$ in lab plasma to $10^{25} m$ in intergalactic nebulae. Lifetimes of the ionized and excited species can

range from $10^{-12}\,s$ to $10^{17}\,s$ and electron densities ranging from nearly zero up to $10^{32}\,m^{-3}$ for internal confinement plasmas. Plasma temperatures can range from $\sim 0K$ for crystalline non-neutral plasma to $10^{8}\,K$ for nuclear fusion plasma.

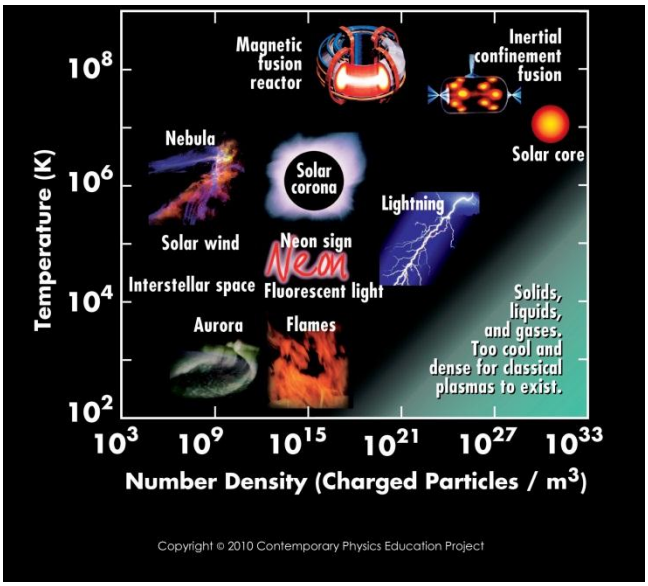

Figure 4-1: Plasma temperature and number density over a vast range

Plasma formation via the electrical breakdown of gas occurs when the dielectric strength of the gas is exceeded and the externally applied fields can begin to partially ionize the gas making it more conductive. The process of ionization can occur through several mechanisms that can be partitioned into five main mechanisms. Firstly, direct ionization by electron impact where an incident electron with energy ε interacts with a valence electron of a neutral atom or molecule and transfers enough energy $\Delta\varepsilon$ such that it is larger than the

ionization energy ε_I : $\Delta\varepsilon > \varepsilon_I$.[82] This method considers the incident electron interacting and ionizing neutral, unexcited atoms, radicals, or molecules and the process is significant to cold or non-thermal discharges.[82] Secondly, stepwise ionization by electron impact is the ionization of previously electronically excited neutral species and is important to thermal or energy-intense discharges.[82] Thirdly, ionization can occur through the collision of heavy particles such as neutrals and ions. This is not as effective as electron impact if the heavy particles are in a ground state because the of the relative velocity difference compared to the electrons bound to the atom result in a low probability of energy transfer. However, even if it is not efficient at ionization it still has a large influence on the particle energetics. If the colliding heavy particle is electronically excited and exceeds the ionization potential of the target heavy particle then a collision can result in an ionization process called 'Penning ionization'. A point of clarification, 'heavy' is generally relative to an electron and can refer to a single proton or larger gas molecules; it is not in this case a reference to a solid particulate. A common example is He(2^3S) that resides at an excited state of 19.8 eV which exceeds the ionization energy of common gases such as N_2 and CO_2.[82] The fourth mechanism is similar to Penning ionization; however the excited state of the incident particle is not high enough to directly ionize the target particle the reaction of the two individual particles results in a molecule product with a combined energy state that is higher than the ionization potential and is called 'associative ionization'.[82] The fifth major mechanism for ionization is photoionization where an incident photon with sufficient energy is able to excite an electron out of its bound state. It is possible to ionize a ground state particle but the photon would require a low wavelength usually significantly below 100 nm; however

similarly to the previously describe ionization mechanisms if the target particle is already in an excited state then a lower energy, higher wavelength photon can be used for ionization.[82]

One common description that covers the progress from ambient conditions to the formation of an arc, such as the one used the work detailed in this dissertation is the Townsend discharge. This is an ionization process where a relatively few number of energetic electrons are able to increase the total number of electrons and thus the conductivity of the gas through avalanche multiplication or a 'Townsend avalanche'. In Figure 4-2 region A is statistical fluctuations in the ionization level due to background effects such as cosmic rays, as the voltage increases towards the breakdown potential (V_B) the current increases by secondary ionization at point B, the region BC is referred to as the Townsend discharge and experiences an increase in current, the cathode fall develops at D, and is intermittent to E, the region EG is a glow discharge which is characterized by having a higher level of ionization than the background but still less than that of a conductive arc, and the GH region has a fall in voltage as it transitions into an arc discharge beyond H. It is in this region that the plasma torch used in the majority of the SERDP WP-1762 project work, PlasmaFlux 5000 (PF5K), operates based on current of 0.25-2 Amps, a voltage of 4 kV, a power of 1-2 kW, and nozzle diameter of 1.25-2.0 mm.

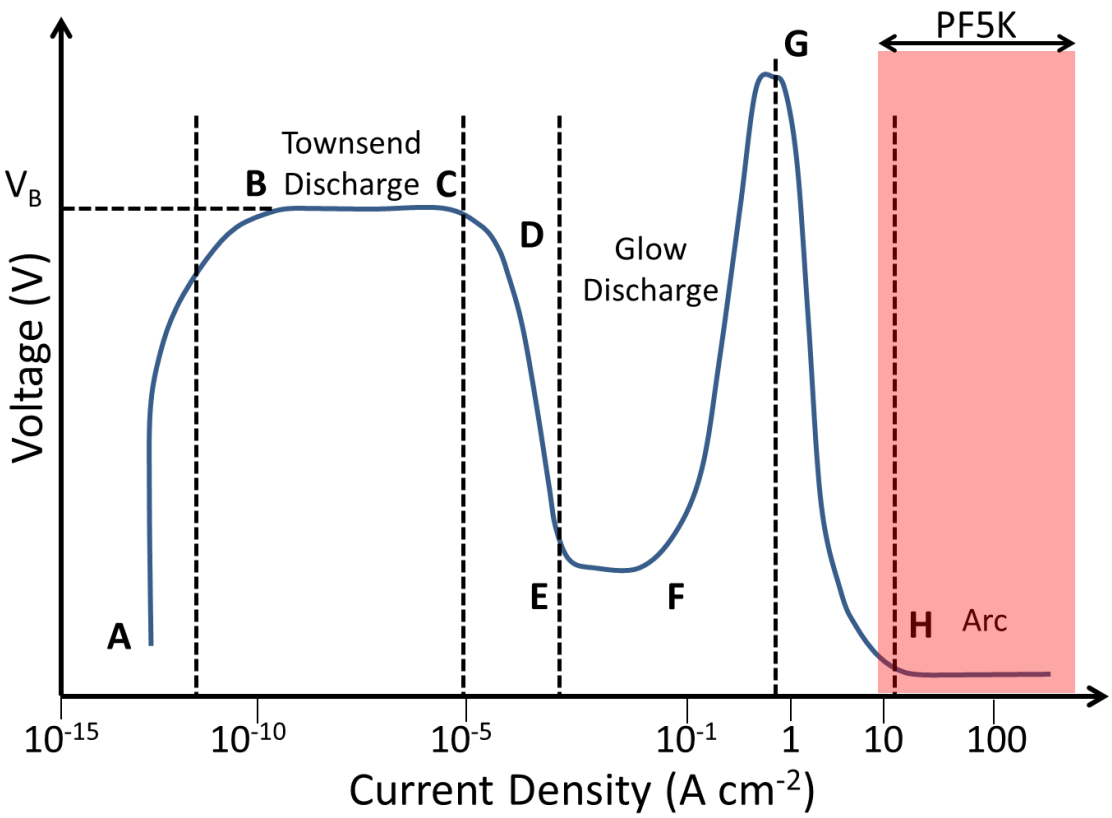

Figure 4-2: Current and voltage characteristics of an electrical breakdown based on Reference [83] with the region that the PF5K is likely occupy.

While the Townsend breakdown is a good introduction to plasma formation it is only apt at describing this process at low pressures and short discharge gaps such that $pd < 4000 \text{ Torr cm}$, which at atmospheric pressure corresponds to an electrode separation of only 5 cm, therefore a different descriptive mechanism for plasma initiation is needed. The spark or streamer mechanism can occur at higher pressures and larger electrode gaps, was originally developed by Raether,[84] Loeb,[85] and Meek and Craggs[86]. This mechanism creates a localized ionization channel much faster than the time required for ions to impact the

electrode providing secondary electron emission making the breakdown potential independent of electrode material. Instead a primary avalanche of electrons, between the electrodes, creates a thin streamer that propagates along the positive wake and also generates photons that spawn secondary avalanches. The electrons produced by these secondary avalanches are pulled into the positively charge wake of the primary avalanche by strong electric fields. [82] As the streamer propagates through space and reaches the opposing electrode a conductive channel now connects the two electrodes.

This conductive channel develops as energy is supplied at a fast rate due to the current passing through it, as generally controlled by the power supply. It then begins to expand forming a cylindrical shockwave, the detailed physics of which are described in more detail elsewhere.[87] The channel diameter reaches equilibrium in approximately 10 μs and based on extrapolating the current:diameter ratios presented in Reference 81[87] the PF5K arc diameter is 40 μm.

Once an arc is generated there is now the problem of removing or extinguishing the arc. As the arc is sustained by a voltage and current flow, a disruption or lowering the voltage below some critical point the arc becomes incapable of sustaining itself.[88] The plasma may still exist for some length of time even in the absence of a sustaining voltage or current due to the delay in recombination or de-excitation.[88] Due to metastable excited states these times can be long, exceeding several seconds.

Plasma parameters of thermal and nonthermal arcs are compared to the parameters from the plasma torch that was built by the NCSU lab, referred to as the Plasma Vortex, in Table 4-1.

Table 4-1: Plasma parameters of thermal and nonthermal arcs adapted from [82] pg 504 compared to the parameters of the Plasma Vortex

Plasma Parameter	Thermal Arc	Nonthermal Arc	Plasma Vortex
Gas pressure	0.1 – 100 Atm	$1*10^{-6} - 1*10^{-1}$ Atm	4-8 Atm
Current	30 A – 30 kA	1 – 30 A	0.1 – 2 A
Voltage	10 – 100 V	10 – 100 V	4 kV
Power per unit length	1 kW cm^{-1}	1 kW cm^{-1}	25 – 250 W cm^{-1}
Current density	10^4-10^7 A cm^{-2}	10^2-10^4 A cm^{-2}	10 – 150 A cm^{-2}

4.3 Thermal-Equilibrium Plasma

Relative ratios of the temperatures for the different species are often used to describe the overall thermodynamics of a certain plasma. A plasma is in thermal equilibrium when electron temperature T_e is approximately equal to the ion temperature T_i and/or neutral temperature T_n: $T_e \approx T_i \approx T_n$.

4.4 Non-Equilibrium Plasma

When the energy distribution differs significantly between species of a plasma, it is described as a non-equilibrium or a non-thermal plasma. This type of plasma has an electron temperature that is far greater than the ion or neutral temperatures: $T_e > T_{i,n}$. Sometimes these non-equilibrium plasmas are referred to as‘cold’ plasma. It can be a bit of a misnomer in that while the overall temperature is less than a plasma in thermodynamic equilibrium,

there can still be a significant amount of thermal energy that can cause damage to the plasma device itself or to whatever is being processed.

4.5 Vacuum

Another major differentiation factor among plasmas is the density of particles. One of the main results is the mean free path or the distance a species can travel between collisions given by

$$\lambda = \frac{kT}{\sqrt{2}\pi d^2 p} \tag{1}$$

where λ is the mean free path, k is Boltzmann's constant, T is the temperature, d is the diameter of the species, and p is the gas pressure. This equation when calculated for nitrogen at room temperature at 1 Torr the mean free path is compared to high vacuum of $10^{-6} Torr$ where the mean free path is $75\ m$.

4.6 Atmospheric

Conversely at higher pressures such as atmospheric pressure, $760\ Torr$, the mean free path drops to $98\ nm$ and for the pressure ranges at which the plasma torch operates, 6 atm or $4{,}500\ Torr$, the mean free path shrinks to about $16\ nm$. The effects of such a reduced mean free path result in drastically different plasma behavior. For instance electronic and magnetic effects or forces from applied fields is significantly reduced since the particle that is being accelerated or acting upon can only move a distance of tens of nanometers before colliding with another particle and loosing or transferring momentum and/or energy. While this does

not allow for certain plasma features that are normally found under vacuum pressures it does offer some redeeming features. The higher pressures allow, in some cases, a higher density of electrons and ionized species per volume of gas. The increased collision frequency also means that there is a higher probability of an excited species colliding with either another excited or neutral species allowing for a chemical reaction to occur. This allows for a higher chemical reactivity and the potential for reactions to take place resulting in chemistry that otherwise would not be possible. For example the mean free path of an electron with respect to elastic collisions with neutrals at atmospheric pressure is approximately 1 μm with an interaction frequency of approximately 10^{12} s^{-1}. [89]

4.7 Plasma Etching

Material removal through plasma treatment has been a mainstay of both vacuum processing and atmospheric pressure treatments with the main difference, aside from the lack of vacuum equipment, being the removal rates. Focusing on atmospheric pressure plasma for coating removal there is a need for higher rates than are offered by the typical 'cold' plasma devices used for surface modification; however, more control is required than is available from the arc cutting and waste remediation type plasma devices.

4.8 Plasma Torches

There exists a plethora of methods and designs to generate plasma. Regardless of how one goes about it at the most simple level there is a transfer of energy for some power source whether it is electrical, chemical, thermal, or some other source to the material that is to be ionized. If the amount of energy transfer is high enough some of the material will become

ionized thereby generating a quasineutral system of electrons and ions in the background gas. The modes of energy transfer can differ widely including the basic separation of electrodes to form an arc, covering electrodes with a dielectric barrier, capacitively or inductively coupling electromagnetic energy, wave heating via microwaves, thermal shock, and lasers.

4.9 General Design for DC and AC Torches

Typically the most ubiquitous plasma torch is the arc, used for cutting, welding, waste remediation and a host of other applications. Power can be applied as DC, AC, or even low frequency RF (100's kHz). Operation of the arcs is sustained by two main modes describing the electrical path of the arc: transferred and non-transferred arcs. Current in a transferred arc travels from the driven electrode to an electrically grounded substrate external and isolated from the torch. Contrastingly, non-transferred arcs flow current from the driven electrode to some part of the torch housing, body, or nozzle that acts as the grounded electrode and a plasma plume is blown through the nozzle. A representative diagram in Figure 4-3 illustrates the differences.

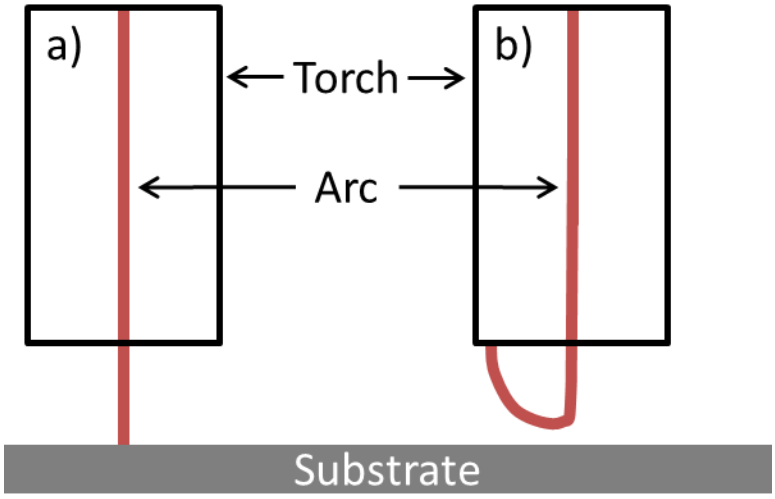

Figure 4-3: Depiction of a) transferred arc and b) a non-transferred arc torch.

The torch body is generally cylindrical in shape along axis coincident with the arc and serves to house the electrode, cooling mechanisms, and nozzle or constricting device. Stabilization can be accomplished by water,[90] gas-vortex,[91] or magnetic stabilization. The latter is possible primarily in vacuum arcs,[92] given the longer mean free path between collisions.

Electrode type and materials depends on the application. If an application with a high electrode consumption rate is desirable such as in metal inert gas (MIG) welding, then a sharp pointed shape is used to ensure ablation of the electrode material which in this case is dependent on the material being welded. Applications that require a longer electrode lifetime, such as tungsten inert gas (TIG) welding, use more thermally stable materials such as tungsten that is commonly alloyed with thorium or zirconium for enhanced performance

due to reduced work function. The shape of the electrode can be a rod, cone, recessed, or hollow for improved operation.

The nozzle can restrict and constrict the plasma as well as make use of properties found in de Laval nozzles, or convergent-divergent nozzle, as depicted in Figure 4-4 showing the associated gas temperature, pressure, velocity, and Mach numbers. Behind the throat of the nozzle the gas velocity is subsonic and accelerates to Mach 1 as the nozzle narrows. As the gas exits the nozzle it expands, accelerating to supersonic velocities and reduced temperature and pressure.

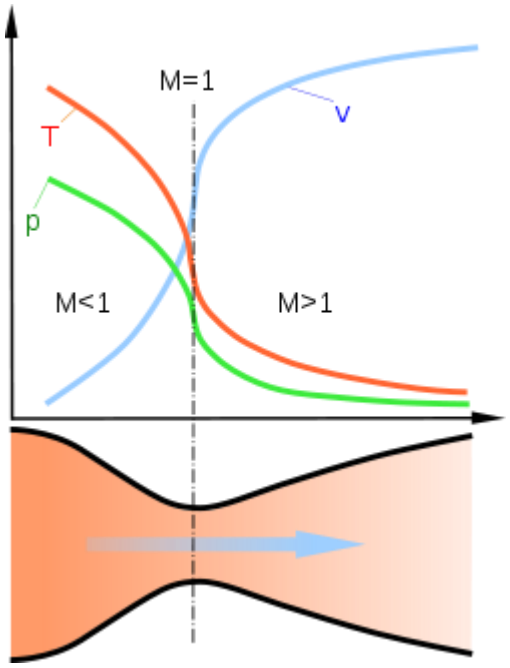

Figure 4-4: A diagram of a de Laval nozzle pictured on the bottom, with the corresponding approximate flow velocity (v), pressure (p), temperature (T) and Mach number (M) located at the top.[93]

A feature common to jet nozzles is the formation of shockwaves (also known as shock diamonds, Mach diamonds, or Mach disks). While the Mach disks are typically associated with aerospace jet and rocket engines, the features are also present with plasma devices.[94-98] The shocks are formed when the compressed fluid on in this case air exist the throat of the nozzle and expands to the point that the expansion wave hits a boundary caused by the environment and is reflected back towards the centerline with some situations resulting in sharp demarcations of high and low pressures.

The powered electrode must be isolated from the rest of the torch otherwise it will short out or have some other catastrophic failure. This is usually accomplished by mounting the electrode to an insulating dielectric material. Low power torches can use polymeric dielectrics that have moderate insulating capabilities but poor thermal stability and higher power torches can use ceramic dielectrics that have high insulating capabilities and thermal stability.

4.9.1 General Applications and Uses

There are numerous applications for plasma torches in areas that need high temperatures or chemically active species that would be difficult to obtain through conventional methods.

Plasma torches initially gained traction in welding applications and supplied the foundation for research performed by Dr. Gage at Union Carbide in the mid-1950's. This research lead to the development of plasma torch cutting by the implementation of a constricted wall stabilized plasma torch which results in a higher plasma arc energy density.[99]

These types of plasma are commonly generated with a low voltage and high current power supply.

As elevated temperatures and unique chemical species are present in these types of high power plasmas, these properties can create a highly reactive environment capable of cutting industrial metals. It also is an attractive solution to the remediation of various waste streams. This is usually achieved through outright combustion or pyrolysis, which is a heating process in an anoxic or anaerobic environment that decomposes materials into their respective molecular components while avoiding a combustion reaction.[100]

Advantages, when compared to conventional incineration or fossil fuel combustion, include that plasma waste remediation uses only 15% volume of air necessary compared to fossil fuel combustion,[100] and as a result uses lower gas input per unit heating power.[101] This allows for smaller and cheaper plants when compared to traditional waste remediation plants,[101-103] and combined with the fact that no fuel is combusted on site to generate the necessary heat also minimize the required footprint.[101,102] Additionally, the torch devices generate plasma with a high energy density and gas temperature[101-103] with steep thermal gradients[102,104] that can produce aster reaction times and highly reactive environment.[101,102] These highly reactive environment can be used to remediate a wide range of liquid, solid, and gas wastes[102] and even treat heterogeneous non-sorted waste directly eliminating the need for an independent separating stage or facility.[105]

Municipal waste and/or biomass waste can be disintegrated by plasma pyrolysis where organic materials are converted into a high caloric synthetic gas (syngas) comprised of

CO and H_2 and inorganic materials are converted into a non-leachable vitrified igneous rock.[101] Hazardous materials and waste from asbestos, healthcare, industrial processing, fiber reinforced polymeric matrix composite materials used in maritime applications, chemical storage and aircraft can be broken down into innocuous products for safe disposal.[102,103] It is even possible to dispose of military ordnance including completely assembled pyrotechnic, smoke, and dye devices as an alternative method to open burning or detonation and conventional incineration.[105,106]

Another area of interest for the high temperatures and energies associated with high power plasma torches is the application in constructive and fabrication applications instead of destructive applications. One such use is soil remediation by 'plasma magmavication' wherein a nontransferred arc is used to melt the soil that upon cooling forms an igneous rock.[107] Another common use is in additive manufacturing termed 'plasma spray' where powders are injected into the plasma to soften or completely melt and are then deposited on a surface where the liquid particles flatten and solidify. This allows for the repair of lost substrate material and deposition of thermal barrier, abradable, wear and corrosion-resistant coatings.[104,108]

While in some cases it is desirable for total vaporization of a material there are certainly cases where a more delicate approach is needed, such as the sterilization of mail. Following the Anthrax attacks of 2001 concern grew over the possible use of mail to deliver and carry out bio-hazardous terrorism. Envelopes containing *Bacillus cereus* as a substitute for *Bacillus anthracis* (Anthrax) were sterilized by reactive oxygen species including

molecular and atomic oxygen produced in a microwave generated plasma.[109] This may be easier to implement as opposed to irradiation or chemical sterilization methods as it cause less damage and avoids incurring public fear over radiation resulting in radioactive mail.

Another more common application of lower powered plasma torches is one that can be used for an analytical characterization technique: inductively coupled plasma (ICP) atomic emission spectroscopy (AES) or optical emission spectroscopy (OES). It operates similar to a flame atomic emission spectroscopy technique but with the major distinction being that instead of using a combustion source such as air/acetylene to heat the gas to relatively low temperatures of 2,500 K it uses an ICP torch that is able to achieve electron temperatures of 20,000 K and higher while keeping the gas and ion temperature low, as a few eV without a combustible agent.[110,111] Pioneering work by T.B. Reed in the early 1960's set the stage for the emergence of this technique.[111] While there are some discrepancies of detection limits, interferences, sample size and other qualifying descriptors between ICP-AES and other techniques such as atomic absorption spectroscopy (AAS) the overall utility and simplicity of the technique ranks it highly amongst atomic elemental analytical characterization.[112] Additionally it allows for the simultaneous multi-element analysis of solutions with detection limits of pg/mL.[113] Another analytical technique that makes use of ICP is mass spectroscopy (MS), often referred to as ICP-MS, which injects the solution into the ICP torch ionizing the molecules and is then differentially pumped into the quadrupole section of the MS.[114]

Other emerging applications and devices are microplasmas denoted by one of the dimensions of the plasma or device is within the micrometer scale, although the term is also loosely applied to plasma devices that can be scaled to millimeters. Examples include large area arrays generated by 13.56 MHz capacitively and inductively coupled devices,[115] the fabrication of a MOS diode at atmospheric pressure and synthesis of carbon nanostructures,[116] and can be small enough to be powered by only 4 AAA batteries.[117] Medical applications of plasma include sterilization of contaminated materials,[19] elimination of necrotic cells,[118] and in-vivo treatment of wounds.[17]

4.9.2 Operation

Since the construction of the PlasmaFlux 5000 (PF5K) was done in such a way that it limits access to critical parts making it not exactly conducive for basic research, a test-bed torch was developed by the NCSU lab in the lab that was designated as the 'Plasma Vortex'. The operation of the plasma vortex type of plasma torches has multiple modes and descriptions. Before steady state operation is achieved the plasma must be ignited through a high voltage pulse that is capable of causing the breakdown of air so that a current carrying channel can be formed. The dielectric barrier discharge (DBD) power supply delivers approximately a 20 kV pulse to assist in the initial arc formation. This potential corresponds to the bread-down potential of about a 0.25" gap based on the Paschen formula. Once the arc is formed and a conductive channel, compared to the background air, is formed, the voltage drops to approximately 4 kV. The arc originates at the driven electrode and the other end is then assumed to be blown down the inside of the tube without interacting with the wall and stabilized by the low pressure region of the vortex. The arc is then forced out the nozzle,

again constricted in such a manner as to avoid contact with the nozzle walls, where the plasma begins to expand and generate the afterglow. The circuit must still be completed and this is achieved by what have been termed secondary arcs which are periodic and jump around in a flickering type manner connecting the primary arc that exits the nozzle to the external face of the electrically grounded nozzle tip. Under this mode of operation the plasma vortex style torch can be considered a non-transferred arc torch as the initiation and termination electrode locations are either contained within the torch or are part of the physical manifestation of the torch itself. There are occasions and conditions where the plasma vortex style torch can operate in a transferred arc mode. For instance, if the sample being treated is conductive (metallic), electrically grounded, and is positioned at a separation distance that is shorter than the existing length of the secondary arcs then the electrical current will follow the path of least resistance. Under these conditions the shortest path is created by the arc to the grounded sample. Once this connection is generated the torch can be moved increasing the separation distance while the transferred arc is maintained, until it reaches a distance such that the resistance to current flow of the increased distance is more than the resistance of the secondary arc length which are then reformed. Under the transferred arc mode there is no appreciable afterglow as the arc is terminated on the sample and not the nozzle preventing the effluent from being blown out of the arc region. While most torches are designed to operate in either transferred or non-transferred mode, the plasma vortex style torches are capable of switching modes depending on the nearest electrically grounded connection. A short distance after the primary arc is connected via the secondary

arcs the plasma transitions from the high intensity arc to a lower intensity afterglow region that extends for a couple centimeters depending on the operating conditions.

5 Optical Emission Spectroscopy

This chapter focuses on the fundamentals of primary analytical technique used to characterize the plasma torch. Pertinent emission systems are covered and a basic overview of OES hardware is included.

5.1 Emission Fundamentals

Optical emission spectroscopy (OES) is the observation of light emitted through the de-excitation of a species existing in an unstable energetic state. The specie transitions from a higher energy state, E_1, to a lower energy state, E_2 emitting the difference in energy between states in a quanta of energy, photon. The energy of the photon is given by

$$E_{Total} = h\nu = E_1 - E_2$$

Where h is Plank's constant and ν is the frequency. The energy state transitions can be electric, vibrational, rotational, or a combination of the different modes. The energy emitted in electronic transitions is in the ultraviolet and visible range of the spectrum, commonly referred to as UV-VIS. Comparably, photons emitted by the transition from an ionized species to ground state are generally in the far-UV range and vibrational transitions are typically in the infrared range. The arrangements of energy states are unique to atomic and molecular species, although there may be some overlap. This allows for the species identification based on the location of peaks in the emission spectrum.

A brief review of spectroscopic nomenclature is provided as a primer on the definitions and background of observed transition states. First, the relevant quantum

numbers include the principle quantum number: $n=1,2,...$ describes the electron shell of an atomic, the orbital angular momentum: $L^2=\hbar\ell\left(\ell+1\right)$ where $\ell=0,1,2,...n-1$ is the angular quantum number where $\ell=0$ is an s-orbital, $\ell=1$ is a p-orbital, and so forth, and the spin quantum number S: parameterizes the intrinsic angular momentum of the particle. Also, when orbital angular momentum is coupled with spin angular momentum it is represented as the total angular momentum $J=\sqrt{j\left(j+1\right)}\hbar$ where the total angular momentum quantum number $j=\ell\pm s=\ell\pm\frac{1}{2}$.

Electronic states of atoms will be detailed using the example of electronic state atomic nitrogen denoted by $N\left(2s^2p^3\,{}^4S_{3/2}\right)$. In this example the "N" obviously refers to atomic nitrogen. Inside the parentheses the "$2s^2p^3$" corresponds to the electrons filling the outer shell of the nitrogen atom where the principal quantum number $n=2$, s and p denote the electron orbital, and the right-hand superscripts indicate 2 s-electrons and 3 p-electrons. The ${}^4S_{3/2}$ term describes the other shell electrons collectively in the ground state. The prefix superscript "4" denotes a multiplicity such that $2S+1$ and corresponds to the number of energy levels in a multiplet if $S\le L$ where these are quantum numbers and not the term itself. Total orbital angular momentum: L=0,1,2 correspond to S,P,D. the subscript $3/2$ denotes the total momentum quantum number $J=3/2$. Another example is the first excited state of helium: $He\left(2p\,{}^1P_1^0\right)$, here the right-hand superscript (0) refers to parity which is the sum of the angular momentum quantum numbers for individual electrons in the atom such that

completed shells have an even parity. Odd parity is denoted by a superscript (0) and even parity is indicated by the absence of a superscript.[82] (pg.74-75)

Electronic states of molecules have a slightly different set of nomenclature. Diatomic and linear polyatomic molecules can be identified by Greek letters $(\Sigma,\Pi,\Delta,\Phi...)$ that correspond to the quantum number $\Lambda = 0,1,2,3...$ which describe the absolute value of the total orbital angular momentum along the internuclear axis. The previously described multiplicity such that $2S+1$ is written as a prefix superscript such that $^2\Pi$ indicates $\Lambda = 1, S = 1/2$. In the case of Σ states $(\Lambda = 0)$ right-hand superscripts (+) and (-) are used to designate if the wavefunction, Ψ, is symmetric or antisymmetric with respect to reflection at any plane including the internuclear axis. Furthermore, right-hand subscripts (g) and (u) are used in order to designate whether Ψ is symmetric or antisymmetric with respect to the interchange of nuclei in homonuclear diatomic molecules, such as N_2,H_2, O_2, F_2, etc… For example a homonuclear diatomic molecule described by the term $^1\Sigma_g^+$ means $\Lambda = 0, S = 0$ and that Ψ is symmetric with respect to both the reflection at any plane including the internuclear axis and to interchange of nuclei. If the molecular specie is in a ground electronic state, the term used is a capital (X) usually written before the term symbol and if the molecular specie is in an excited electronic state with the same multiplicity as the ground state the capital letters A,B,C,… are used as the terms and if the multiplicity is different than the ground state lowercase letters a,b,c,… are used as the terms. [82](pg.74-75) More detailed explanations of the quantum state, wavefunctions, transitions, and other basic properties of

atoms and polyatomic molecules are commonly found in physical chemistry text books such as: X & Y.

OES is a convenient non-invasive technique capable of measuring excited species and relative changes. An air plasma of modest power levels will have an assortment of nitrogen and oxygen compounds and species such as NO, N_2, N, and O. The distribution of these species is critical to the interaction with and removal of coatings as the species are a significant source of highly chemically active reactants and an energy reservoir stored in the various vibrational and electronic modes of the species.

Molecular nitrogen has several significant emission features commonly observed in atmospheric air plasma. The 1st Positive $\left(B^3\pi_g \rightarrow A^3\Sigma_u^+\right)$, 2nd Positive $\left(N_2C^3\pi_u \rightarrow B^3\pi_g\right)$, and 1st Negative $\left(N_2^+B^2\Sigma_u^+ \rightarrow X^2\Sigma_g^+\right)$ systems,[119] and are depicted in Figure 5-1 and the wavelengths of several of the bands of the 1st Negative system and 2nd Positive system are given in Table 5-1. The state $N_2C^3\pi_u$ can be considered to be populated by direct electron collision from the state $N_2(X^1\Sigma_g^+)$: $e + N_2\left(X^1\Sigma_g^+\right) \rightarrow e + N_2\left(C^3\Pi_u\right)$ and de-populated by radiative transition to the state, with emission of the second positive system $N_2\left(C^3\Pi_u\right) \rightarrow N_2\left(B^3\Pi_g\right) + (h\nu)$.[119]

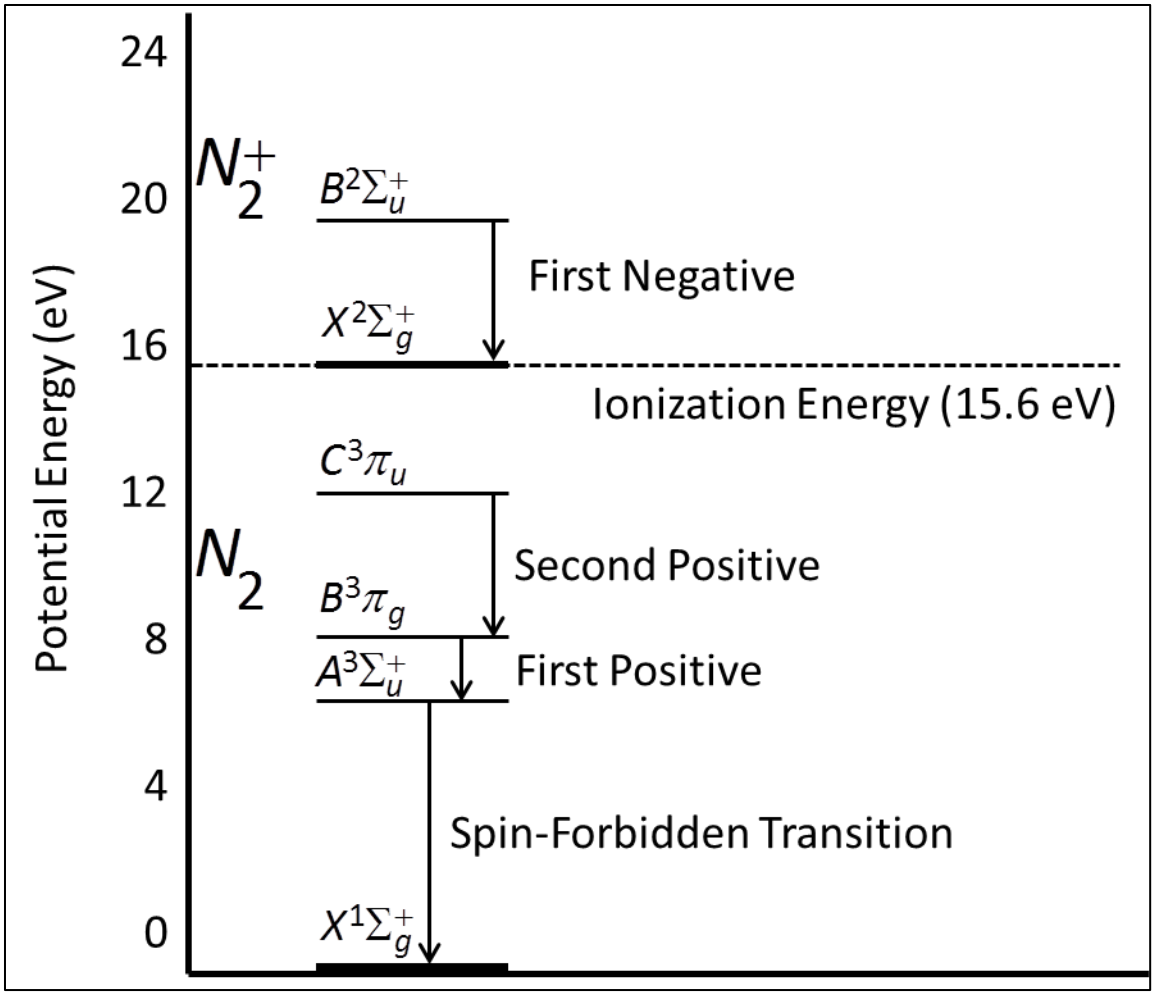

Figure 5-1: Depiction of the different states of molecular nitrogen addapted from reference[120] and reference[121].

Table 5-1 Wavelengths of the various N_2 second positive system and N_2 first negative system bands adapted from reference [122]

N_2^+ $B^2\Sigma_u^+ \rightarrow X^2\Sigma_g^+$ (1st Negative System)		N_2 $C^3\Pi_u \rightarrow B^3\Pi_g$ (2^{nd} Positive System)	
Band (v'-v'')	Band Origin (nm)	Band (v'-v'')	Band Origin (nm)
0-0	391.1	0-0	337.0
1-0	357.9	1-1	333.8
2-1	356.1	2-2	330.9
3-2	354.6	1-0	315.8
4-3	353.5	2-1	313.5
2-0	330.5	3-2	311.5
0-1	427.5	4-3	310.2
1-2	423.3	2-0	297.6
2-3	419.6	3-1	296.1
3-4	416.4	4-2	295.2

The excited molecular nitrogen species can act as an energy reservoir for several reactions such as steel nitriding and the deposition of Si_3N_4,[119] as the vibrational excitation of molecules essentially accelerates endothermic chemical reactions.[123] Molecular nitrogen is capable of acting as an energy reservoir given that it has a large effective cross section of the vibrational levels excited by electron impact $\left(3 \bullet 10^{-16} cm^2\right)$ compared to a relative small effective cross section of vibrational relaxation $\left(3 \bullet 10^{-24} cm^2\right)$ and a small factor of vibrational

energy loss on the surface making it easy to excite N_2 molecules while retaining the vibrational energy.[123] Other methods that enable de-excitation include natural photo radiation: $N_2^* \rightarrow N_2 + h\nu$, quenching by the background gas: $N_2^* + A \rightarrow N_2 + A^*$, or by chemical reactions: $N_2^* + A \rightarrow products$.[121]

The metastable molecular nitrogen species are readily generated by electron collision and function as a medium to store electron energy by conversion to internal energy.[120] Molecules excited to $C^3\pi_u$ relax to $B^3\pi_g$ and then to $A^3\Sigma_u^+$ with an accompanying emission of light, with a radiative lifetime of 37 ns for $C^3\pi_u$, 8 μs for $B^3\pi_g$, and a long period of 1.9 s for $A^3\Sigma_u^+$ as the $A^3\Sigma_u^+ \rightarrow X^1\Sigma_g^+$ transition is forbidden by the spin selection rule.[120]

Another significant molecular species typically found in atmospheric air plasma is the NO_x (NOX) group of compounds is responsible for the ubiquitous greenish yellow glow. Lord Rayleigh determined that nitric oxide was necessary, though erroneously attributed ozone to be the other reactant,[124] later confirmed to be atomic oxygen in the reaction: $NO + O \rightarrow NO_2 + h\nu$.[125] The NO is produced through the reaction $N_2(\nu) + O \rightarrow NO + N$ for $\nu > 12$.[126,127] This nitrogen and oxygen chemical process produces a quasi-continuum emission spectra over a wavelength range of 400-900 nm with a maximum near 620 nm arising from electronically excited NO_2 molecules, the long-wavelength range from 700-1200 nm is the 'thermal' radiation of NO_2 molecules caused by collisional E-V excitation (molecular $^1B_2$-X^2A_1 electronic transitions) and the short-wavelength range from 400-600 nm is the 'recombination' radiation emitted by the NO+O reaction.[128] The intensity of the

afterglow increases with decreasing gas temperature, typically along the plasma flow direction, agreeing well with the strong negative temperature dependence of the rate of NO+O radiative recombination: $I_\lambda \sim [NO][O]T^{-1.9}s^{-1}cm^{-3}$.[128]

It is also possible to form atomic oxygen through an exothermic dissociative quenching of nitrogen metastables: $N_2(A,B,C)+O_2 \rightarrow N_2(X)+2O$ with the primary nitrogen metastables contributing to the O_2 dissociation by $N_2(B,C)$ while $N_2(A)$ was deemed less critical.[129]

Atomic oxygen excited by electron impact in the $^3P \rightarrow ^3P$ (10.99 eV) and $^3P \rightarrow ^5P$ (10.76 eV) transitions cannot radiate to the ground state due to the electric dipole selection rules and instead transition to lower energy states $^3P \rightarrow ^3S^0$ (844.6 nm) and $^5P \rightarrow ^5S^0$ (777.4 nm) and then the subsequent transitions to the ground state $^3S^0 \rightarrow ^3P$ (130.4 nm) and $^5S^0 \rightarrow ^3P$ (135.6 nm) as depicted in Figure 5-2.[130]

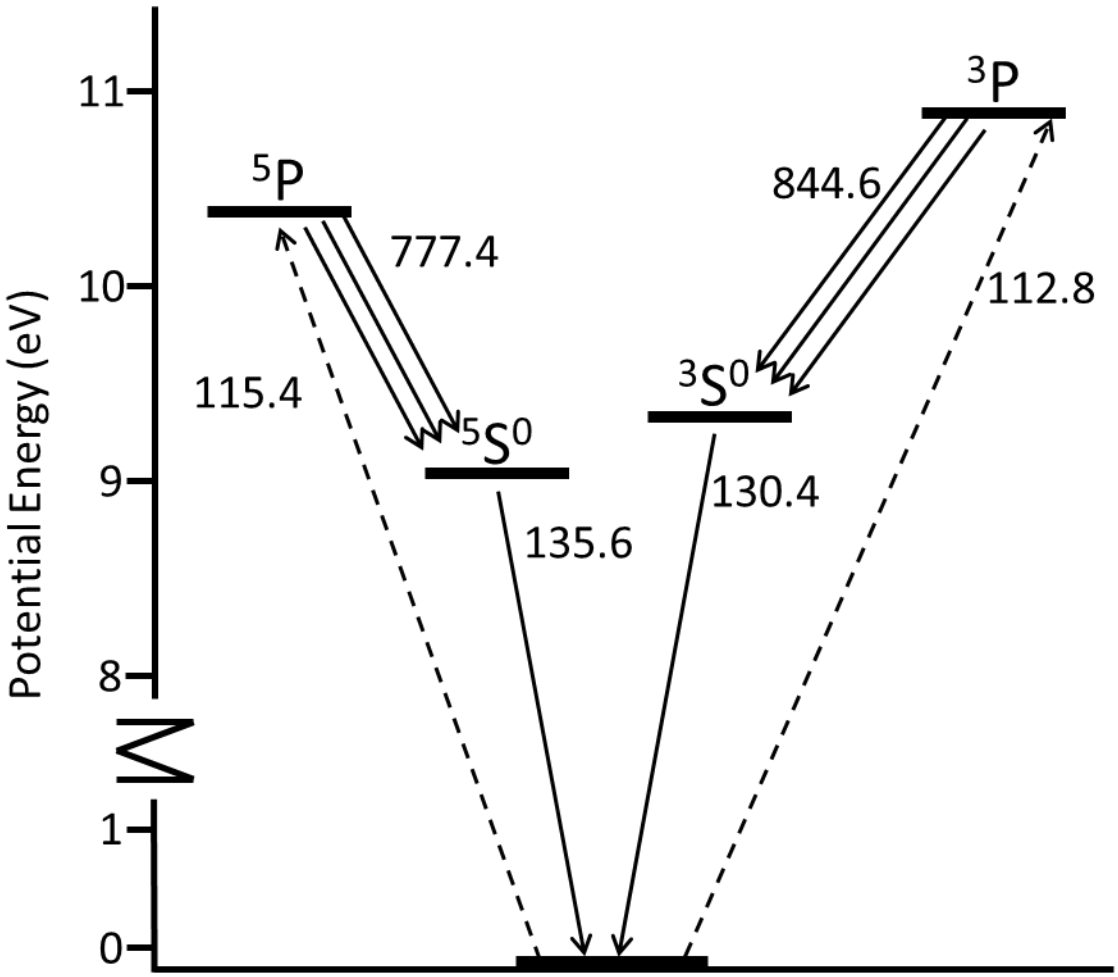

Figure 5-2: Energy diagram of atomic oxygen adapted from [130]

Atomic nitrogen can be generated by electron-impact dissociation reaction $N_2 + e^- \rightarrow N_2^* + e^- \rightarrow N + N + E_{Trans} + e^-$ where an electron impact with molecular nitrogen produces an electronically excited N_2 state that then dissociates into atomic nitrogen with a release of translational energy.[131] It was determined by Cosby[131] and Walter et al.[132] that the dominant dissociation mechanism of N_2 into $N(^2D^o) + N(^4S^o)$ occurs for excited N_2 states

lying below 13.91 eV and energy levels above this increasingly dissociate to the more highly excited $N(^2P^o) + N(^4S^o)$ limit. While it is possible to generate atomic nitrogen from molecular nitrogen, there exist only three electronic states of atomic nitrogen (^4S, ^2D, and ^2P) that are energetically accessible below the ionization energy of molecular nitrogen.[121] There are four atomic nitrogen transitions that are significant to the PF5K. The first is the $3s^4P - 3p^4S^o$ transition that produces a NIR triplet located at 742.3, 744.2, and 746.8 nm, secondly the $3s^4P - 3p^4P^o$ transition produces seven-line multiplet between 818.5 and 824.2 nm, thirdly the $3s^2P - 3p^2P^o$ transition generates a four-line multiplet at 856.8, 859.4, 862.9, and 865.5 nm, and lastly the $3s^4P - 3p^4D^o$ transition emits the region from 868.0-872.8 nm.[133] The energy levels are depicted in Figure 5-3.

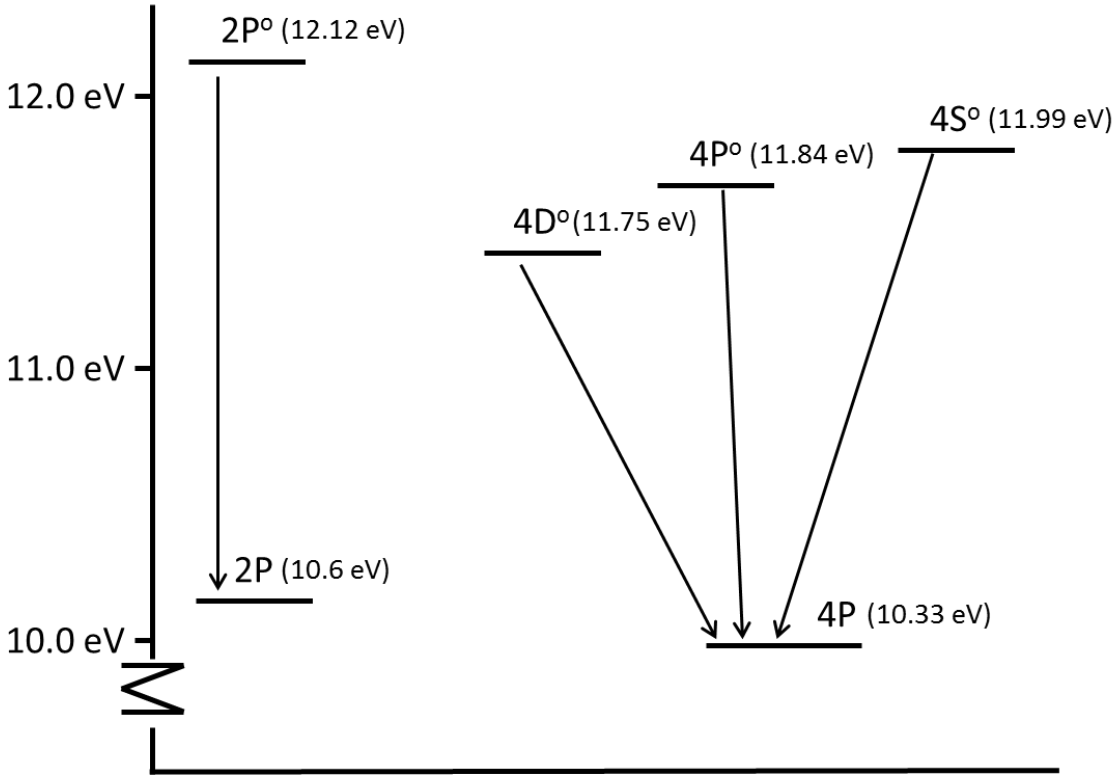

Figure 5-3: Atomic nitrogen energy levels

Several atomic Cu I emission lines are present in the OES spectra of the PF5K and the energy levels and emission wavelengths are given in Figure 5-4 and the spectroscopic data are given in

Table **5-2**. The most intense peaks arise from the two exited $3d^{10}4p^1$ states at 3.8187 eV and 3.7879 eV that transition to the $3d^{10}4s^1$ ground state emitting at 324.75 nm and 327.40 nm, respectively. Given the emission wavelength of these transitions the lines overlap with the nitrogen second positive system leading to difficulty in identification in the presence of strong nitrogen metastable emissions. The other easily identified Cu I lines arise

from the two $3d^{10}4d^1$ states at 6.1953 eV and 6.1944 eV that transition to the two previously described $3d^{10}4p^1$ states emitting at 512.82 nm and 515.32 nm, respectively. Another transition occurs following $3d^{10}4d^1\left(6.1953eV\right)\rightarrow 3d^{10}4p^1\left(3.8187eV\right)+h\nu\left(512.82nm\right)$ is the $3d^{10}4p^1\left(3.8187eV\right)\rightarrow 3d^9 4s^2\left(1.3905eV\right)+h\nu\left(510.55nm\right)$ transition. While, these lines are relatively isolated from overlapping bands in the arc region, when the plasma transitions to the afterglow the lines are enveloped by the broadband continuum.

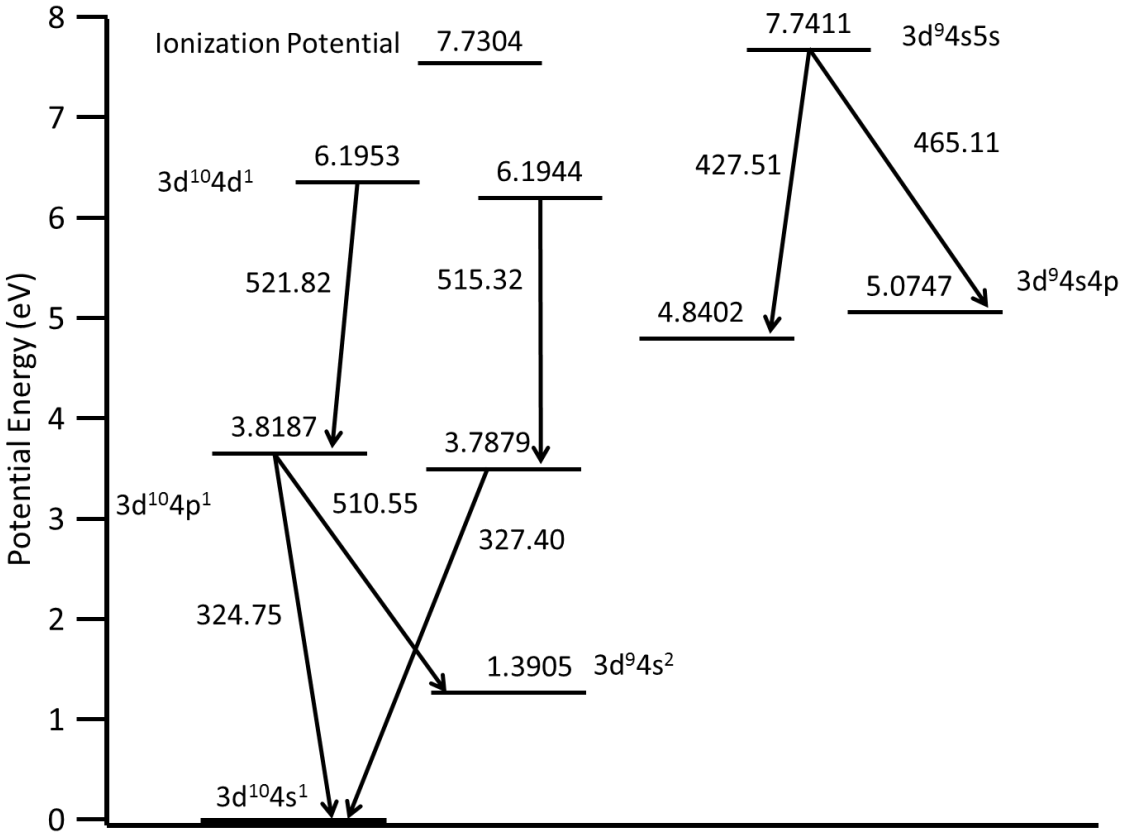

Figure 5-4: Energy levels in eV and emission transition in nm of Cu I, adapted from [134]

Table 5-2: Table of spectroscopic values used for Cu I lines[134,135]

λ (nm)	g	A_{ik}	E_i (eV)
324.75	4	1.39E+08	3.817
327.39	2	1.37E+08	3.786
427.34	8	3.45E+07	7.7458
464.84	8	3.80E+07	7.7458
510.554	4	2.00E+06	3.82
515.324	4	6.00E+07	6.19
521.82	6	7.50E+07	6.19

The inclusion of the Cu I lines in this dissertation is twofold. Firstly, as there is no intentional addition of Cu to the plasma feed gas it is apparent that the Cu that is in the effluent is from the erosion of the electrode and/or nozzle, both of which are copper alloys. The presence of these emissions is important to the process control of the industrial applications as the measurement and monitoring of the lines can be used to track the wear and erosion of the torch consumables. Properly calibrated or calculated it would enable the operator to know more precisely when to replace critical parts thereby decreasing downtime and frivolous use of materials by early replacement. This could be accomplished either by calculating a continuous wear rate from the time averaged Cu I emission intensity or by the observation of fluctuations in the instantaneous emission intensity compared to the time

averaged emission obtained during normal operation. Secondly, the presence of Cu I lines enables an additional calculation of plasma temperature by the relative atomic line intensities.[136,137] This method is also referred to as the 'Boltzmann Plot' method and has been previously employed to calculate the temperature of electrothermal-chemical launchers[138] and arcs [139] in addition to the electrode erosion rate of the later by the relationship[140]:

$$Ln\left(\frac{\lambda I}{gA}\right) = C - \frac{E_i}{k_B T}$$

Where λ is the spectral wavelength, I emission line relative intensity, g statistical weight of the upper level, A transition probability, E_i energy of the upper level, k_B Boltzmann's constant, T plasma temperature, and C is a constant.

5.1.1 OES Hardware

Emission spectroscopy is the measurement of radiation intensity as a function of wavelength, in this dissertation the radiation being measured is in the ultraviolet (UV), visible (VIS), and infrared (IR) spectrum. There are several basic critical components to OES, first is the emission source, then the separation of the light with respect to wavelength, and finally the measurement of the photons. As this chapter focuses on the hardware aspect of OES the separation and measurement components are of interest and discussed.

There are multiple methods available to disperse the wavelengths of an emission source. Material dispersion is a method that utilizes a prism which disperses light based on

the refractive index of the material causing different wavelengths of light to refract at different angles resulting in a spatial separation as depicted in Figure 5-5. Another common method of dispersion is using a diffraction grating depicted in Figure 5-6.

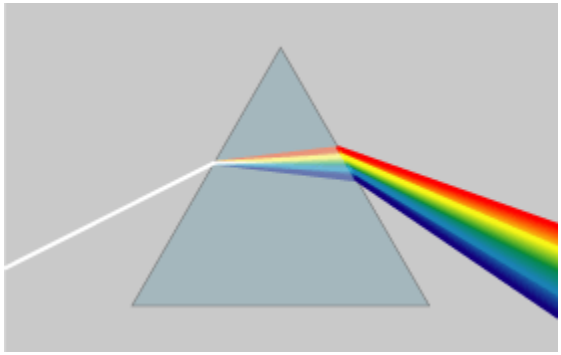

Figure 5-5: The dispersion of white light through a prism, used under the terms of the GNU Free Documentation License.[141]

Figure 5-6: A diffraction grating

The diagram in Figure 5-7 shows the general layout for the Ocean Optics spectrometers. 1: SMA 905 connector, 2: fixed entrance slit, 3: optional longpass absorbing

filter, 4: collimating mirror, 5: grating and wavelength range (installed on platform and rotated to select the starting wavelength and permanently fixed at the factory), 6: focusing mirror, 7: Optional detector collection lenses to ensure aberration-free performance, 8: detector for the USB2000+ is a 2048 element Sony ILX511 linear CCD array detector, 9: optional filter, & 10: optional UV detector upgrade for enhanced performance below 340 nm by replacing the standard window with a quartz window.

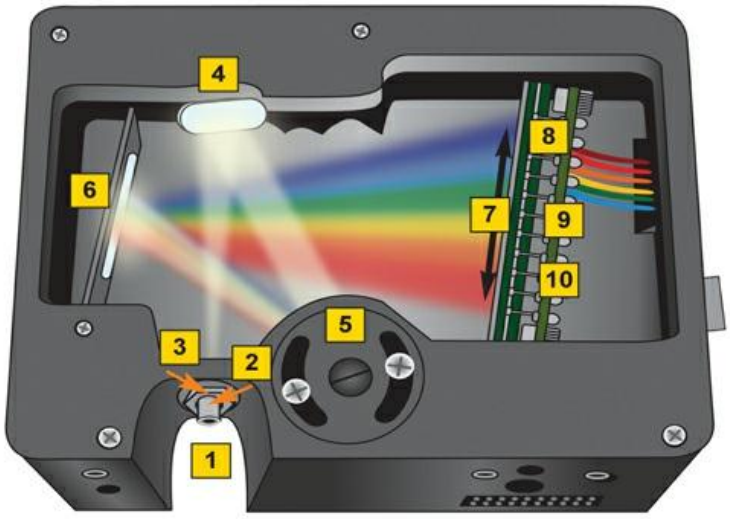

Figure 5-7: Ocean Optics USB2000+ and USB4000 spectrometer layout (http://www.oceanoptics.com/Products/benchoptions_usb4.asp)

The detector is a charge-coupled device (CCD) or a photomultiplier tube (PMT). A CCD operates where the incident light impinges on a capacitive pixel of photoactive material that develops a charge that is proportional to the light intensity and a control circuit then

transfers the charge to the neighboring pixel until it reaches a charge amplifier that generates a voltage that can be measured and recorded. When a linear or matrix array is used each pixel corresponds to a different wavelength of light impinging. In contrast a PMT combines the photoelectric effect and secondary emission whereby incident light strikes a photocathode material that generates an electron via the photoelectric effect that is then focused toward staggered electrodes called dynodes that are each held at a more positive potential than the previous one such that the emitted electron that has the energy of the incident photon minus the work function is accelerated toward the first dynode by the electric field and thus striking it with more energy and thereby releasing more electrons that are then accelerated toward the next dynode and so forth causing a cascade effect that eventually reaches the anode electrode giving a sharp current pulse. The dynodes are generally charged to ~ 1,000 V. The benefit with this device is it can achieve a much higher sensitivity that is useful in low light intensity environments; however, since there is no spatial component the different wavelengths of light must be rastered across the PMT which can take a significant amount of time in comparison to the lifetime of what is being measured.

A common monochromator design is the Czerny-Turner as shown in Figure 5-8 where light from a source A) enters the monochromator through an entrance slit B) is then reflected of a mirror C) and off another mirror D) onto the grating E) that disperses the light onto another mirror F) that focus the light onto the final mirror G) that reflects the dispersed light through an exit slit H) that allows narrow wavelength ranges to strike a detector I) such as a PMT. In order to scan different wavelength the grating is rotated so that the different wavelength are moved across the exit slit.

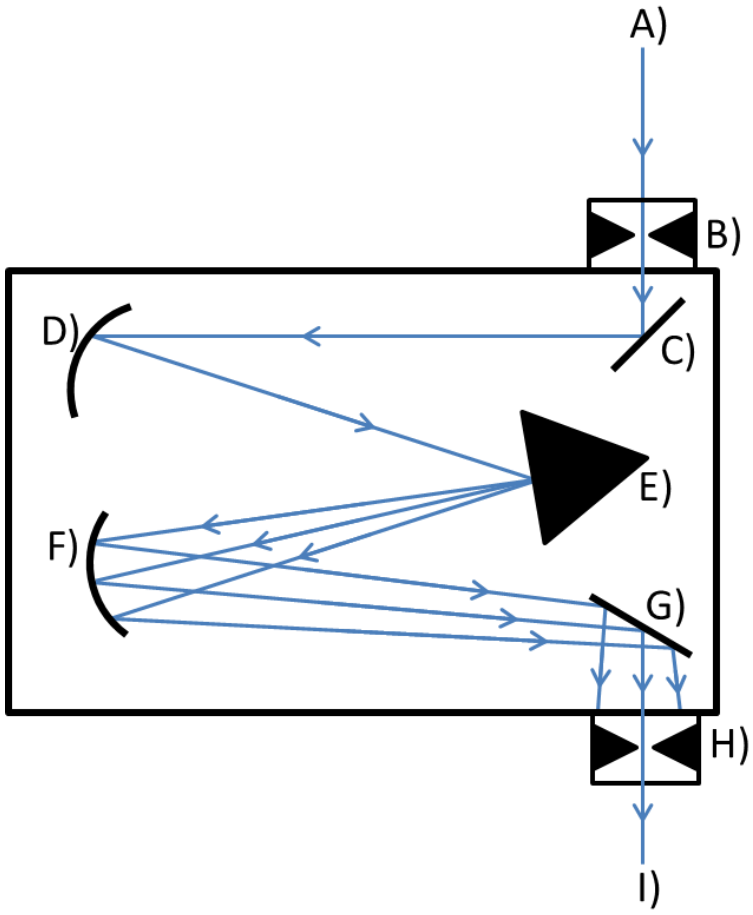

Figure 5-8: Czerny-Turner monochromator

As the light source for the OES studies presented in this dissertation is generally an air plasma the species of interest include molecular N_2 and NO and atomic O I and N I. Additionally, there are Cu I lines from the torch electrode and nozzle that can be used to monitored component wear. It is also conceivable to use Fe I peaks as an 'endpoint' signature to indicate when and where the plasma has bored through the coating and reached

the steel surface, this should be straight forward as there are 6,700 emission lines for Fe I between 200-1,000 nm according to the NIST Atomic Spectra Database.[142]

6 Equipment

6.1 Plasma Devices and Power Supplies

Over the course of the various research projects several plasma devices were used. The primary plasma torch used in the research supporting the SERDP project and dissertation is based on the PlasmaFlux™ Power Supply manufactured by Atmospheric Plasma Solutions, Inc. (APS or AP Solutions). The plasma torch model is PlasmaFlux™ 5000, under the assumption that it is capable of 5 kW power output. This device will be referred to as PF5K. Notable features include two user controlled interlocks where one can be connected to a programmable timer and the other is generally used in conjunction with a dead man type switch. The power supply is controlled via an 'ON/ OFF' toggle switch and the plasma is initiated by depressing the ignition button and 'RESET' button for the case when an internal fault is activated. The PF5K has useable frequency range of 95-110 kHz that is controlled by an unmarked dial knob and displayed on a LCD. The power is controlled in a similar fashion with an unmarked dial knob and a LCD displaying in units of Volts, with a maximum of 275 V. As there has been no clarification from the manufacture and tamper proof seals are placed on all access points to the power supply making direct electrical measurements impossible, it is assumed that the power, even though it is given in units of potential (V), refers to the potential prior to a step-up transformer and not the actual potential across the torch. The operational gas is stated by the manufacturer to be dry compressed air, with the torch operating with a flow range >85 SLM of air with the upper limit determined by the other plasma parameters such as frequency and power where it is possible to 'blow out' the plasma

if the flow is high enough. There are additional internal interlocks that require a minimum air flow of >85 SLM, a thermocouple located on the lower portion of the torch body that trips if the temperature exceeds a predetermined value, and an internal photodiode that is intended to trip if there is an arc failure, i.e. something blows up inside, to prevent further damage although it also trips if the power supply is in direct or reflected sunlight as it is able to reach the interior through vent holes and possibly the front panel or other gaps.

Other research was performed on the PlasmaFlux™ 1000, an earlier model built by AP Solutions Inc. with a supposed 1 kW power output and a more primitive torch design built from primarily stainless steel vacuum parts as shown in Figure 6-1. The main controls consist of a 0-10 dial for the power and an LCD output panel indicating the driving current. The device is owned by the Industrial and Systems Engineering Department at NCSU. This device will be referred to as PF1K. The torch is housed in a 2" diameter steel tube, the electrical power is supplied through a flat steel disk and is connected to the back end of the electrode assembly with a bolt through a ring crimp connector as shown in Figure 6-2. The electrode assembly consists of the HV wire connected to a metal rod that is isolated from the torch housing which is at electrical ground by a ceramic dielectric most likely Macor and a graphite nozzle is threaded into the other end of the metal rod. Air flow is supplied with a 1/8" tube that had been welded in a tangentially aligned through hole in the torch housing located near the tip of the nozzle providing a vortex flow. A conflate flange was bolted to the bottom of the torch housing with a threaded center hole serving as the mount for the nozzle which comprised of a tapered steel rod with a matching tapered hole machined through the center.

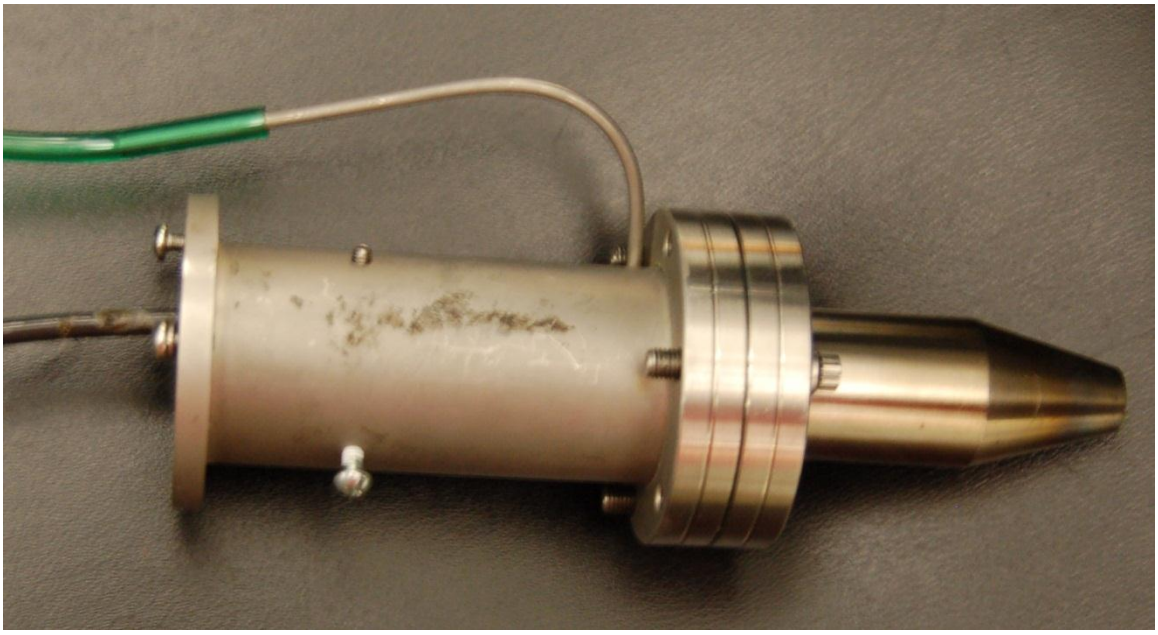

Figure 6-1: PlasmaFlux™ 1000 (PF1K) torch body.

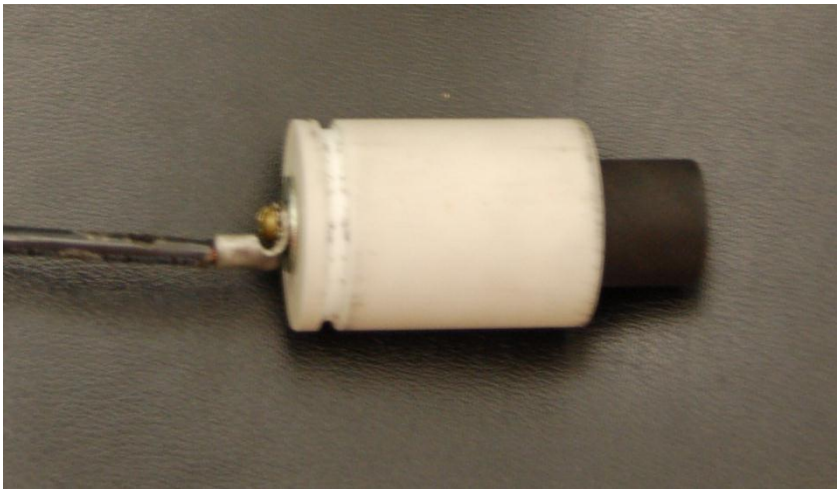

Figure 6-2: PF1K dielectric and electrode assembly

The other power supply unit used in this research was the AIR-DBD-5000 Plasma Power Supply that was originally intended for a dielectric barrier discharge (DBD) type plasma and has since been repurposed for AP-torch style research. The device has a usable frequency range of ~ 30-160 kHz. This device differs from the PlasmaFlux™ devices in that the step-up transformer is a separate exterior device. It is with this system that the 'in-house' designed plasma torches and devices were tested. This device will be referred to as the DBD-power supply. The 'in-house' plasma torch was dubbed the Plasma Vortex as diagramed in Figure 6-3, the side, front, and rear isometric views of the actual device shown in Figure 6-4, the electrode components in Figure 6-5, and the individual components in Figure 6-6.

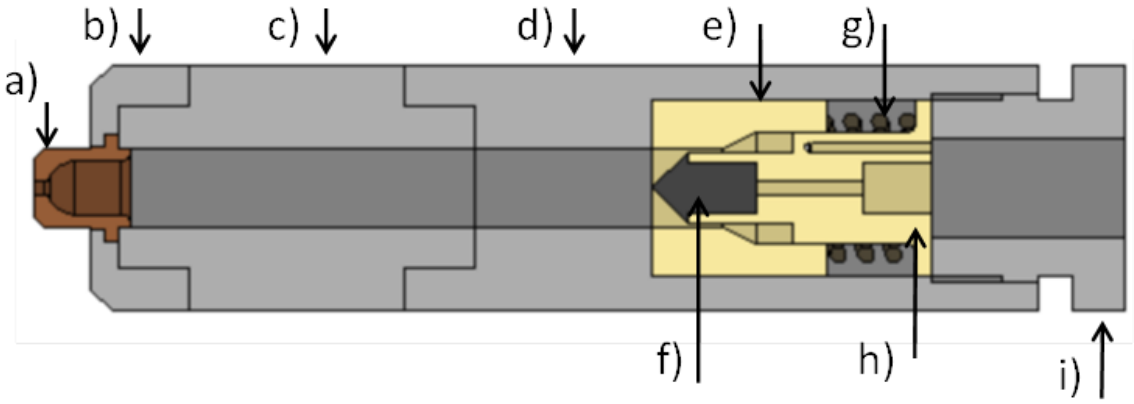

Figure 6-3: The Plasma Vortex torch with components of a) nozzle, b) nozzle retaining nut, c) barrel length extender, d) primary barrel, e) dielectric spacer, f) electrode, g) spring, h) dielectric electrod holder and gas delivery, and i) end cap

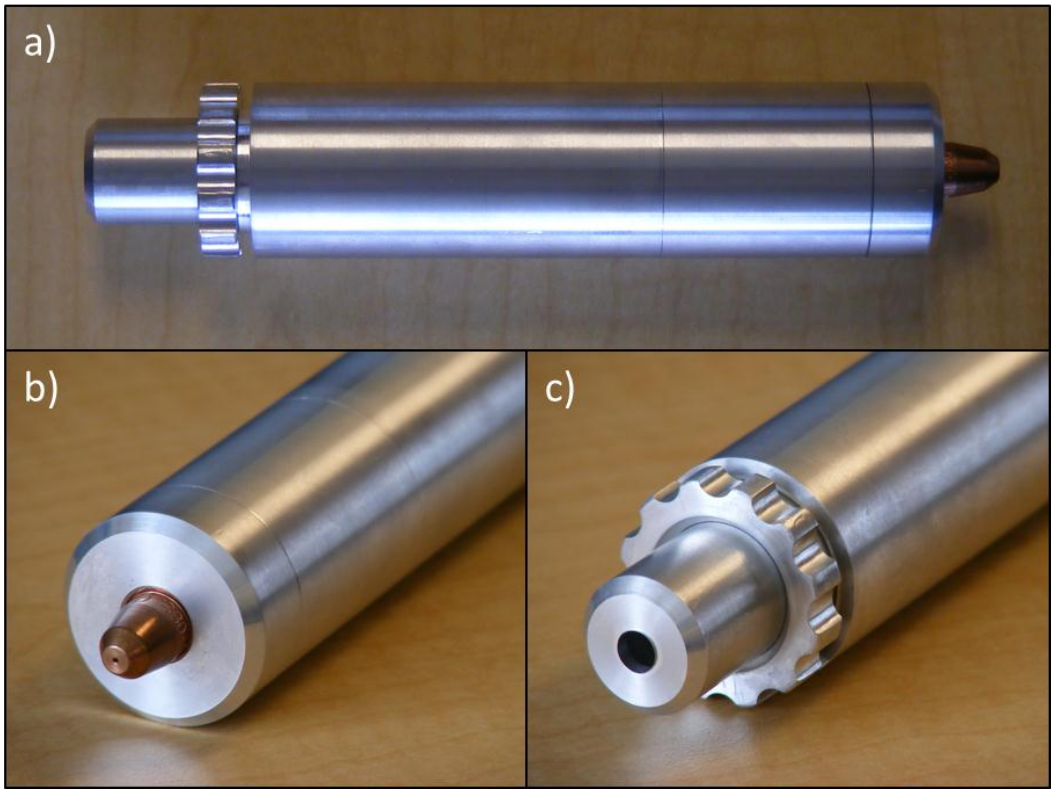

Figure 6-4: The Plasma Vortex shown in a) side view, b) front isometric, and c) the rear isometric view

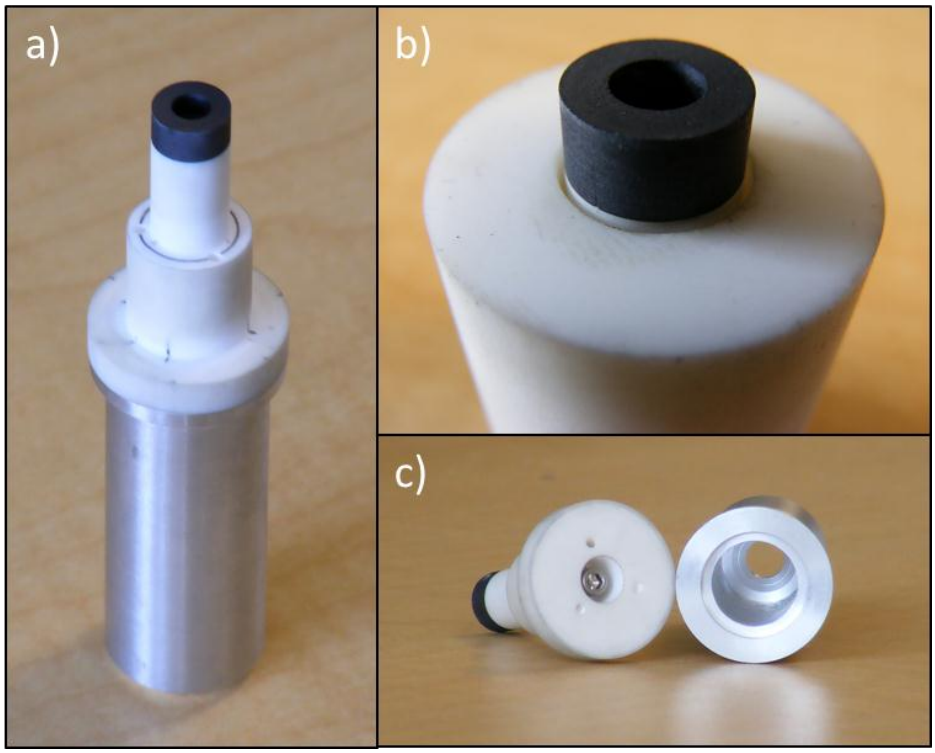

Figure 6-5: The assembled a) electrode components of the Plasma Vortex, b) a close up of the electrode and dielectric, and c) a separated view of the dielectric showing the three angled through holes for gas delivery.

Figure 6-6: The various components of the disassembled Plasma Vortex

6.2 Lab Equipment

Plasma treatment of various samples required consistent manipulation of either the torch or sample in several dimensions and time. Three dimensional positioning was controlled by a computer numeric control (CNC) machine the ShopBot Buddy model PRSstandard BT32, serial number 10-1560-SP38 manufactured by ShopBot Tools, Inc. It has a tool movement area of 25" x 33" x 7" in the lab convention of X, Y, and Z axis where X is front-to-back with positive direction to the rear, Y is left-to-right with positive direction to the left, and Z is vertical with positive direction toward the top. The maximum speed is 12"/s with a resolution of ~± 0.005 mm. The device includes the necessary power supplies, control boards, and computer interface. Simple changes in position can be controlled by directly entering values into the command console or through the arrow keys on a keyboard. More complicated positioning requirements such as raster patterns or treatment of complex shapes such as a helicopter rotor blade can be made using a programing language software supplied by ShopBot Tools, Inc.

The effectiveness of the plasma treatment on material removal was, unsurprisingly, based on the amount of the coating or material removed; however, for this type of application this type of measurement is not straightforward. One such method for determining this quantity is by calculating the volume of material removed. This technique is typically employed with vacuum plasmas, or other more uniform techniques, by measuring a step height between the untreated material and the treated material giving a etch rate in distance/time (e.g. μm/min). If a treated area is measured then the etch rate becomes a

volume rate (e.g. μm^3/min). Directly measuring these values, however, is a non-trivial task for coating or material removal with a this type of plasma torch as the treatment path, width, and depth is far from uniform and to get a close approximation the number of individual stylus scans would be prohibitively large, 3D scanning would also be impractical, and a coating thickness gauge largely ineffective in spatial resolution. Therefore, for simplicity and quicker data acquisition with a moderate level of precision, it was determined that measuring the mass removed could give a more accurate representation of the material removal by plasma treatment. Mass measurements were made using a balance from A&D Company Limited model GX-1000 serial number 50004 with a maximum capacity of 1,100 g and a resolution or minimum weighing value of 0.001 g as shown in Figure 6-7. When acquiring the mass of steel panels a plastic disk approximately 2" thick was placed on the weighing pan to limit any magnetic interactions, samples such as the HDPE panels were placed directly on the weighing pan as on page 8 of the User Manual it is mentioned that the "balance uses a strong magnet as part of the balance assembly".[143] The User Manual recommends, on page 7, that the balance be installed and operated away from equipment that either have or produce magnetic fields. This is an issue when the balance is used in an environment that has magnetic materials such as electric motors or equipment that produces electromagnetic interference such as the plasma torch and these interferences can significantly alter mass measurements.

Figure 6-7: A&D model GX-1000 balance
(http://www.andonline.com/weighing/products/details.php?catname=Balances&product_num=GX_Series)

The different plasma devices used in this research required a constant supply of gas for stable operation. Gas flow was controlled using a pair of mass flow controllers (MFC) manufactured by Advanced Energy model Aera® FC-7720C with a full-scale range of 35 to 200 SLM and a response time of < 3 sec to within ±2% of set point. An aside, the Aera® series MFCs were bought out by Hitachi shortly after the acquisition of the MFCs. The operation of these MFCs are controlled through a mass flow control unit (MFCU) manufactured by Advanced Energy model ROD-4A serial number R10/1021 that allows for digital control through a face mounted keypad and LCD panel or an optional computer interface be means of a RS-232 cable.

As the plasma consists of a highly energetic plume, the transfer of this energy in the form of heat to the substrates is an issue of concern and monitoring the substrate temperature was necessary. Direct contact measurements at multiple locations simultaneously were made

using a DATAQ® Instruments model DI-1000-TC-8 serial number 1324 with a built in RS-422 interface with USB adapter shown in Figure 6-8. This device is an 8-channel thermocouple (TC) data logger designed to work with type J, K, T, E, S, B, or R thermocouples. Temperature measurements were made with K-type TCs from OMEGA Engineering, Inc. model XCIB Series Style 3 that are 1 m long with Inconel 600® over-braided ceramic fiber insulation. K-Type TCs have a sensitivity of approximately 41 μV/^{o}C with a range of -200^{o}C to +1350 ^{o}C although the manufacturer specifications list the maximum temperature at 1090 ^{o}C. Style 3 is an exposed bead welded TC junction with an Inconel collar to clamp the probe to a surface or secure it into a hole as shown in Figure 6-9.

Figure 6-8: DATAQ Instrument model DI-1000-TC-8 (http://www.dataq.com/products/hardware/di1000tc.htm)

Figure 6-9: Thermocouple (http://www.omega.com/ppt/pptsc.asp?ref=XCIB)

Experiments that required data recording of various digital or analog singles were performed with a DATAQ® Instruments data logger model DI-710-UHS serial number 406BDAFA as shown in Figure 6-10. This device interfaces directly with a computer via USB cable and it has the capability to record directly to a SD memory card. It has a 14-bit measurement resolution with 16 analog input channels that can be configured for single ended or differential measurements and an 8-bit (8-channel) digital bi-directional port through screw terminal blocks. In PC operated mode, the acquisition rate can range from 0.048 Hz to 4,800 Hz for a measurement period of 20 seconds to 0.2 ms and in standalone mode it can range from 0.0017 Hz to 10,000 Hz or a period of 9.8 minutes to 0.1 ms. Each channel has a measurement range of ± 10 V over 4 gain ranges of either 1, 2, 4, & 8, with each channel input impedance of 1 MΩ and a maximum voltage of 30 V DC or peak AC. The device also has two channels that provide a + 5 V supply.

Figure 6-10: DATAQ Instrument model DI-710-UHS (http://www.dataq.com/products/hardware/di710.htm)

The coating thickness of as-delivered painted samples and lab-painted samples were determined using a gauge manufactured by ElectroPhysik model MiniTest 720 as shown in Figure 6-11. This device is a magnetic induction sensor with a measuring range of 0-2 mm (80 mils) with a minimum substrate thickness of 0.5 mm (20 mils) with an accuracy of ±1.5 µm (±0.06 mils) with a low range resolution of 0.1 µm (0.005 mils).

Figure 6-11: Coating thickness gauge (http://www.elektrophysikusa.com/sub/page.asp?page_id=38)

Electrical measurements were made using a high voltage (HV) probe manufactured by Tektronix model P6015A HV Probe. This type of HV probe has a 1000X attenuated

readout value and can measure up to 20 kV_{RMS} and pulses up to 40 kV for 100 ms duration, and a 3.0 pF compensation range. Current measurement were made with a Pearson™ Current Monitor model 4100 that has a sensitivity of 1V/A with an output resistance of 50 Ω and is capable of measuring a maximum peak current of 500 A and a maximum RMS current of 5 A. The probes were monitored with a Tektronix TDS5034 Digital Phosphor Oscilloscope serial number 200714, this model is discontinued.

Figure 6-12: Current probe (http://www.pearsonelectronics.com/products/current-monitors)

Instant non-contact point temperature measurements were made using a Fluke® IR Thermometer model 561 as shown in Figure 6-13. This device has a temperature range of -40 ^{o}C to 550^{o}C with a display accuracy of ±1.0% of reading or ±1^{o}C, whichever one is greater. Additional, thermal imaging was acquired using a FLIR® IR camera model SC5000 as shown in Figure 6-14.

Figure 6-13: Fluke IR (http://www.fluke.com/fluke/usen/thermometers/infrared-thermometers/fluke-561.htm?PID=56089&trck=561)

Figure 6-14: FLIR IR (http://www.flir.com/cs/emea/en/view/?id=42577)

Experiments that required the ambient environment to be controlled were performed in a glove box manufactured by Plas Labs model 830-ABC serial number 08101. Linear motion in the glovebox was achieved using a pneumatic slide manufactured by Tol-O-Matic Minneapolis, Mn model BC215 Band Cylinder with a 1.5" bore size and a maximum operating pressure of 100 psi. The slide is 22" in length, the range of the midpoint of the carriage is 14", with the carriage length is 5", and a 0.5" stopgap between the carriage and end of the slide on both ends. The velocity was calibrated at a constant pressure using the DATAQ system.

Exhaust handling was performed with a vacuum system from Oskar Environmental, Inc. model SPC-G3 serial number 83110 with specifications of 3 HP, 230 V, 60 Hz, 7.5 Amps, 3 phase, and 3450 RPM. The company later changed its name to Avani Environmental Intl., Inc. This device has a capacity of 1500 CFM with dual 6" diameter 10' articulating arms.

6.3 Optical Emission Spectroscopy

OES characterization of the various plasma devices was performed using several spectrometer configurations. A portion of the spectroscopic research was completed on a CCD based Ocean Optics 4-channel model S2000 serial number MC2J358 with an analog to digital converter model ADC1000-USB serial number ADUD 1263. The four separate channels are arranged in a master-slave configuration with each channel covering an effective range of 194.65-522.42 nm, 394.45-725.95 nm, 595.03-895.87 nm, and 794.53-1055.71 nm; however, the data are spliced together at the following ranges: 200-400 nm, 400-600 nm, 600-800 nm, and 800-1,100 nm. The given pixel resolution is 0.5 nm with a calculated FWHM of 0.72 nm from Figure 6-15 of the atomic oxygen triplet at 777.4 nm. Light is supplied to the channels through three bifurcated steel jacketed fiber optic cables ganged together such one fiber is split into two fibers each of which is then bifurcated into four total fibers. This assembly was acquired after the original fiber bundle that split directly from one fiber to four fibers had two of the separate fibers stop working, and it is a custom order that increased the cost and lead times significantly, hence the steel jacketed modular version. Control software used is the Ocean Optics developed SpectraSuite that allows for individual channel control over integration times, averages, smoothing, acquiring a

background spectrum, background subtraction, and other common features. This device is powered through the USB-data cable.

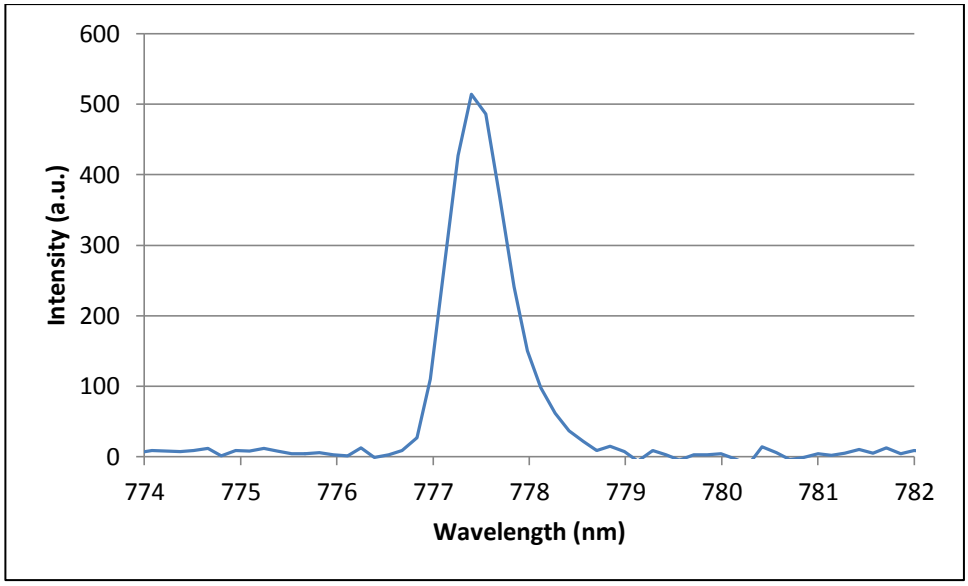

Figure 6-15: Spectra of the non-resolved atomic oxygen triplet

Broad band spectroscopy was also performed using the Ocean Optics 7-channel LIBS2000+ serial number LIBS A056 spectrometer that, from the model name, was originally developed for a LIBS system. Each channel has a range of about 100+ nm starting at 200 nm and going to ~1,000 nm with a given pixel resolution of 0.1 nm. This device is powered through an external power supply. The experimental light is supplied through a custom fiber optic cable that splits a single fiber into seven fibers that connect to the individual channels.

High resolution spectroscopy, for measurements that required rotational and vibrational levels to be resolved, was performed using a Czerny-Turner monochrometer outfitted with a photomultiplier tube (PMT). The device is a Princeton Instruments Acton SP2500 ½ meter Czerny-Turner monochromator with a 1200 g/mm grating blazed at 500 nm and operated with an entrance and exit slit width of 2 µm giving a FWHM resolution of 0.03 nm. The monochromator output is measured with a Hamamatsu H7546B-03 PMT. Monochromator and PMT settings were computer controlled via a Princeton Instruments SpectraHub USB controller with high voltage output and picoamp current measurement for PMT control and measurement. Alignment of the torch and optical setup was performed with a laser diode using a 600 µm diameter bifurcated fiber optic, allowing for frequent realignment without disassembly. The collimating lens attached to the acquisition side of the fiber resulted in a circular sample spot size of approximately 2 mm. The median of 5 scans with an integration time of 25 ms were used for data processing.

6.4 Analytical Equipment

The majority of the analytical work characterizing the plasma treated samples was performed at Duke University in the Shared Materials Instrumentation Facility (SMiF). This was done because, in general, the facility has better equipment available for a lower cost than what is available at the NCSU Advanced Instrumentation Facility (AIF). Specific equipment that was used to characterize the plasma treated samples includes:

- X-Ray Photoelectron Spectrometer (XPS) model Kratos Analytical Axis Ultra and data processing software used is CasaXPS located at SMiF.

- X-Ray Diffractometer (XRD) model Panalytical X'Pert PRO MRD HR X-Ray Diffraction System. X-Ray source is the Cu Kα (1.5405 Å) line located at SMiF.
- Scanning Electron Microscope (SEM) with Energy-Dispersive X-Ray Spectroscopy (EDS or EDX) located at SMiF, Model FEI XL30 ESEM with Bruker XFlash 4010 EDS Detector located at SMiF. The SEM has a resolution of 100 nm for high vacuum analysis. The Peltier cooled EDS is capable of detecting elements from Boron to Americium over an area of 10 mm^2.
- Surface profiles were obtained with a Zygo NewView 5000 that utilizes white light interferometry to produce 3D topographical representations of the surface and it is also located at SMiF. It can measure profile heights over a range of < 1 nm – 15 mm with < 1 nm resolution with a lateral resolution of < 1 μm. It is capable of single area acquisitions or automated image stitching can cover a larger area and has 2.5X, 10X, and 50X microscope objectives.

7 Materials

The paint systems used in the SERDP project are complex mixtures of several inorganic fillers and an intricate organic matrix binder. Initial experiments aimed at understanding the basic mechanisms of the plasma removal of the organic material were based on a simplified model substrate, thus minimizing complicating factors stemming from the fillers or complex chemistries. As such, an organic compound, high density polyethylene (HDPE), was chosen since it has a simplified composition of carbon and hydrogen in the approximate ratio of [CH_2]. The HDPE samples used in the removal experiments were obtained through two sources. Preliminary experiments were conducted with HDPE supplied by McMaster-Carr that were delivered as panels of ¼" x 4" x 48" size with a width tolerance of +1/16" and a thickness tolerance of ±0.013". The original supplier was King Plastic Corporation (www.kingplastic.com) with a manufacturer # 26487 and dimensions of ¼"x49"x97". These panels were cut into smaller test panels approximately 6" in length. Follow up experiments were performed using samples that had been made from 'scratch' starting with Hival™ PE HD 521054 NAT RESIN, acquired through Nexeo Solutions, with a melting point of 240^{o}C and a density of 0.906 g/cm^3 at 25 ^{o}C. This HDPE resin was then extruded by the Polymers Center of Excellence (PCE) and injection molded into ¼"x2"x3" samples. The extrusion process was completed using a Theysohn TSK 21 mm Twin Screw Extruder shown in Figure 7-1 and the injection molding was completed using a 165 ton Engel injection molding machine shown in Figure 7-2. The PCE is a 501-c6 not-for-profit organization that is partnered with NC State University and UNC-Charlotte and focuses on research, development, and training in the polymer industry. [144]

Figure 7-1: Twin screw extruded located at the Polymers Center of Excellence.

Figure 7-2: Engel injection molding machine located at the Polymers Center of Excellence.

As the primary focus of the SERDP WP-1762 project is to investigate plasma removal of paint, it was later determined that the possible effects of the inorganic fillers needed to be taken into account. In a similar fashion to the choice of using HDPE, TiO_2 was chosen as a model filler for its wide use as a paint filler and overall stability. The inorganic filler used in the HDPE loading experiments was Ti-Pure® R-960 manufactured by DuPont™ that has a minimum TiO_2 wt% of 89, alumina wt% of 3.3, amorphous silica wt% of 5.5, a median particle size of 0.5 µm. The reason for specifically going with Ti-Pure® R-960 is that it was cited in the MIL-DTL-24441/21A [37] detail specification sheet for the Formula 150 haze gray epoxy-polyimide paint.

In addition to determining the correlation between torch axial position and the effective removal rate, the next critical factor is the underlying removal mechanism(s). Experiments were conducted to elucidate the effect of oxygen on the removal process by diluting the air feed gas with nitrogen gas. These dilution experiments were conducted using N_2 acquired from Machine & Welding Supply Company. The product was under the 'Industrial Products' listing and cylinder tank part number AG NI300 with a volume of 300 ft^3 and a purity grade equal to or below Grade 0 nitrogen as it was significantly cheaper. Low purity nitrogen was used primarily due to significant quantities that would be required for operating the torch. A single 300 ft^3 tank would not even last 85 minutes with the torch operating at 100 SLM, without even considering the substantial amount of gas used in purging the glovebox. While the additional levels of purity to the tens of thousandths might be justifiable for some applications, such as the demanding nanometer-sized high purity applications; that level of purity is not justifiable at atmospheric pressure and the volumes required for operation of the plasma.

The experiments that were completed with coatings representative of the primary paint systems used by the US Navy were primarily International® brand distributed through Surfaceworx. Primer paints include Intergard 264 a red two part epoxy primer Part A sales reference is FPL 274/1GL MSDS reference is FPL274/P9 and Part B sales reference is FPA 327/1QT and the MSDS reference is FPA327/N9. This primer is mixed at A:4-B:1 by volume. Formula 150 Primer is a green two part epoxy primer both parts are Type III Part A sales reference is 5747/5GL with MSDS reference 5747/B2 and Part B sales reference is 5748/5GL with MSDS reference 5748/B0. This primer is mixed at A:2-B:1 by volume.

Topcoats include the red antifouling coating Interspeed 640 sales reference BRA640/5GL with MSDS reference BRA640 revision B3. It is described as a polishing antifouling with enhanced biocide release mechanism and is TBT free. The freeboard or haze gray topcoat is Interlac 665 alkyd finish sales reference CLA033/1GL with MSDS reference CLA033/B2 and the color is described on the can as "Base Deep". (AF: primer: Intergard 264 top coat Interspeed 640, FB: primer formula 150 top coat interlac 665)

The steel that was used as substrates for some of the test samples was of the variety DH36 commonly used in shipbuilding and are standardized by the American Bureau of Shipping and thus sometimes referred to as 'ABS steels'. DH36 is listed as a higher-strength ABS steel where the '36' grades have a yield strength of 51,000 psi (355 MPa) and an ultimate tensile strength of 71,000-90,000 psi (490-620 MPa) as opposed to the '32' grades with a yield strength of 45,000 psi (315 MPa) and an ultimate tensile strength of 64,000-85,000 psi (440-590 MPa). The initial ¼" x 4" x 6" DH36 panels were procured through internal means by NAVSEA. The panels used for the subsequent large area removal were acquired through Chapel Steel and were cut to ~ 3/8" x 24" x 36" and sand blasted to SSPC-SP 10 near-white finish. Twelve such panels were acquired.

Expanding foam used to seal the massive hole needed to pass the PF5K torch through was manufactured by DOW Chemical Company as "Great Stuff" Insulating Foam Sealant, Big Gap Fillers.

8 Experimental Methods

This chapter focuses on the methodology used in the experiments. There are three main groups of experimentation: 1) plasma based material removal, 2) plasma characterization, and 3) a catch-all that includes experiments that do not fall in to either previous category.

8.1 Plasma Material Removal

This section can be further divided into two main areas: 1) the primary focus of the SERDP project being coating removal of US Naval paints from ship grade steel substrates and the primary focus of the dissertation scientific research 2) is the investigation of the removal mechanism using HDPE as a substitute substrate.

8.1.1 Plasma Coating Removal

The SERDP project WP-1762 grew out of prior work done in conjunction with Vertical Lift Center of Excellence (VLCOE) on the removal of paint from aircraft frames as well as sealants. The SERDP WP-1762 project focusing on the two main paint systems employed by the US Navy: the freeboard (FB) and antifouling (AF) systems and the respective primers. For the purpose of the SERDP project a DOE was constructed early in the project by the NCSU partners and tasked to AP Solutions for completion. As an initial experiment it was intended to demonstrate the removal of these paint systems with a plasma device, determine the parameter space of the removal rates for the FB and AF paint systems, any differences between the two paint systems, and set the baseline of paint removal with a one plasma torch device that would be used for comparison during the later scale up efforts. The samples used in this experiment were the ¼" x 4" x 6" DH36 steel panels that were

acquired through NAVSEA and delivered with both FB and AF paint stacks already applied. When the samples arrived the coatings were still somewhat tacky and maintained a noticeable volatile organic compounds (VOC) odor. Due to the limited time frame of the project it was decided to accelerate the curing process in order to give test samples that would be more indicative of fully cured and aged paint. Panels were loaded onto racks made with 2" x 4" boards and placed in an oven over night at an elevated temperature. After the samples were dried the panels were delivered to AP Solutions for testing.

As the SERDP project continued the focus shifted to address the issue of scale-up, since the whole purpose of the project is to remove paint from capital ships. To achieve this transition from the lab to a field deployable device it was calculated that to reach removal rates comparable to grit blasting it would take approximately 14-18 plasma devices based on the PlasmaFlux design. This approximation was reached based on the assumption that a single plasma device could clear a 101.6 mm x 5 mm swatch (a single stripe on a 4" x 6" test panel) while traveling at 100 mm/s; however, a more realistic speed of 20 mm/s or slower results in 70+ plasma devices needed to match the rates of grit blasting. AP Solutions decided a step-wise approach is needed for scale up and employees a pre-existing rectangular 4 nozzle device with the nozzle arranged in a linear fashion, where each nozzle effluent was essentially the result of a separate torch that had been constructed in a large block of aluminum. However, the current model of power supplies can only operate two of the plasma torches at full power otherwise all four torches could be operated simultaneously but at reduced power. The scaled-up test samples were made from the DH36 steel purchased through Chapel Steel and grit blasted by A-1 Sandblasting out of Fuquay-Varina and the

appropriate paint systems were acquired through Surfaceworx. At the time of writing the dissertation this portion of the project was still in progress.

8.1.2 Plasma HDPE Removal

This section addresses the removal of HDPE by plasma treatment. The plasma removal can be divided into four subsections: 1) initial HDPE removal using commercial off the shelf (COTS) McMaster-Carr HDPE, 2) follow up removal experiments based on a parametric DOE with HDPE samples that were injection molded by PCE, 3) the HDPE loaded with TiO_2 compounded and injection molded by PCE and 4) other related plasma HDPE removal work that focused on determining the removal mechanism through gas mixing.

8.1.2.1 Initial HDPE Plasma Removal

The initial HDPE plasma removal was performed with the PF5K on the COTS HDPE from McMaster-Carr. The PF5K was operated at 100 kHz, 250 V, and 100 SLM air and the ¼" thick HDPE panels were cut to approximately 4" x 6". The plasma treatment consisted of rastering the plasma over the panels in a boustrophedonic method using the ShopBot Buddy™ at a velocity of 150 mm/s with an observed repeatability of $\pm$ 0.005 mm. The samples were individually massed using the W.B. Porter & Co., Inc. GX-1000 scale prior to treatment. After which a plasma treatment was administered for a given number of passes, for Z values of 2-20 mm 10 passes were used, for Z values of 20-25 mm 50 passes were used, and for Z = 30 mm 100 passes were used. The number of passes was chosen depending on the separation distance with the higher number of scans being used at farther distances in

order to obtain a more consistent and measureable mass difference. This was needed since at the farther separation distances the effective removal rate drops significantly such that a large number of passes were required to achieve a measurable mass difference. The samples were again massed, within approximately 15 seconds after the plasma treatment, to determine the final mass after plasma treatment. As a control the plasma torch was passed over a HDPE sample with the plasma off but with the air still flowing and showed no measureable mass loss clearly indicating that the plasma is responsible for the mass removal and not due to high velocity airflow. This set of experiments was performed as a function of Z to investigate the spatial relationship to removal, removal rates were obtained for Z-values of 2, 4, 6, 8, 10, 12, 14, 16, 18, 20, 22, 25, & 30 mm.

8.1.2.2 Parametric Plasma HDPE Removal

This set of experiments was performed to investigate the relationship between the driving parameters of the plasma and the removal rate. For this study the parameters that were manipulated were the operating frequency, power, and air flow. The HDPE samples used in this experiment were the 'neat' or non-loaded resin injection molded by PCE. The DOE for this study was designed with three factors being frequency, power, and air flow and for each factor there were three levels each covering a relative low, medium, and high value giving a total number of 27 unique parameter combinations. The levels for the frequency factor were: 95, 100, 110 kHz, power factor were: 225, 250, 275 V, and air flow factor were: 90, 100, 125 SLM. The low and high values represent the maximum range that the PF5K could operate with a stable plasma; while the medium values are the standard operating parameters used in several previous experiments and was chosen to hopefully minimize confusion between

various data sets if the exact middle values were used. In order to minimize any error due to drift in performance either from the plasma or analytical related equipment, the set of unique conditions was laid out in a factorial form and assigned a random value using an MS Excel 2010 spreadsheet random number generator function: "RAND()" which returns a random value 'x' such that $0 \leq x \geq 1$. The data set was then ranked according to the newly assigned random number using the function: "RANK()" in order from least to greatest value. The freshly shuffled list or ranked set was then given a number 1-27 as the sample ID # which then dictated the order in which the samples were tested. As this set of experiments was design to investigate the driving parameters, the separation distance between the torch and the substrate was not a design factor. However, for enhanced comparison to other data sets multiple Z values were used for each unique condition, 4 values of 10, 12, 14, & 16 mm were chosen. While this range did not have the highest removal rates as compared to the lower separation values, which are inherently of great interest to the various partners associated with the SERDP WP-1762 project, it was still chosen due it its relative invariance of removal rate with respect to Z compared to the smaller and larger Z ranges. This separation range is important to consider when small changes in the separation distance, between the torch and substrate, can arise mostly due to warping of the panels due to increased temperature as a result of plasma exposure. Being on the order of magnitude of ~ 1 mm, these small discrepancies in Z can lead to large variations in the effective removal rates for the close range of 2-10 mm and the farther range of 16-30 mm. This is also an issue that will need to be addressed as the technology transitions from a laboratory experiment to a field deployable device as the fluctuations in the thickness of paint on a ship returning from a 10 year stint

between repainting maintenance is going to be anything but uniform combined with the presence of biofouling and even the fact that as the thick coatings are removed the distance increases from the surface to the torch. Additionally, there were three replicate samples that were plasma treated at the same time for a given Z value. A typical set would consist of

1) setting the frequency, power, and flow to the prerequisite values
2) massing three HDPE samples and recording the values
3) placing the three samples on the stage and immobilized such that the plasma or air flow does not launch a sample from the stage
4) set the Z value to the appropriate value in the ShopBot program file
5) run the plasma treatment program and turn of the plasma torch when the program has been completed
6) remove and mass the samples recording the values
7) then repeat outlined numbers 2)-6) for the remaining Z values
8) repeat outlined numbers 1)-7) for each remaining unique parameter combinations

Each plasma treatment consisted of ShopBot parameters such that: velocity: 200 mm/s, Δx: 5 mm (the space between each subsequent pass), and the number of passes: 10.

8.1.2.3 HDPE-TiO_2 Loading Plasma Removal

This set of experiments was performed to investigate the relationship between inorganic fillers and the removal rate and the possible effects or ramifications it might have on the removal of more complex paints or coatings with substantial amounts of inorganic fillers present. The samples utilized were prepared by PCE and extruded with 0, 10, 20, 30,

40, 50, & 60 weight percent of DuPont Ti-Pure R960. The naming convention used with these samples is the inverse of filler wt.% and are described in HDPE wt. % such that the samples were identified as 100, 90, 80, 70, 60, 50, & 40 HDPE wt. % respectively. This was adopted after the samples received from PCE were labeled as such, which considering the primary focus of PCE is on the polymers it is not unexpected. The DOE consisted of two factors being the HDPE % and Z value with 7 and 12 levels respectively. The HDPE % levels were the previously stated values and the Z level covered a range from 2-24 mm at even values i.e. (2,4,…22,24) resulting in 84 unique combinations. The other plasma parameters remained constant at frequency: 100 kHz, power: 250 V, flow: 100 SLM, velocity: 200 mm/s, Δx: 5mm, and 10 passes. In a similar fashion as previously described the test matrix consisting of unique factor and level combinations was assigned a random number, sorted, and given a sequential sample ID # 1-84. The methodology used was straight forward: for each # the correct HDPE-TiO_2 samples were selected and appropriate Z value was entered into the ShopBot program, then each sample was massed individually with the value recorded, placed on a sample holder, that only immobilized one sample, plasma treated, and subsequently massed and recorded and repeated for each of the three replicate samples before moving onto a different #-ed combination.

8.1.2.4 Nitrogen Plasma

One of the innate aspects of the interaction of the atmospheric pressure air plasma torch with organic materials is the resulting removal; however elementary this phenomenon is; the mechanism is not well understood. It has been commonly postulated that the mechanism is simply chemical oxidation. The premise is that oxidizing species present in the plasma, such

as energetic metastable molecular and atomic oxygen species created from ionizing air, react with the organic components of the paint or coating producing CO_2 and H_2O. This pathway is summarized in the following generalized chemical equations:

$$O + [R - CH_2 - R] \rightarrow CO_2 + H_2O$$

or

$$O_2^* + [R - CH_2 - R] \rightarrow CO_2 + H_2O;$$

however, these reactions have never been confirmed nor substantiated with this plasma device or technology. As the mechanism for removal is the critical component of this technology applied to material or paint removal it is essential to investigate the possible mechanisms so that there is an understanding of the science behind the technology which can then be utilized to optimize devices and have more awareness of the capabilities, limitations, and hazards.

Therefore, experiments were conducted to examine the possible removal mechanisms. These sets of experiments focused on elucidating the contribution to removal due to the presence of oxygen and the validity of the chemical oxidation mechanism. This was achieved by altering the plasma feed gas as a method to control the active species that could be present in the plasma and possibly responsible for material removal.

The first experiment changed the plasma feed gas from solely compressed air to consist of just nitrogen delivered from a tank. As an initial attempt at gas modification the

experiment was completed under ambient open air conditions. The gas inlet to the PF5K was connected directly to a high pressure high volume regulator on a standard 300 CF nitrogen tank replacing the air supply. The torch setup and treatment of HDPE samples remained the same as the previous air-feed-gas experiments such that the torch was mounted to and controlled by the ShopBot with the discharge and panels exposed to the open air environment with sufficient exhaust handling capabilities. Operating parameters were similar to previous experiments: the ShopBot was set to a speed of 150 mm/s in the Y-direction across the width of the sample, a ΔX = 12 mm, X_i=10 mm denoting the position of the first pass with respect to the front edge of the sample, and 10 passes were used. The PF5K was set to a frequency of 100 kHz and power of 250 V and the nitrogen gas flow was set to 100 SLM to match the regular flow of air. The samples tested were six HDPE samples from McMaster-Carr and were treated at three torch heights of 4, 6, & 8 mm with two replicate samples at each given position. As described before the sample were massed prior to plasma treatment and promptly massed after treatment with the data recorded.

The next experiment was designed to investigate entrained oxygen into the nitrogen plasma plume from the surrounding air and could be contributing to the removal. Thus, a glovebox was modified allowing the torch to be confined within the walls and confines of the box. A feed-through setup had to be devised allowing transmission of power and gas flow to the torch through the solid walls or ceiling of the box. Due to the manufacturer covering the torch with heat-shrink material which prevented disconnecting the torch from the power line and the RF power line was terminated with the connectors inside the sealed power supply again preventing the device to be disconnected. This was a non-trivial issue since the outer

diameter of the torch assembly is roughly 1.5” compared to less than 0.5” for the insulated cable which could have been connected to a bulkhead style electrical connection. However, as it was not possible to separate the electrical connection from the torch, such that only a small hole would need to be drilled through the glovebox wall for an electrical bulkhead connector a much larger hole approximately 1.5”+ in diameter had to be drilled through the top of the glove box so that the entire torch plus the outcropping of the thermocouple could pass through. This now presents the problem of a massive hole with a significantly smaller cable passing through that needs to be sealed in order to maintain a controlled environment. Another through hole had to be drilled for the gas supply line to the torch as it was not fed through the previous torch hole as any gaps between the cable and sealant needed to be avoided. As a result of drilling this additional feed through, three cracks propagated from the hole which were subsequently covered in an epoxy on both internal and external faces to mitigate further crack growth and gas exchange. A 3/8” Swagelok bulkhead connector was screwed through the hole and bolted in place, further sealed using epoxy slathered between the bolt and glovebox wall prior to tightening. The 3/8” tube was reduced inside the glove box to the ¼” size tube accepted by the plasma torch. Initially, a pneumatic slide was operated using a line ‘T’-ed off from the torch gas supply; however, it was quickly noted that when the slide was actuated the plasma would invariably cut off presumably from a transient drop in pressure, even though the ‘fault’ light was not tripped. This was solved by a using a pre-existing feed through present in one of the sidewalls and assembling a bulkhead using plumbing fittings with various sized Swagelok adapters to take it from a 3/8” tube from the N_2 tank to a ¼” tube connected to a series of toggle valves located inside the glovebox that

manipulated the slide. A two axis position milling vice was affixed to the bottom of the glovebox using foam mounting tape. This held the pneumatic slide in place and allowed for sample to be advanced by changing the positioning screw so that multiple passes could be completed on the same sample over fresh untreated surface. The torch was held in place with a ring stand clamp with the base weighted down with steel plates in an attempt to minimize movement of the stand or torch. Additionally, the torch power cable exiting the top of the glovebox was held in place by another ring stand to prevent any damage to the foam sealant and subsequent loss of containment. A small mechanical pump was attached to one of the pre-existing exhaust valves to assist in controllably removing gas and moderating the internal pressure. Finally, the GX-1000 mass balance was placed in the back left corner so that mass measurements could be made promptly and without exposing sample to ambient air.

A relatively minor issue of the glovebox location proved to be a sizable one instead. It was located on a large metal table that also accommodated a sizeable milling machine, grinding wheels, and vice. Herein lays the problem the first attempt at plasma treating HDPE samples was complicated by the sample mass varying wildly by up to 0.100 mg between individual massing attempts. In one case a plasma treated sample appeared to have gained a substantial amount of mass compared to the initial untreated mass. After ruling out pressure, turbulent gas flow, and RFI from the torch, it was then determined that the location of balance was causing the variance in mass readings. This was due to the presence of large quantities of iron, steel, and magnets in electrical motors that could interact with the balance measuring system. The balance was relocated to the glove box load lock which is elevated off the surface of the table and the mass readings stabilized. A single reference sample of

HDPE from PCE was massed between each experimental sample that was tested to monitor if there was any drift of the balance.

This experiment used a batch of 6 HDPE samples from the PCE batch with no inorganic fillers present. Initially, the torch separation distance was set to 5 mm and the samples were all treated under this distance. Although by the end of the experiment, the distance had decreased to approximately 3 mm most likely due to some slippage in the clamps attaching the bar holding the torch to the vertical ring stand. As a consequence the effective Z values were adjusted from 5 mm to 5, 4, and 3 mm for the corresponding samples.

The intent of this experiment was to confirm the removal of HDPE by a nitrogen gas plasma. As the separation distance remained 'fixed' the number of passes for each sample was changed to gauge consistency and repeatability of removal. Values of 10, 15, and 20 passes were used and two replicate samples were treated at each given number of passes.

The PF5K was set to the standard frequency of 100 kHz and power of 250 V, while the gas flow was set to 95 SLM as this slightly lower flow rate produced a more stable plasma resulting in fewer 'blow-outs'. The methodology implemented with this set of experiments involved the mechanical pump operating throughout the plasma treatment process. Then, the gas flow was turned on using preset values of the MFC system and once the gas flow reached the targeted value and equilibrated the plasma was ignited. The plasma was monitored for a short period of time before sample treatment commenced in order to ensure it had stabilized as it would occasionally cut off unexpectedly and no 'fault' light

indication was activated. Once a stable plasma was confirmed, the pneumatic slide was activated by depressing a ¼" Swagelok toggle valve and the plasma was quickly turned off followed by the gas flow. The pneumatic slide holding the sample stage was advanced one turn of the vice positioning screw and the carriage was manual pulled back to the starting position. This process was repeated until the desired number of passes was reached. After that point the sample was removed from the sample holder and placed on the balance with the mass being recorded. The somewhat elaborate and complicated methodology was developed and necessary in order to maintain a pressure inside the glove box that would allow for the operator hands to be placed in the gloves and easily manipulate objects within the box thereafter.

Additional gas mixing experiments were performed using the glovebox, that investigated the plasma HDPE removal as a function of oxygen content in the feed gas. The oxygen concentration was controlled by admixing a flow of N_2 gas to the compressed air flow. Each gas supply was controlled by a separate MFC and combined using a 'T' connector prior to entering the PF5K power supply. The nitrogen concentration was metered such that the concentration relative to oxygen doubled for each condition. The total flow rate was maintained at 100 SLM with a ratio of N_2:Air flows in SLM being 0:100, 50:50, 75:25, and 90:10. These flow ratios resulted in $[N_2]$:$[O_2]$ by volume % of 4.1, 9.36, 19.89, and 51.47. The only reason 100% N_2 was not used in this set of experiments was that the plasma failed to remain ignited under 100% N_2 flow. After depressing the 'ON' button the plasma would ignite but would instantly extinguish once the 'ON' button was released. The flow was varied over the range of 90-105 SLM to no avail. The other main difference compared

to the previous nitrogen glovebox work is that the sample motion was controlled by attaching the sample to bar rotated by a motor. The average sample speed was calculated using a stopwatch and treating the samples a total of 20 times.

8.2 Plasma Characterization

The effects of the plasma on various materials and the innate capacity for material removal has been the main focus of the SERDP project WP-1762 and prior work associated with this plasma technology and have been well studies. The characterization of solely the plasma has not been as rigorous or detailed by comparison. As one of the main goals of the work associated with this dissertation has been to investigate the driving forces behind the removal process, a comprehensive analysis of the plasma was required.

8.2.1 Optical Emission Spectroscopy

The analytical technique OES was implemented in the characterization of the various plasma devices utilized in this dissertation as an effective non-perturbing method capable of identifying the presence of excited species within the plasma. This data contributes to the overall understanding of the nature of the plasma and can be related to the effects of removal inferring interaction relationships between the plasma and materials.

8.2.1.1 Rotational Temperature

The optical emission spectra of a plasma can be analyzed to discern several important properties of the discharge. One such property is the gas rotational temperature that can be measured based on the relative emission intensities of two rotational bands of nitrogen. Identifying the rotational temperature allows for a comparison to the removal rates to

determine if this is a significant contributor to the predominant removal mechanism(s) and will enable optimization of the plasma device to maximize removal of organic materials. The experiments investigated the rotational temperature of the predominant gas present in the plasma, nitrogen, at various axial positions of the plasma torch. In order to make these measurements light emission from the plume of the plasma torch was measured with a standard high resolution optical emission spectroscopy system as shown in Figure 8-1. A Princeton Instruments Acton SP2500 ½ meter Czerny-Turner monochromator with a 1200 g/mm grating blazed at 500 nm and operated with an entrance and exit slit width of 2 µm giving a FWHM resolution of 0.03 nm is used to separate the light into spectral components. The monochromator output is a Hamamatsu H7546B-03 PMT. Monochromator and PMT settings were computer controlled via a Princeton Instruments SpectraHub USB controller with high voltage output and picoamp current measurement for PMT control and measurement. Torch alignment was performed with a laser diode using a 600 µm diameter bifurcated fiber optic allowing for frequent realignment without disassembly and a sample spot size giving a spatial resolution of approximately 2 mm. The median of 5 scans with an integration time of 25 ms were used for data processing.

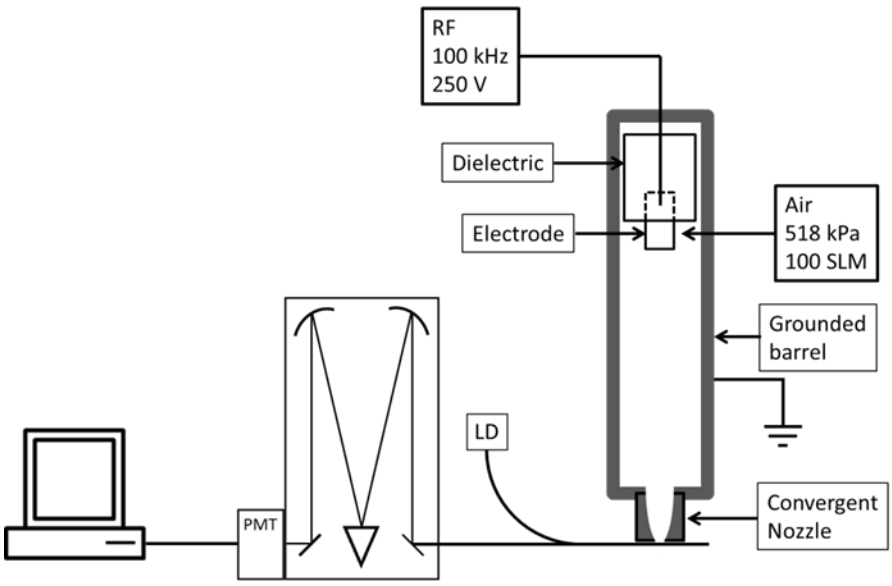

Figure 8-1: The plasma torch is constructed out of an electrically grounded metal tube with a convergent nozzle at one end and a driven electrode isolated by a ceramic dielectric at the other end. Power is supplied to the driven electrode at 100 kHz and 250 V, air is supplied at a rate of 100 SLM at 518 kPa in such a manner as to form a vortex. The optical setup consists of a 600 µm diameter bifurcated fiber optic with one leg connected to a laser diode (LD) for alignment and the other end connects to the monochromator where the signal is generated by a photomultiplier tube (PMT) with the output going to a computer.

8.2.1.2 Preliminary Spatial Broadband OES

This section covers several experiments conducted to investigate the presence of plasma species across the UV/VIS/NIR (200-1,000 nm wavelength) range of the light spectrum. This type of analysis provides a much broader and encompassing view of the spectrum with significantly quicker acquisition times, on the order of milliseconds, as compared to the slower rastering speeds of the monochromator but at the penalty of lower resolution of ~0.75 nm compared to <0.05 nm for the monochromator setup. The fairly rapid

spectra acquisition over a large wavelength range allows for spatial profiles to be developed which provide insight into the evolution of plasma species as a function of time and/or space.

8.2.1.3 Detailed Spatial Broadband OES

Refined spatial OES experiments were conducted at the request of the dissertation Committee following the preliminary exam in order to achieve a higher spatial resolution. The experiments were performed using the 4 channel S2000 Ocean Optics Spectrometer on the PF5K. The first attempt at higher spatial resolution OES was mostly unsuccessful due to practical and physical limitations of the plasma and optical equipment. The initial design consisted of two apertures separated by 8" and housed in an aluminum tube. The apertures were a pair 100 μm diameter pinholes and a pair of 100 μm x 3 mm slits acquired through Thorlabs, Inc. At these length scales the spatial resolution became diffraction limited as each aperture essentially acted as a single-slit diffraction setup; this posed a dual set of issues. First, the actual area that was resolved be far larger than the area of the 100 μm slits or pinholes. Secondly, the diffraction would decrease the amount of light entering the fiber and ultimately reaching the detector by a factor of 1×10^{-3} for the slits and 1×10^{-6} for the pinholes. While this decrease in intensity probably would not be an issue for highly sensitive spectrometers, the Ocean Optics spectrometer would not be capable of registering a noticeable signal compared to the noise. Even using a single slit, the attenuation would approximately be a factor of 0.04 which on the 4,000 count scale the output would only register a signal of ~160 counts that is comparable to the observed noise level.

The optical setup was revised by sacrificing spatial resolution to gain signal intensity. Instead of a double slit or pinhole collimation design an Ocean Optics Gershun Tube field of view collimation device was incorporated into the setup. This device utilized a single disk with a pinhole of diameter 1 mm held in place and centered in line with respect to the fiber by a short tubular coupler. It was designed to produce a 1^{o} angle field of view for the fiber that resulted in a sample spot size of 1.35 mm in diameter at the separation distance the plasma would be characterized. This spot size was confirmed by shining a laser through the fiber and out the pinhole onto a ruler. While the sample area is obviously larger size than the 100 μm apertures, it still produces a 5x reduction in sample area compared to the 3 mm diameter collimation lens used in the preliminary work; 1.43 mm^2 compared to 7.07 mm^2 respectively and is still a significant improvement. The integration time and number of averages were adjusted for each of the four channels at each spatial location that spectra were acquired. The values for these parameters were normalized to 5 seconds such that the total acquisition time was the same for each channel, e.g. a channel with a 10 ms integration time and 500 averages would have the same acquisition time as a channel with a 500 ms integration time and 10 averages. A radial profile was acquired at Z=0 mm over a radial range from -3.0 to 3.5 mm with 0.0 mm being the physical center point with respect to the nozzle and spectra were taken in 0.5 mm steps. Further radial profiles were obtained at axial positions from 1-5 mm in 1 mm steps and the radial range from -3.0 to 3.0 mm also in 1 mm steps.

8.2.2 Thermal

Thermal measurements were made of the plasma and of steel substrates during plasma treatment to measure the heating effect of the plasma on the substrate to monitor the possibility of thermal damage. Direct measurements of the plasma were made by inserting a TC into the center of the discharge at axial positions of 20, 30, and 40 mm from the nozzle and recorded as a function of time using the DATAQ DI-1000-TC-8. The justification for choosing axial positions this far away from the nozzle is that at any appreciable distance closer the TCs and/or the measuring equipment experience strong interference from the high potential and current contained in the primary arc. Indirect measurements of the plasma heating capability were performed on the ¼"x4"x6" DH36 steel panels. As to avoid interfering with the torch or plasma impinging on the surface 5 TCs were placed in contact with the backside of the panel and aligned the length of the panel. The plasma torch was centered on the sample in the width and length directions creating a relative coordinate origin such that the TC locations on the opposing side of the sample were at -75, -25, 0, +25, & +75 mm centered along the length of the sample.

8.2.3 Electrical

As the plasma torch is an electrical discharge, characterization of the voltage and current delivered to the torch provides valuable information that can be used to identify and at least provide rough values for certain plasma parameters, such as power density and electron density that could then be compared to the removal data or OES data. However, as described previously the PF5K is not accessible for electrical measurements and as such a

limited number of measurements were made on the torch constructed by NCSU and powered by the DBD power supply in order to obtain general information.

8.3 Additional Experiments

This section covers any additional experiments that warrant a brief mention but perhaps not fully investigated or directly related to the main goals of the dissertation and are found in appendix #5.

8.3.1 Plasma Interaction with DH36 Steel Surface

Following the In-Progress-Review in the spring of 2011, the SERDP review committee raised a valid question that centered on the reason the samples, which had coatings removed with the plasma torch, were a darker shade of gray compared to the 'near-white' surface generated with grit blasting. In order to answer this question samples were prepared from cutting grit blasted DH36 steel samples into test samples approximately 1cm x 1cm in size. These test samples were then plasma treated under conditions similar to ones used in the paint removal experiments and then characterized. Additional analysis was made of painted samples that had been treated with the plasma torch down to bare metal to characterize the surface roughness and possible contamination. The samples used were full size ¼"x4"x6" that had been plasma treated and then cut into smaller samples approximately 1cm x 1cm in size so that the samples could loaded into the XPS and SEM analytical machines.

8.3.2 Plasma Acid and Calorimeter

The thermal output of the plasma torch was investigated using in a similar approach to a standard calorimeter setup. The exhaust of the plasma torch was placed underwater in a thermally isolated system so an assumption could be made that the thermal energy of the torch was transferred to the water and not conducted away through the container. Given the initial and final water temperature and the heat capacity, an effective value of power could be calculated. Following a conversation with Dr. Cuomo regarding the experimental setup, it was determined that the pH of the water needed to be monitored during the same set of experiments to determine if the exposure of the plasma discharge into the water caused any chemical changes. The initial work was completed using the PF1K. A 1 L glass beaker was filled with 250 mL of DI water, as determined by mass, which was placed on a thermally insulating block (wooden 2"x4"). The nozzle of the torch was submerged with an air flow resulting in a line pressure of 10 psi. Then a plasma was ignited at a power setting of 5.0 resulting in 118 V and 7.4 A electrical input being displayed by the power supply. The temperature was measured using a submerged thermocouple with care taken that it was not in contact with the beaker wall, torch body, or near the discharge volume. The plasma was left on for a predetermined amount of time, after which the pH was promptly measured using a pH probe and the tarred beaker was massed to determine any water loss due to splatter or evaporation. This process was repeated several times for differing lengths of time: 5, 10, 15, 20, 30, 45, 60, 90, & 120 seconds to identify the evolution of pH and temperature with time. A follow-up experiment was briefly attempted with the PF5K; however, the required flow

rates splashed considerable amounts of water out of the container, in this case a 5 gallon bucket and the water measurements would not have been accurate.

8.3.3 Coating thickness

The coating thicknesses of the FB and AF 4”x6” panels and the 2’x3’ panels were made using the coating thickness gauge.

8.3.4 Pneumatic Slide Speed Verification

The nitrogen plasma removal of HDPE performed in the glovebox under inert nitrogen atmosphere required the speed of the pneumatic slide to be verified such that mass removal could be converted to a reliable removal rate. In order to obtain a valid speed several methods were attempted. The first approach was to film the slide operation with a digital home-video type camera with an analog stopwatch present but due to the limited frame rate of the camera there were only about 4 frames of the carriage in the appropriate range and the stopwatch did not have the resolution to make any accurate time estimates, this method gave speeds of 100-1,000 mm/s. The next approach was essentially a photogate where there is a light source on one side and a receiver on the other, in this case an IR LED and compatible receiver, and the slide would interrupt the light path causing a change in output signal. However, the approach was not able to produce a functioning device with a high enough response. The final and successful approach made use of a simple mechanical switch and the DATAQ™ DI-710-UHS, the circuit diagram and layout is shown in Figure 8-2. The switch has a metal spring lever attached to one side of the switch with a roller attached to the free end of the lever; it has three connector leads that are normally closed,

normally open, and common. In Figure 8-2 the leads are arranged such that the non-used lead is the normally closed lead and the lead going to channel 1 is the normally open lead and the lead going to the + 5 V port is the common lead. The switch was attached with two through screws to an OEM mounting bracket that was then with a DIM adapter plate of Al 1/8" x 1 ½" x 3" was attached to a short 2" piece of 80/20 which was then connected to the torch using a hose clamp. It was mounted such that the lever faced downwards so that when the HDPE sample passed underneath the torch it would depress the lever activating the switch and then when the sample had passed the torch the lever would relax deactivating the switch. The data output displayed as voltage across time with it nominally 0 V with the switch open and + 5 V while the switch was closed.

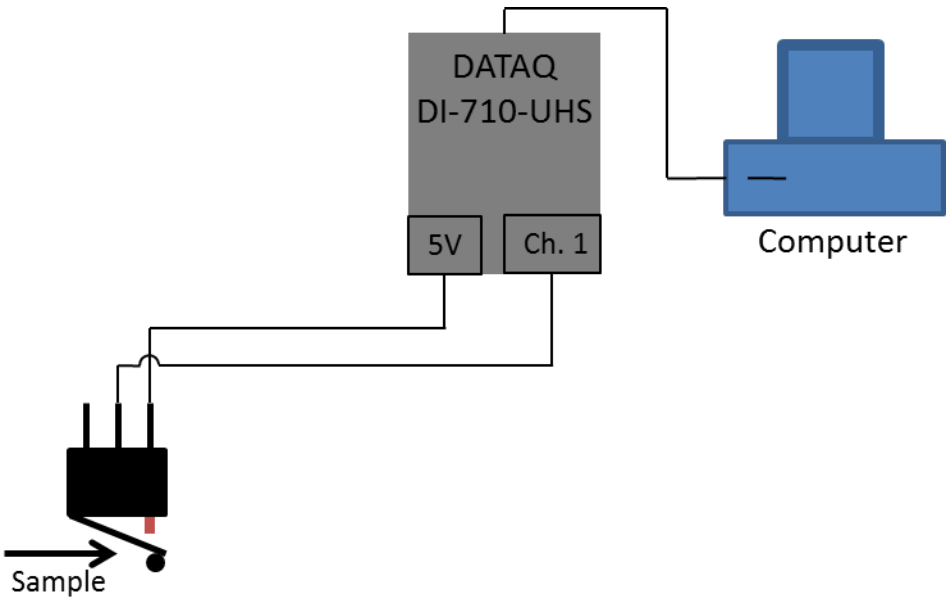

Figure 8-2: Circuit diagram for switching mechanism.

9 Plasma Material Removal Results

9.1 Plasma Coating Removal

The central composite design (CCD) DOE was arranged to investigate several of the factors that the SERDP team believed to be critical to the removal rate. From this set of experiments it was determined that although there does not appear to be a significant relationship between the thickness of the paint and the removal rate, the JMP software was able to illicit a positive correlation. The CCD was formed with 5 process parameters with low and high values: temperature 0:42 ^{o}C, speed 30:100 mm/s, air flow 95:135 SLM, plasma torch angle with respect to substrate -30:+30^{o}, and plasma torch height from substrate 2:4.5 mm and the included center and axial points. The analysis employed was a response surface model using a Least Squares Analysis to determine the statistically significant factors affecting the average mass removal.

The average mass removed response surface can be seen in Figure 9-1. The average removal rate response surfaces for the different factors can be seen in Figure 9-2.[†]

[†] This information was obtained through the course of the SERDP WP-1762 project and has appeared in varying degree in several reports.

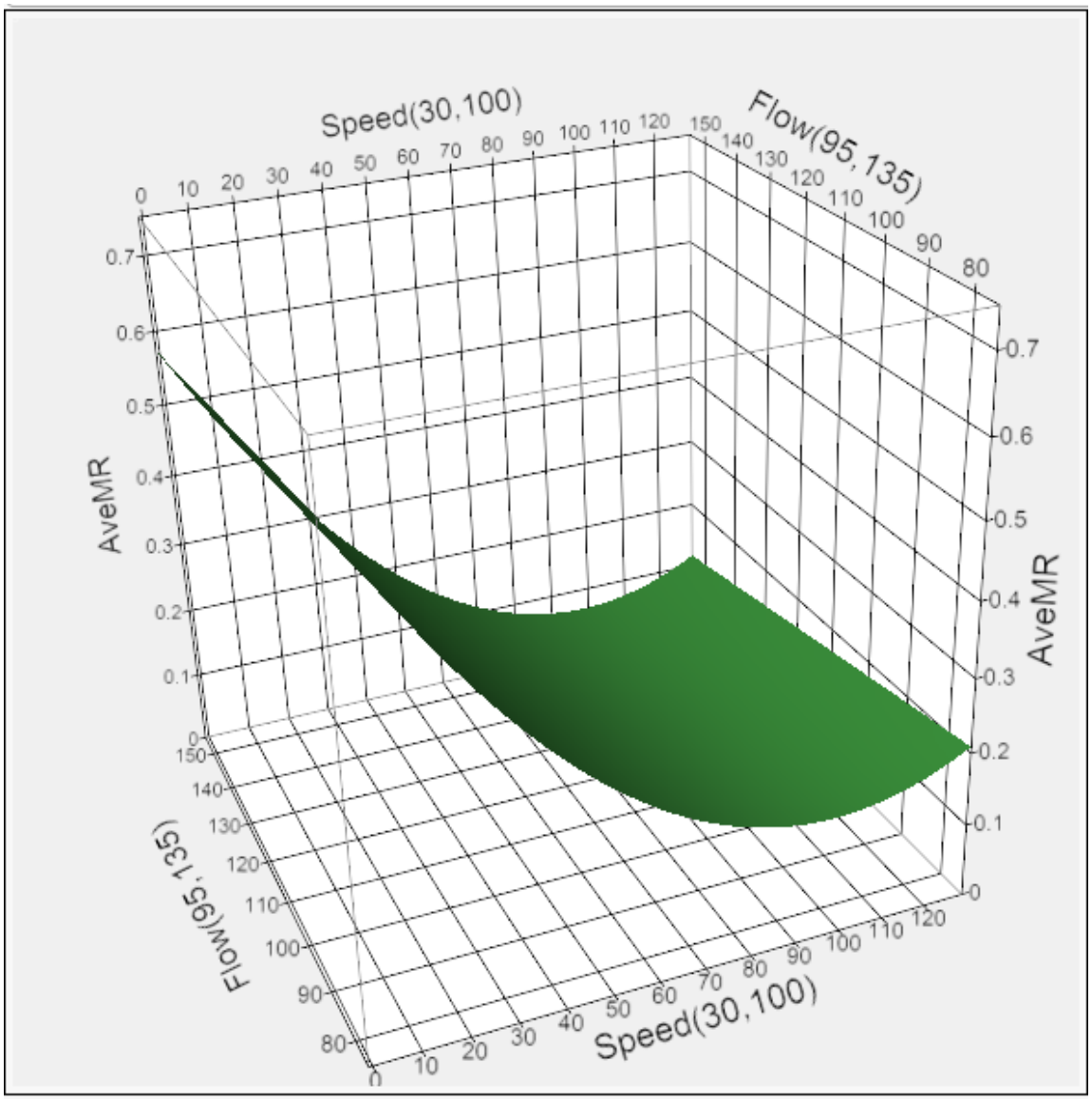

Figure 9-1: Response surface showing there is a speed quadratic effect that is most influential in this process for mass removal

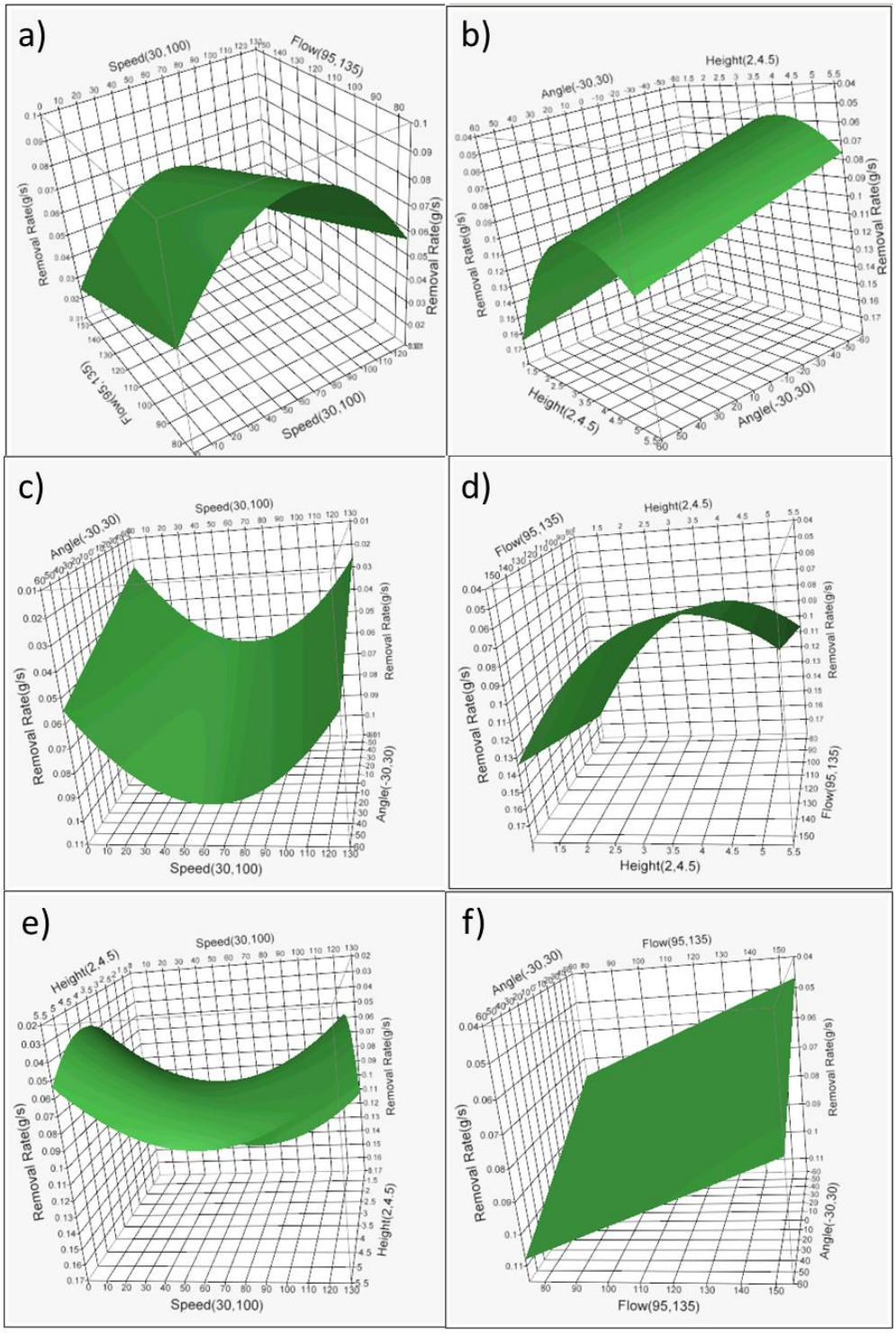

Figure 9-2: The removal rate g/s response surfaces for the factors a) speed and flow, b) height and angle, c) angle and speed, d) flow and height, e) height and speed, and f) angle and flow.

9.2 Initial Plasma HDPE Removal

The tabulated data for the mass removal is given in Appendix # 1 and graphed in Figure 9-3. This shows a strong correlation with a negative relationship between the axial separation distance of the torch and sample and the removal rate.

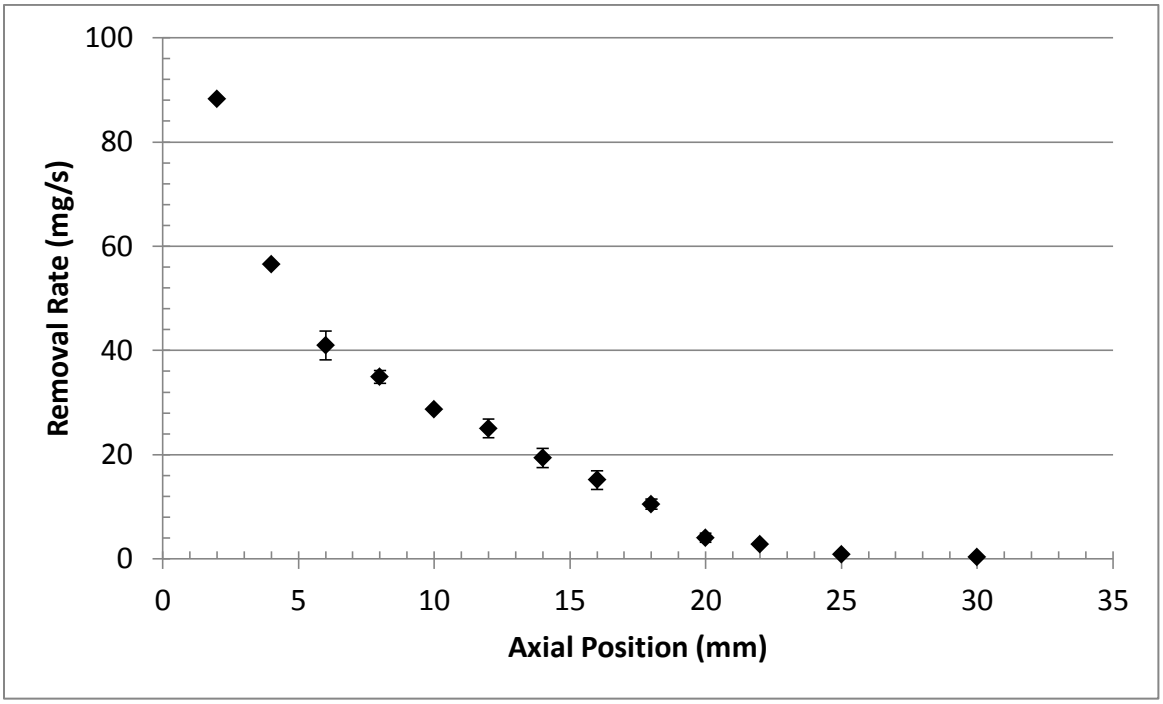

Figure 9-3: The removal rate of COTS HDPE from McMaster-Carr with the PF5K plotted against axial position.

9.3 Parametric Plasma HDPE Removal

The parametric study of the plasma removal of the PCE-HDPE determined the removal as a function of frequency, power, and air flow. The tabulated data is given in Appendix # 2.

The removal rate is plotted as a function of frequency and power for the three air flow values in Figure 9-4. The removal rate is plotted as a function of frequency and air flow in Figure 9-5 for the three power values. The removal rate is plotted as a function of power and flow in Figure 9-6 for the three frequency values.

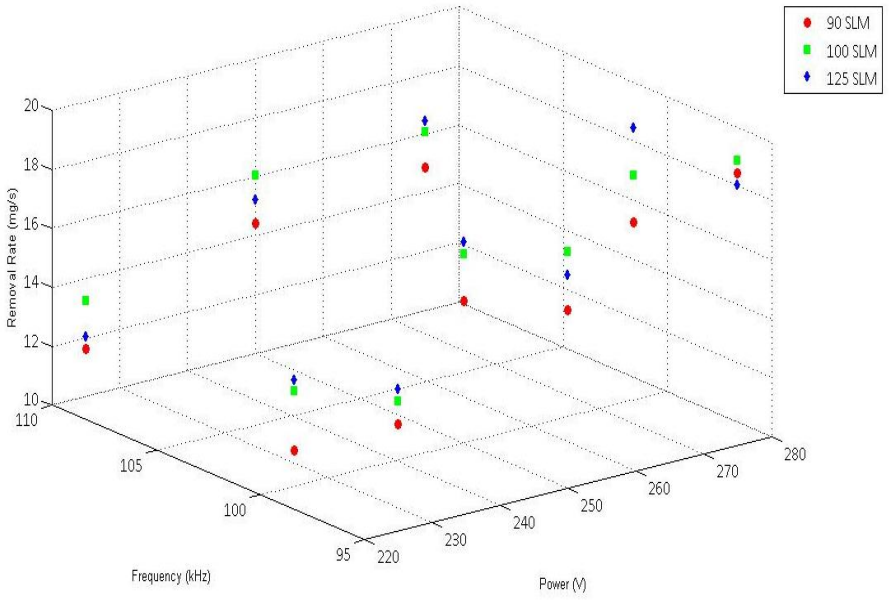

Figure 9-4: Removal rate of PCE-HDPE as a function of frequency and power for the three different flows of 90, 100, & 125 SLM

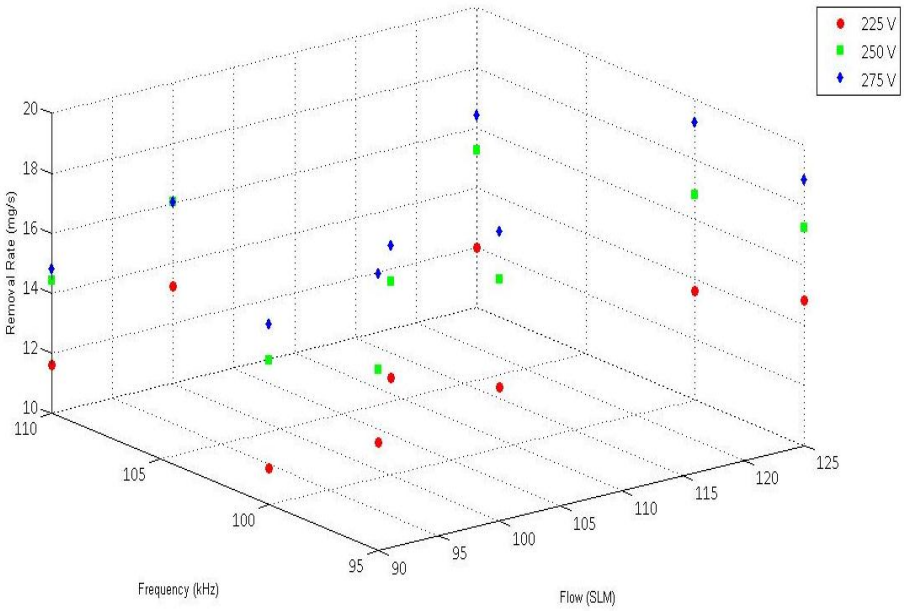

Figure 9-5: Removal rate of PCE-HDPE as a function of frequency and flow for the three different powers of 225, 250, & 275 V

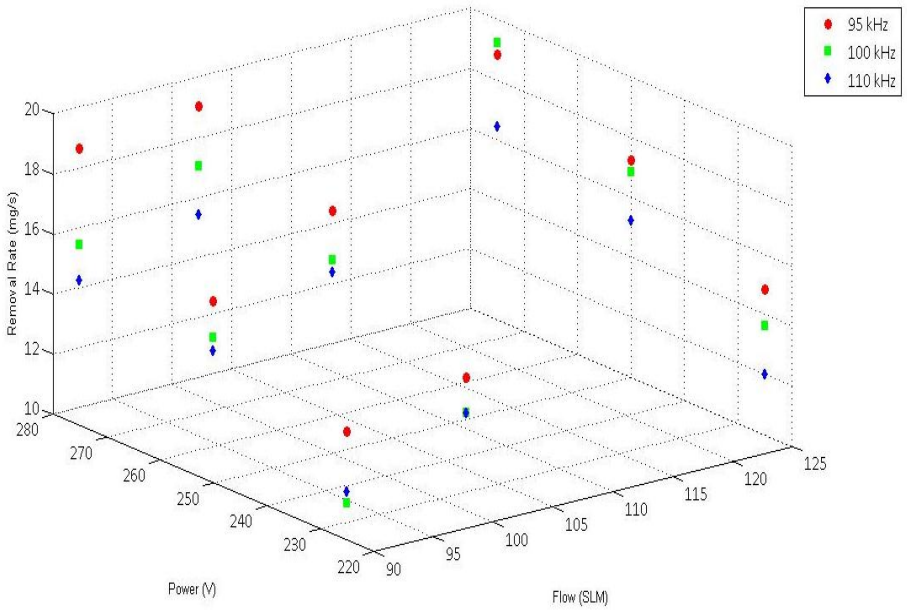

Figure 9-6: Removal rate of PCE-HDPE as a function of power and flow for the three different frequencies of 95, 100, & 110 kHz

9.4 HDPE-TiO_2 Loading Plasma Removal

The removal rate of HDPE loaded with varying concentrations of inorganic fillers as a simulation of actual paint systems is tabulated in Appendix #3 and shown in Figure 9-7. This seemingly indicates, at first glance, relatively similar removal rates for the various HDPE percentages across the axial range. There is, as expected, a higher variability in the removal rates at the closer axial positions due to the variability of the torch discharge and the sensititvity of the removal rates on small changes in Z. The removal rate series for a reduced number of HDPE percentages, for clarity, are graphed on a log scale in Figure 9-8 in order to show that the lower removal rates do not just flatten out but continue to decrease significantly with increasing axial position. The mass removal rate is plotted against the

HDPE concentrations for several fixed axial positions in Figure 9-9 showing relativly little change in the mass removal rate at a given axial position over the range of HDPE concentrations. The mass removal rates have been adjusted to a volume removal rate given the sample mass and avearage measured volume for each HDPE concentration tabulated in Appendix # 4. The volumetric removal rates are plotted against the HDPE concentration as shown in Figure 9-10 for the same fixed axial positions as in Figure 9-9. This data indicates a decreasing trend in volume removal rate with respect to increasing the amount of inorganic filler. Overall it appears that the mere presence of inorganic fillers in the matrix does not significantly alte the removal rates of organic polymers. It should be noted that the extrusion of the HDPE and inorganic fillers by PCE was just that, there were no surfactants, binders, or other additives that might increase the bonding between the matrix and filler.

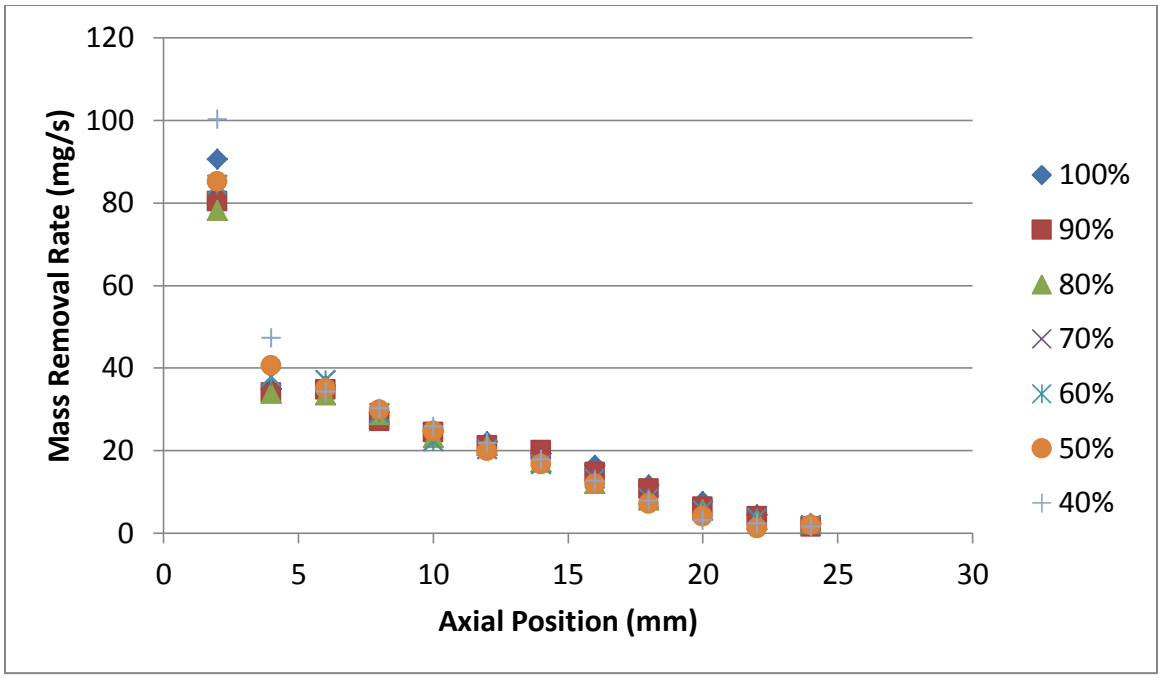

Figure 9-7: Removal rate of HDPE samples plotted against axial position for 7 different loadings given in HDPE wt. concentrations.

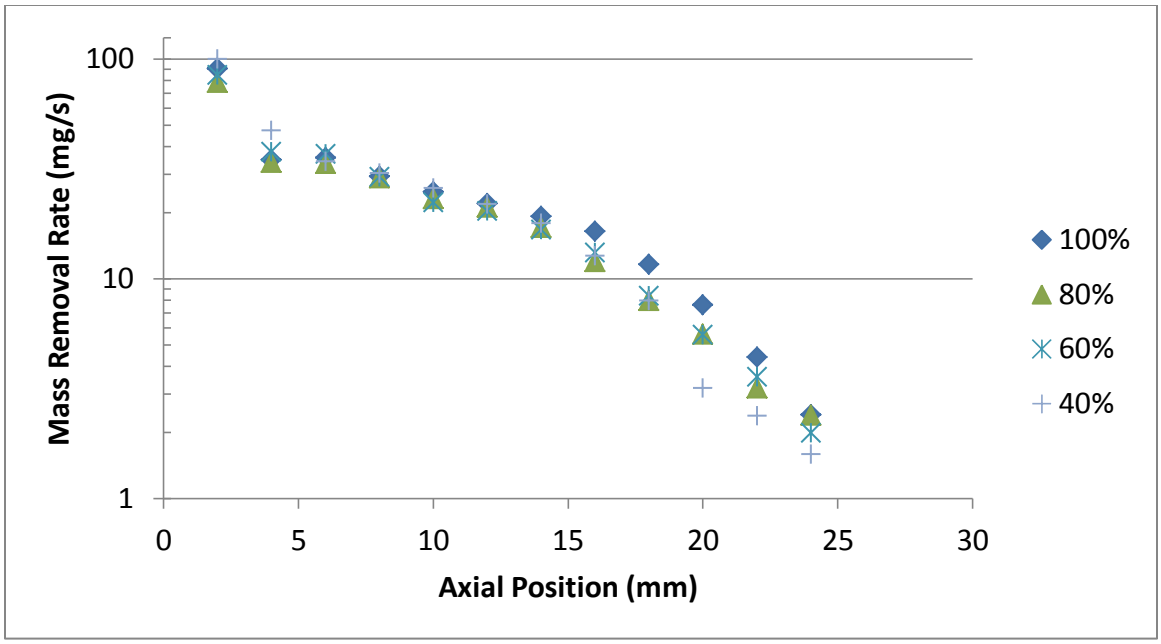

Figure 9-8: The log of the removal rate plotted against axial position

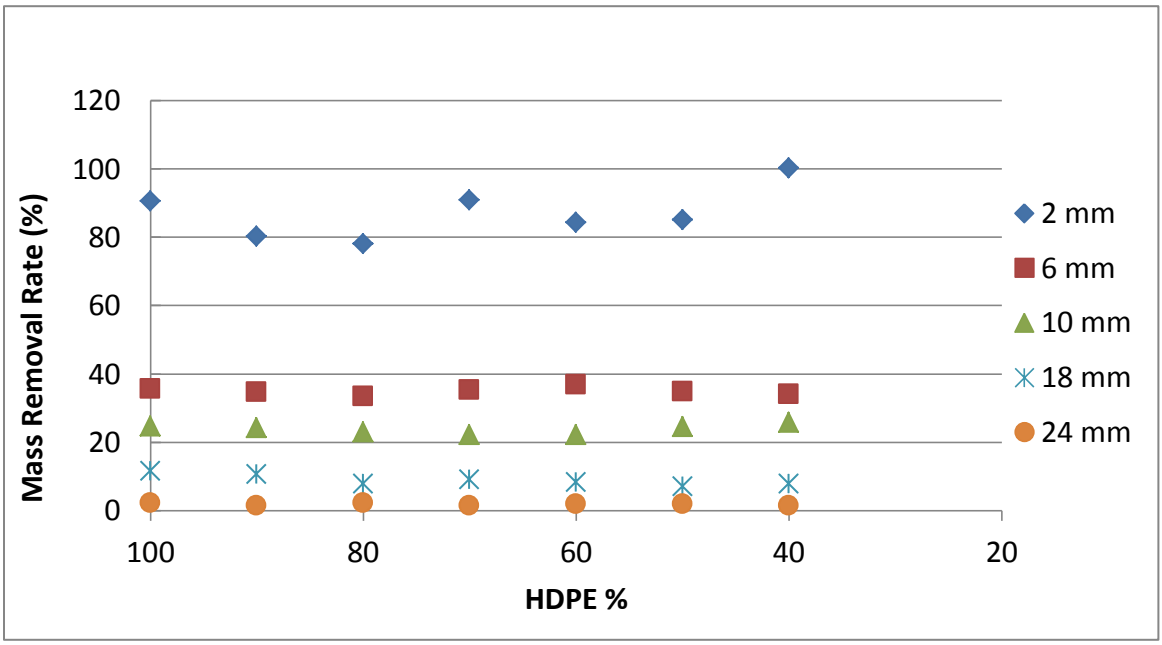

Figure 9-9: Removal rate plotted against HDPE % for several axial positions

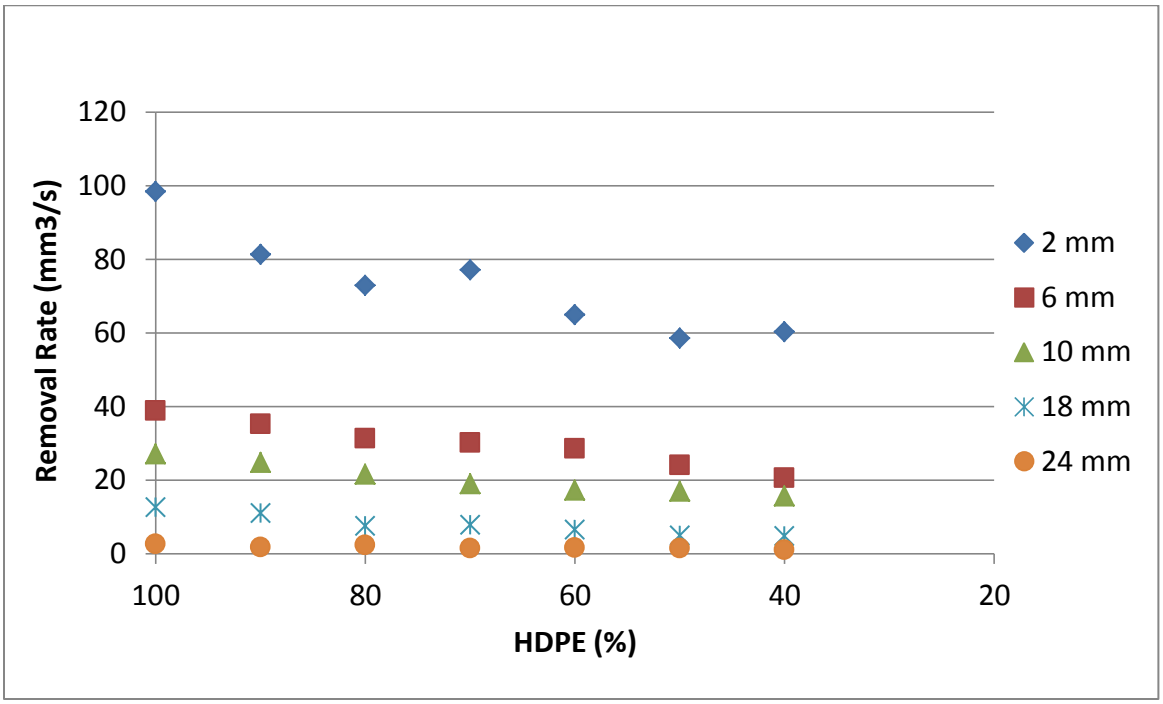

Figure 9-10: Volume removal rate plotted against HDPE % for several axial positions

9.5 Plasma Gas Composition Dependent HDPE Removal

The removal rate of HDPE using a nitrogen plasma feed gas in ambient air environment, or open lab conditions, is shown in Figure 9-11 for three axial locations with each point being the average of two replicate samples. The removal rate of HDPE using a nitrogen plasma feed gas in a controlled nitrogen environment in a glove box is shown in Figure 9-12. The two nitrogen plasma removal rates are plotted with the air plasma removal rates for comparison in Figure 9-13 showing the nitrogen plasma in air is comparable and the nitrogen plasma in nitrogen is at least on the same order of magnitude.

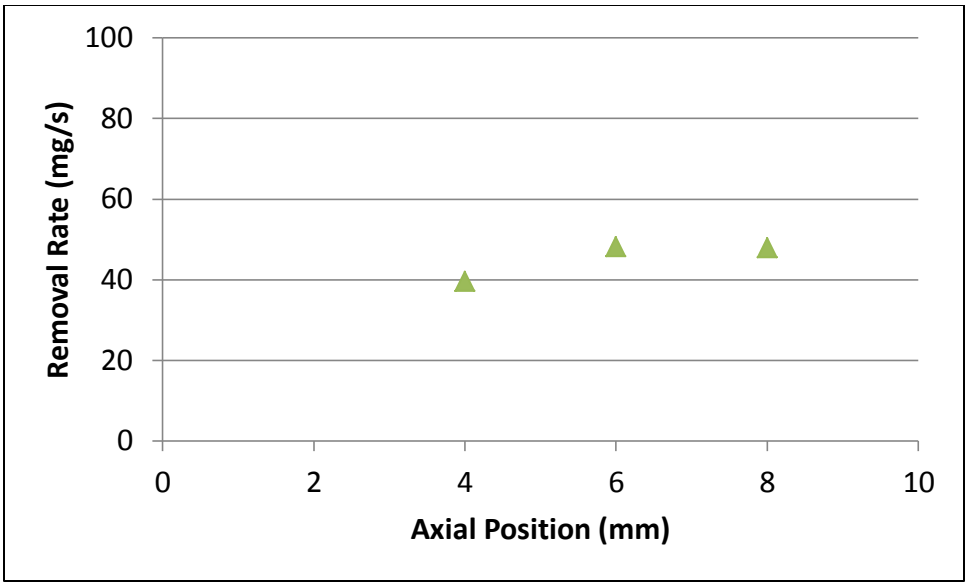

Figure 9-11: HDPE removal with nitrogen plasma in ambient air plotted against axial position for the average value of two samples per point

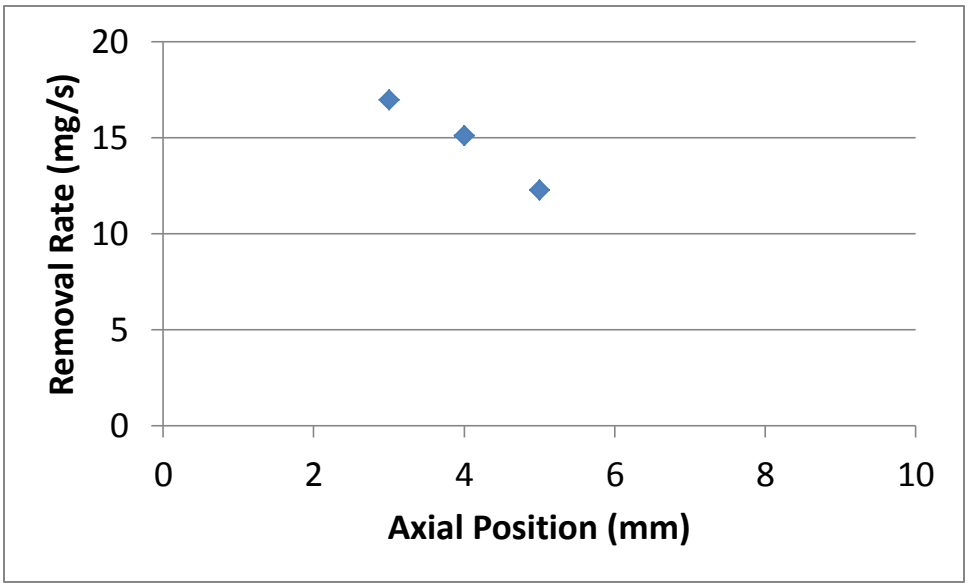

Figure 9-12: Removal rate of HDPE with a plasma feed gas of nitrogen in a nitrogen environment

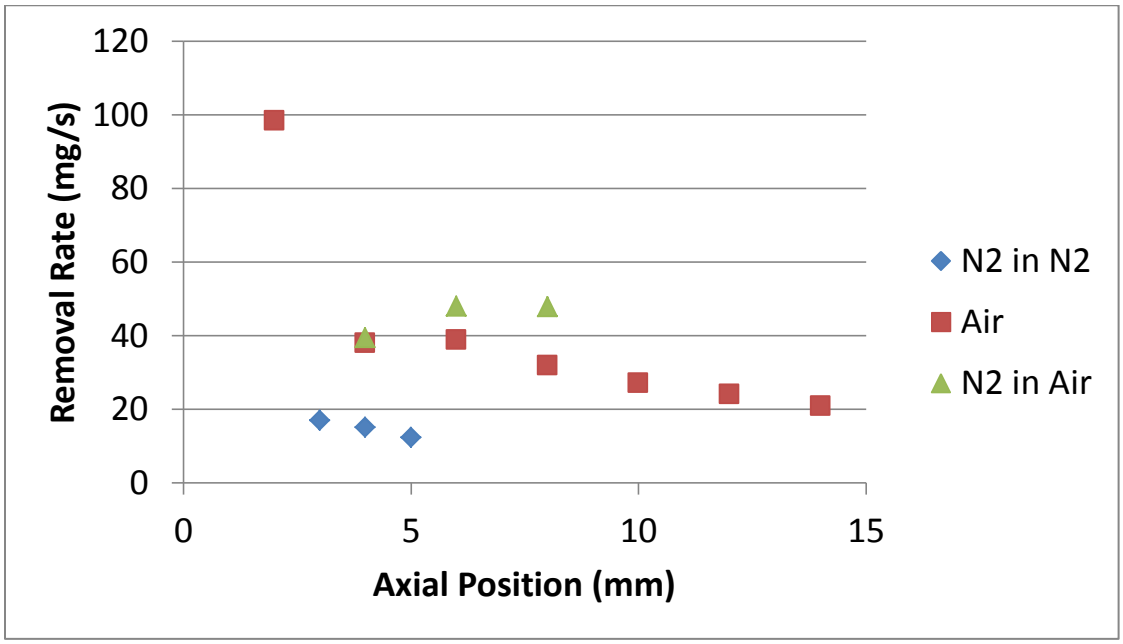

Figure 9-13: The different nitrogen plasma removal rates overlaid with the removal rates using a plasma feed gas of air for comparison

The removal rates from the plasma feed gas composition experiment are shown in Figure 9-14. These data clearly show a drop in removal rate from the air composition at 78% N_2 to the first admixture of N_2 at just under 90% representing approximately a doubling in the volume percent of nitrogen. The removal rate remains relatively flat over the next two volume percent doublings before dropping again at the 100% N_2 concentration.

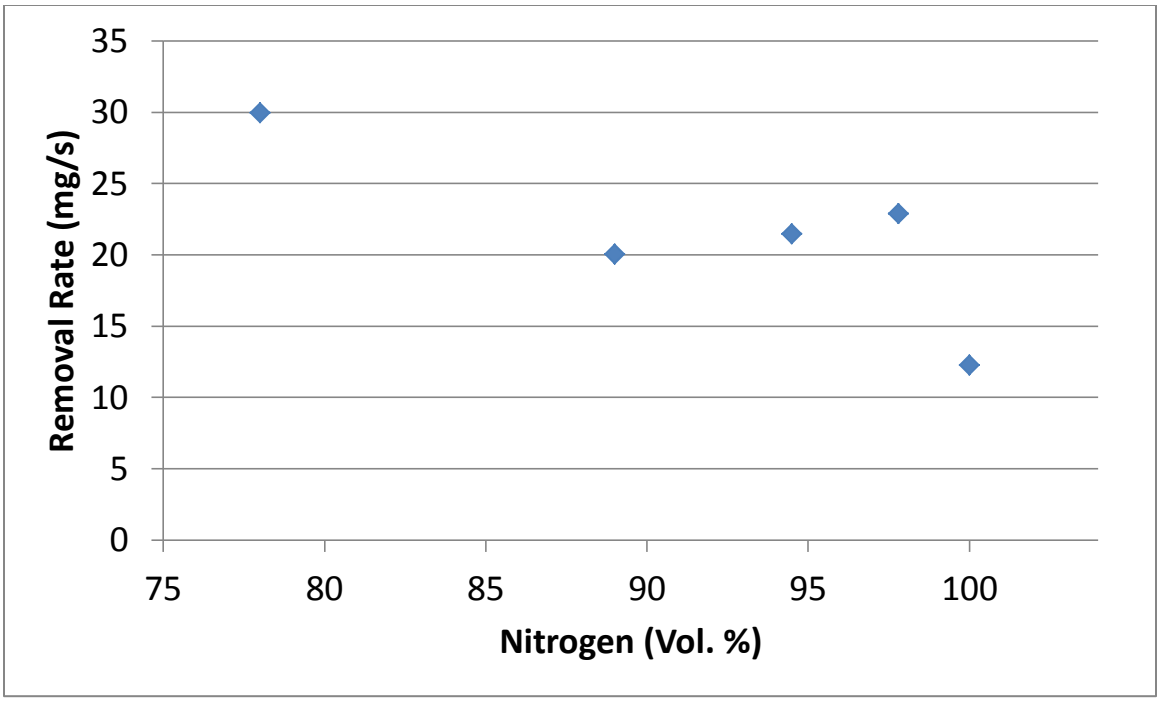

Figure 9-14: The mass removal rate of HDPE as a function of N_2 volume percent of the plasma feed gas.

This data set gives strong credence to a removal mechanism that is not solely dominated by the chemical oxidation of organic material by oxygen species. It does appear that oxygen has a positive contributing effect on the overall removal rate increasing the rate above what is achieved with solely nitrogen.

10 Plasma Characterization

10.1 OES Based Rotational Temperature Measurements

Indicative spectra of the high resolution spectroscopy are shown in Figure 10-1 and Figure 10-2 with the 375.95 nm line and the (0,0) band head at 391.5 nm, respectively, identified and highlighted. Using the methodology outline by C.O. Laux *et al.*[145], the rotational temperature was calculated and is shown in Figure 10-3 as a function of axial position. This shows a relatively stable rotational temperature across the 16 mm axial range that was measured with a median temperature of 8,570 K.

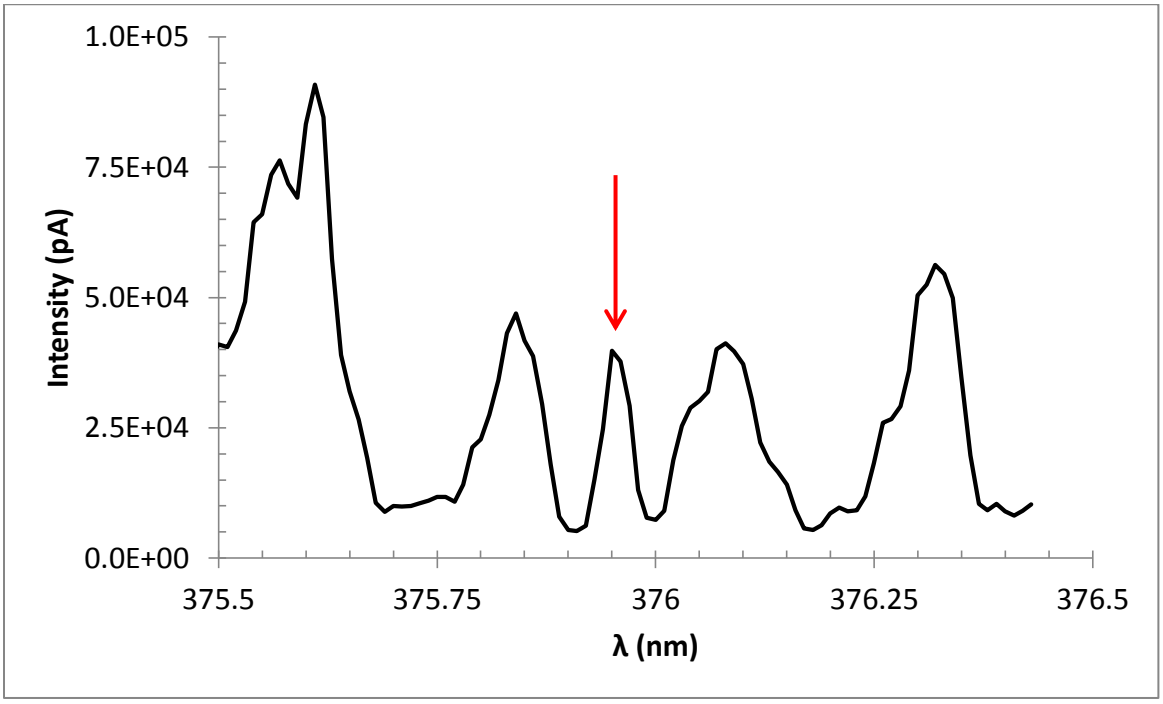

Figure 10-1: High resolution spectrum denoting the isolated 375.95 nm line

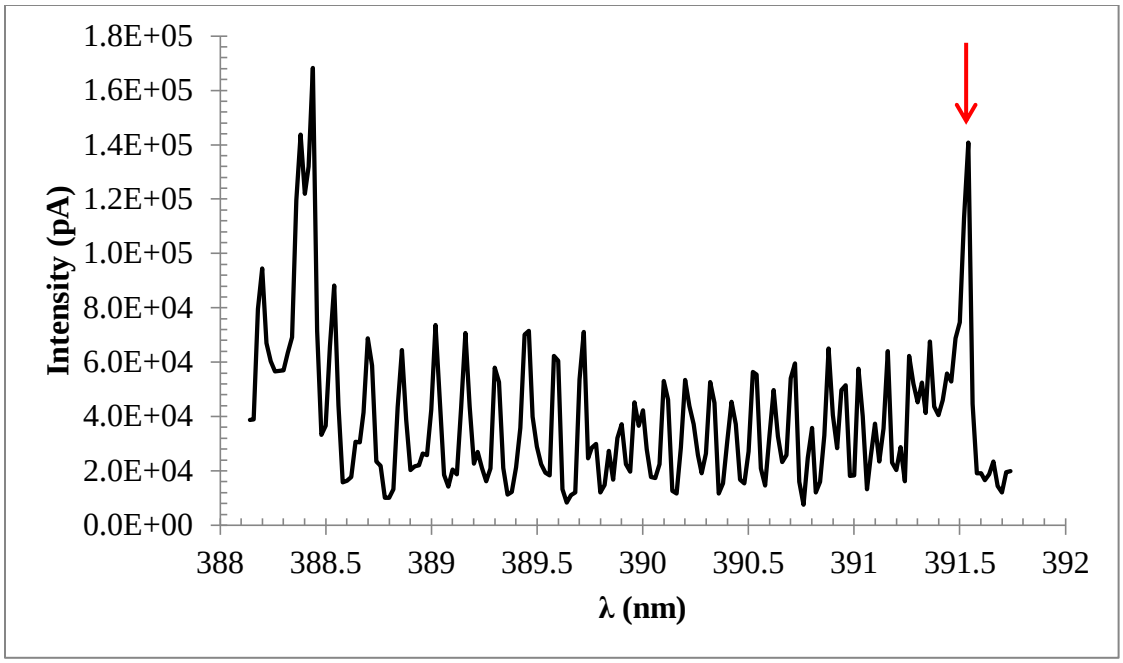

Figure 10-2: High resolution spectrum over a range of the nitrogen first negative system with the (0,0) band head at 391.5 nm

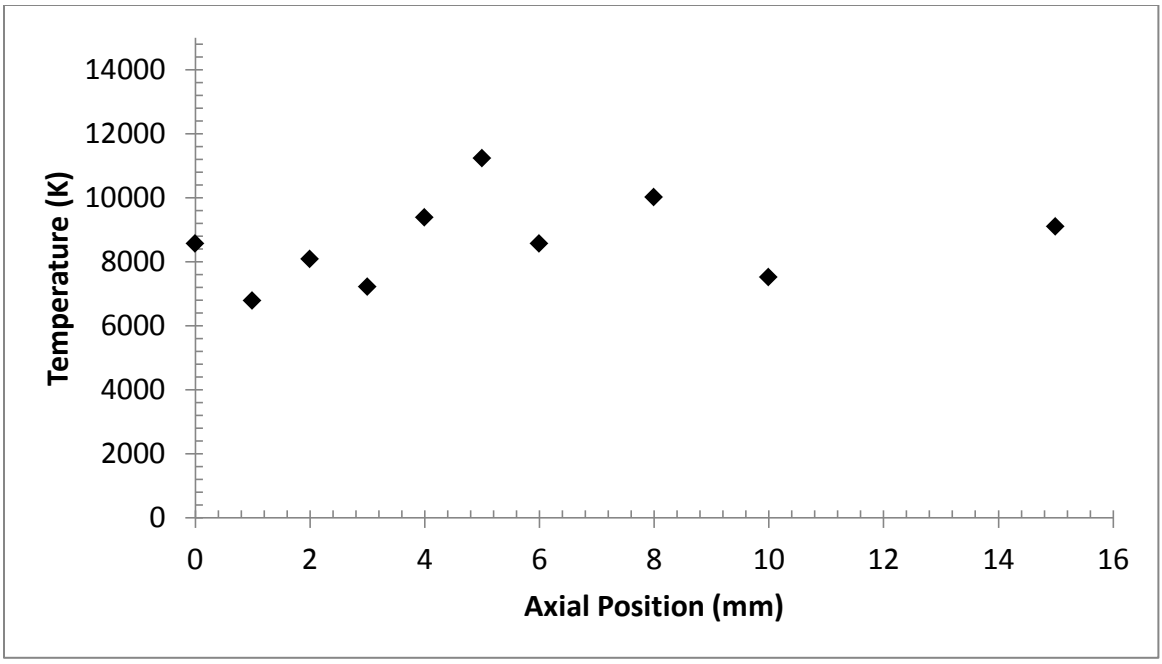

Figure 10-3: Rotational temperature as a function of axial position from the nozzle tip to 15 mm

The intensities of three nitrogen first negative system transitions are shown in Figure 10-4 as a log function against the axial position. This indicates that the relative intensities of the different nitrogen species track similarly with axial position. The intensity of the atomic oxygen line as a function of axial position is shown in Figure 10-5 indicating a relatively smooth decline with increasing axial position. The slight discontinuity at an axial position of approximately 5 mm is where the torch transitions from an arc to an afterglow and also where the secondary arcs complete the electrical circuit from the arc to the grounded nozzle.

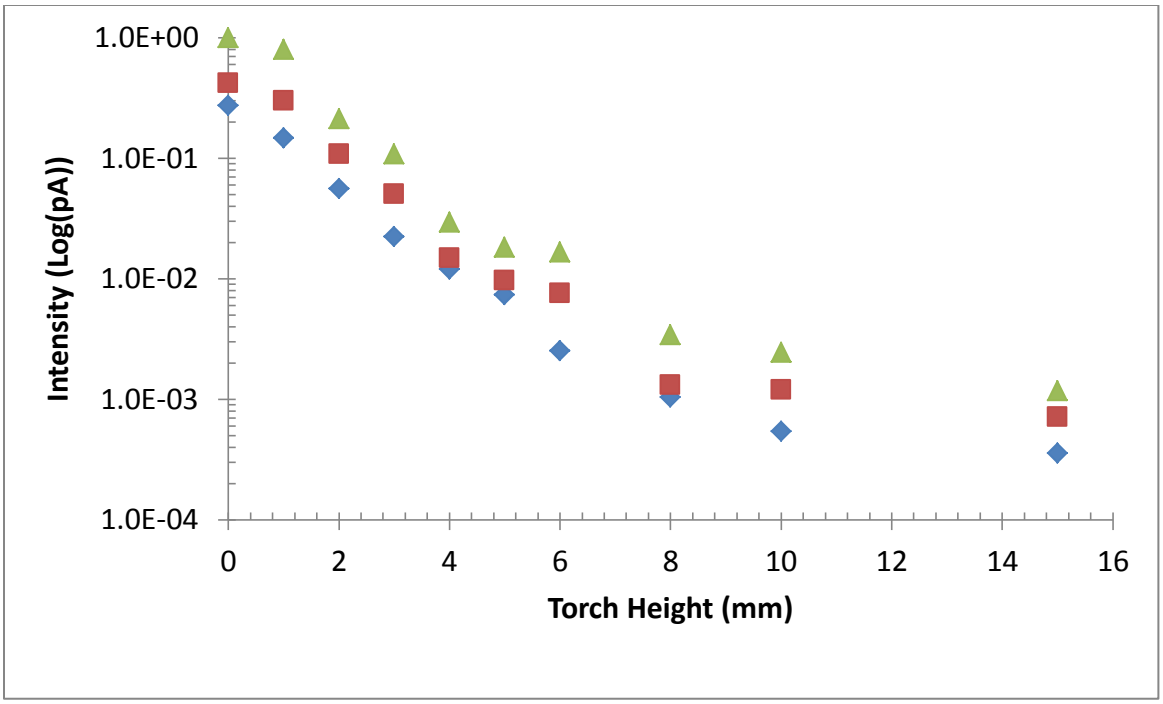

Figure 10-4: Log intensity of 375.95 nm (◆), 388.7 nm (■), and 391.5 nm (▲) peaks as a function of distance from torch nozzle.

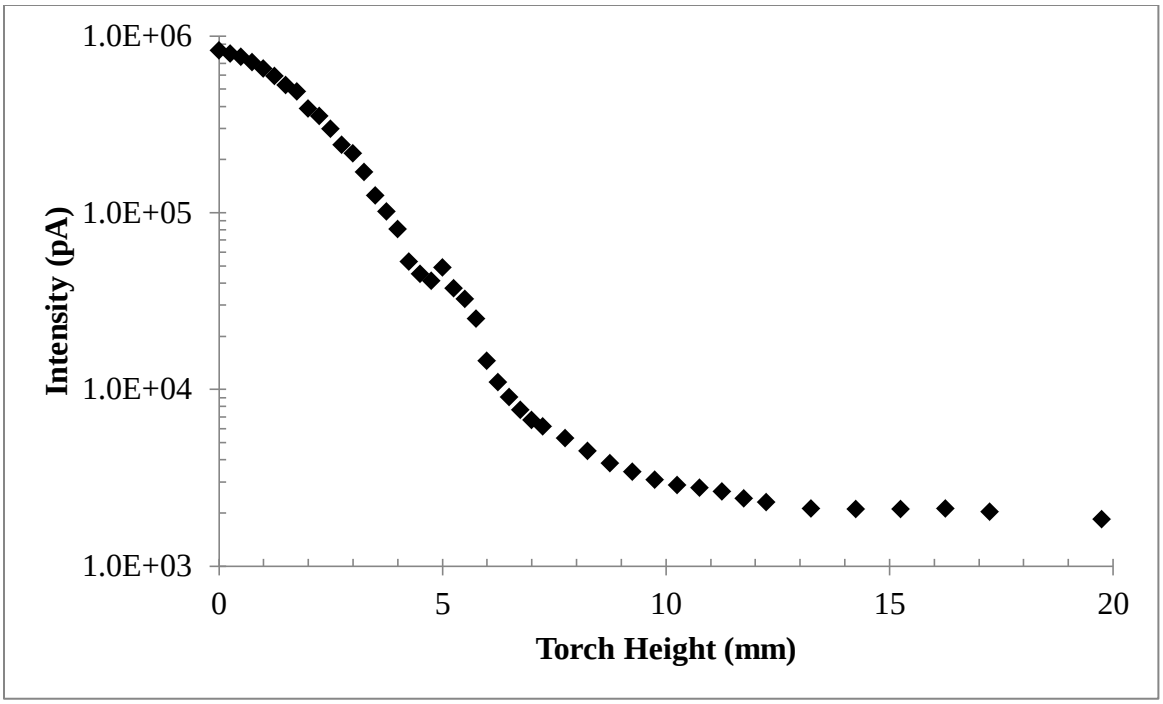

Figure 10-5: Atomic oxygen intensity as a function of distance from the torch nozzle as indicated by the emission line at 777.19 nm

The mass removal rates of the McMaster Carr HDPE plotted as a function of the rotational plasma is shown in Figure 10-6 resulting in a relatively high level of scatter and slight positive trend. The removal rates for the same HDPE samples are plotted against the log of the normalized intensity of the two nitrogen first negative lines and the atomic oxygen line and are shown in Figure 10-7. Firstly, these data show a much stronger correlation to the removal rate than one from the rotational temperature. Secondly, these data show relatively similar relationships between the various emission intensities and the removal rate. From these data sets it was concluded that the removal rates did not track well with rotational temperature, and while there was not much distinction between the molecular nitrogen and

atomic oxygen lines, the removal rates did appear to track more strongly with emission intensity. Based on this analysis it was decided to investigate the contributions to the removal rate from the different plasma constituents.

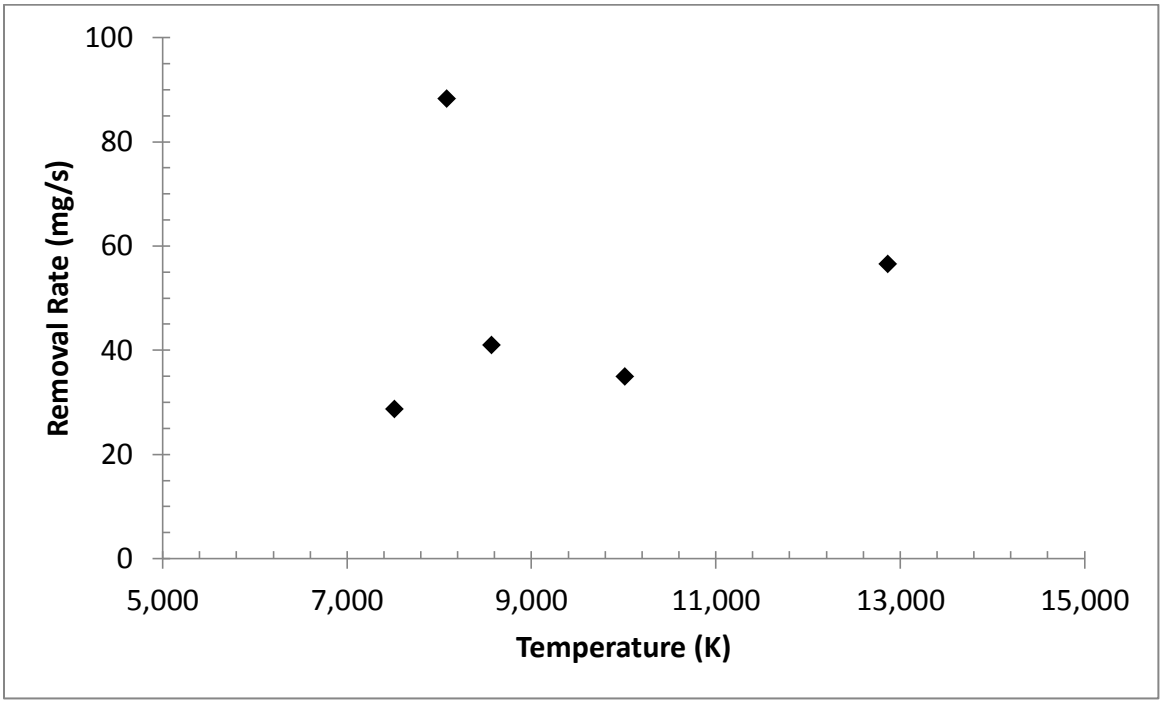

Figure 10-6: Mass removal rate as a function of rotational temperature

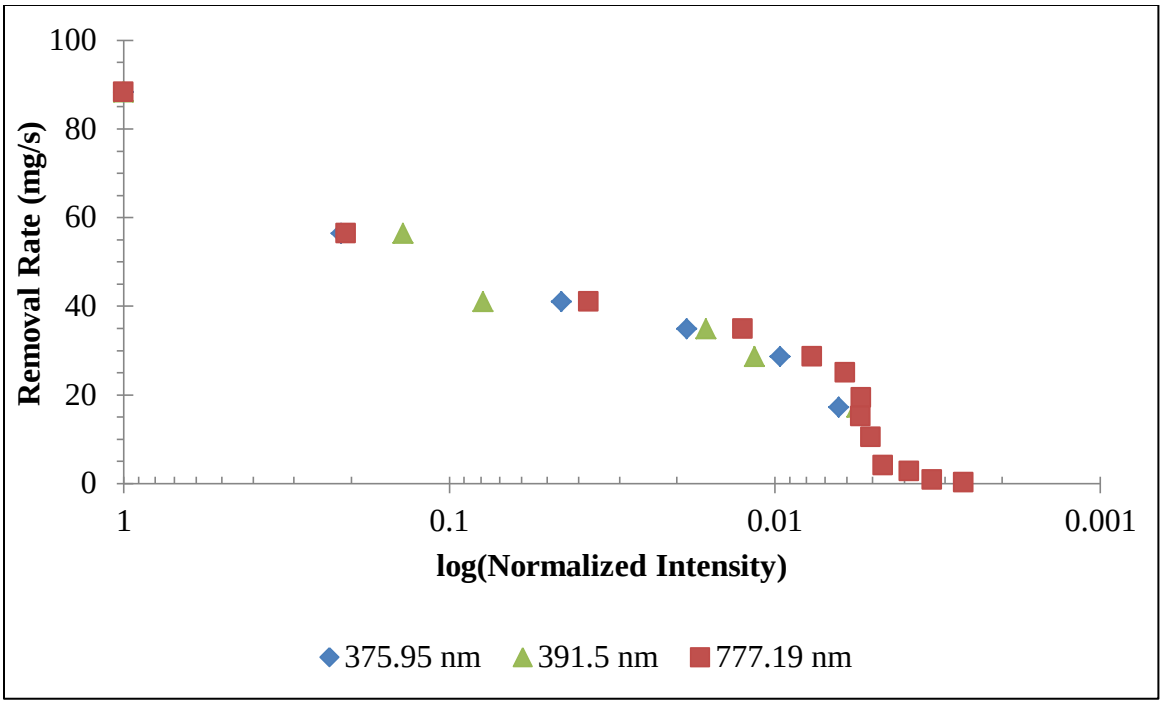

Figure 10-7: Removal rate as a function of peak intensity for the 375.95 nm and 391.5 nm peaks of the nitrogen first negative system and the 777.19 nm line of atomic oxygen

10.2 Preliminary Spatial Broadband OES

Initial broadband OES characterization was completed to provide insight into the spatial profile of the plasma species. An indicative spectrum of the arc region of the plasma torch from 200-1,000 nm compiled from the spectra generated by each of the four spectrometer channels, is shown in Figure 10-8. As identified and indicated on the spectrum, the primary emitting species are NO, N_2, O, N, and Cu species, there are additionally two Cu I lines at 324.92 nm and 327.57 nm that were not labeled for the sake of clarity but should not be confused as part of the nitrogen vibrational bands that are located in the same region. An expanded view of the broadband spectrum showing more detail over the lower

wavelength ranges is shown in Figure 10-9, with the major nitrogen transitions and Cu I emission lines labeled.

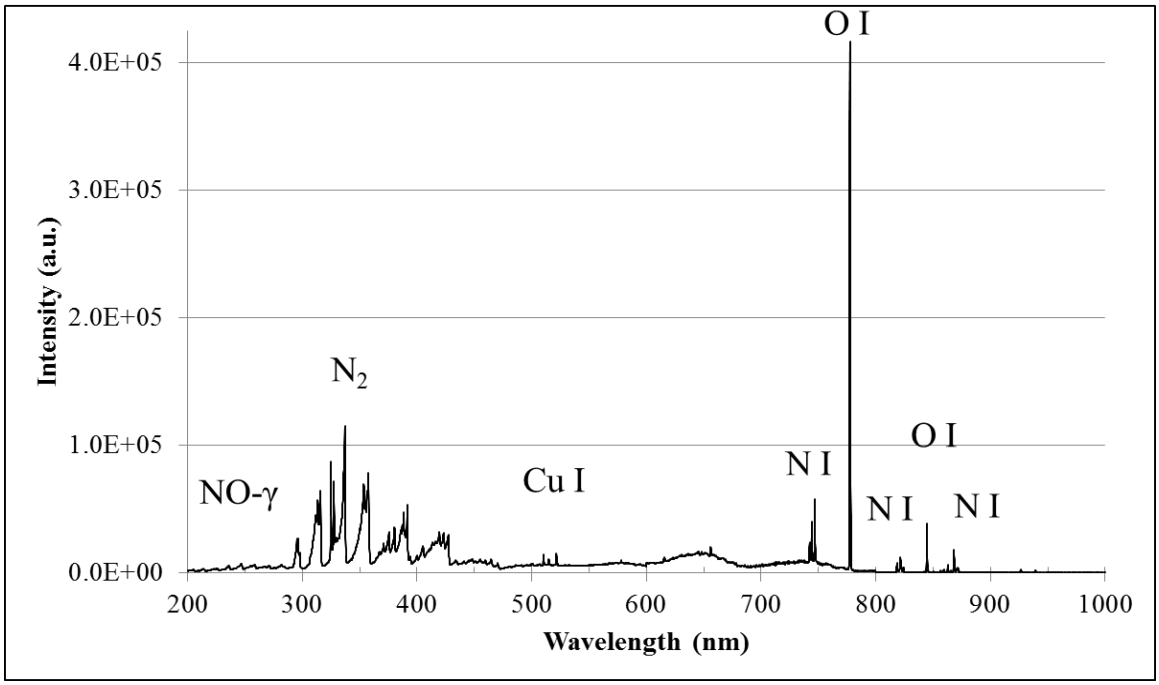

Figure 10-8: Broadband spectrum compiled using the 4-channel Ocean Optics S2000 spectrometer at an axial and radial position of 0 mm

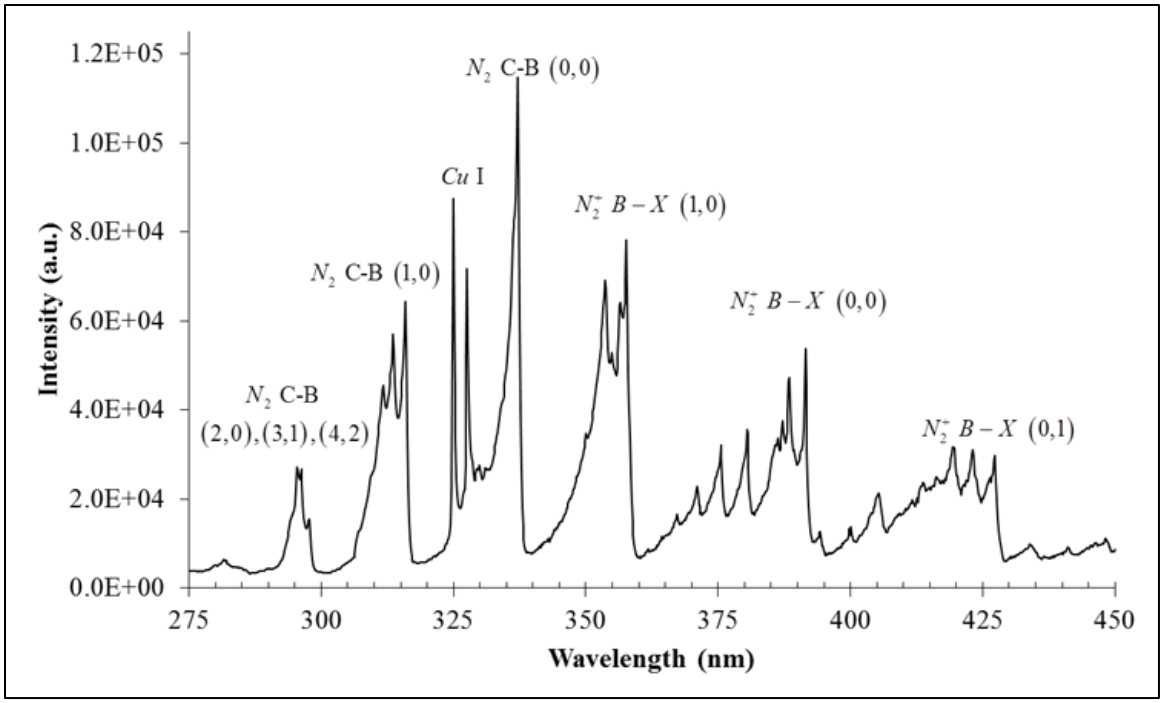

Figure 10-9: An expanded spectrum over the lower wavelength range with the significant bands and emission lines labeled such as the nitrogen first negative system, nitrogen second positive system, and Cu I.

Initial investigating of the spatial distribution of plasma species began with the spatial distribution of total emission intensity. This value was calculated as the area under the curve using the Riemann trapezoidal approximation $A = \sum_{\lambda=200nm}^{\lambda=970nm} \frac{I_1 + I_2}{2}(\lambda_2 - \lambda_1)$, where A is the area, $I_1 \& I_2$ are the intensity of two neighboring points located at the wavelengths $\lambda_1 \& \lambda_2$, and the summation $\sum_{\lambda=200nm}^{\lambda=970nm}$ as indicated is taken over the 200-970 nm range. A graphical representation is given in Figure 10-10. The emission intensity summation was then calculated for each axial and radial position that was analyzed and normalized to the most

intense value for each axial and radial data sets. The radial distribution at an axial position of 2 mm is shown in Figure 10-11 and appears to be slightly asymmetric with respect to the centerline of the torch and to itself. These asymmetries are generally attributed to the numerous irregularities in the throat and exit of the nozzle and those arising from the vortex gas flow. The axial profile was acquired at a radial position of 1 mm, as that location contains the most intense signal and is shown in Figure 10-12. From these data the summated axial emission intensity appears to have a slight increase over the first couple millimeters that is then followed by a substantial drop with increasing axial position. There are several possible justifications for the initial intensity increase. The first possible explanation considers the fluid dynamics of the gas exiting the nozzle. The issue is that as the plasma gas and non-ionized gas exits the throat of the nozzle the gas undergoes a volume expansion thereby either reducing the concentration density of emitting species or reduces the energy density of the plasma gas. The following increase would then be explained by a compression of the gas as the expansion wave is reflected inward. Secondly, the discontinuity could be a result of competing excitation and de-excitation mechanisms. The emitting species might be a delayed de-excitation giving the appearance of an increase or a self-excitation process whereby highly energetic photons emitted by ionized atomic transitions to the ground state, which are outside the range of wavelengths that are observable using the available spectrometers, and are able to excite energy states that have transitions that are observable. Or thirdly, the increase could arise from a quirk in the electrical circuit model of the torch. Where even though the plasma exits the torch at the throat of the nozzle, the circuit is not completed in the same location, rather not until further down the arc length.

This is where the periodic secondary arcs connect the plasma to the electrically grounded nozzle.

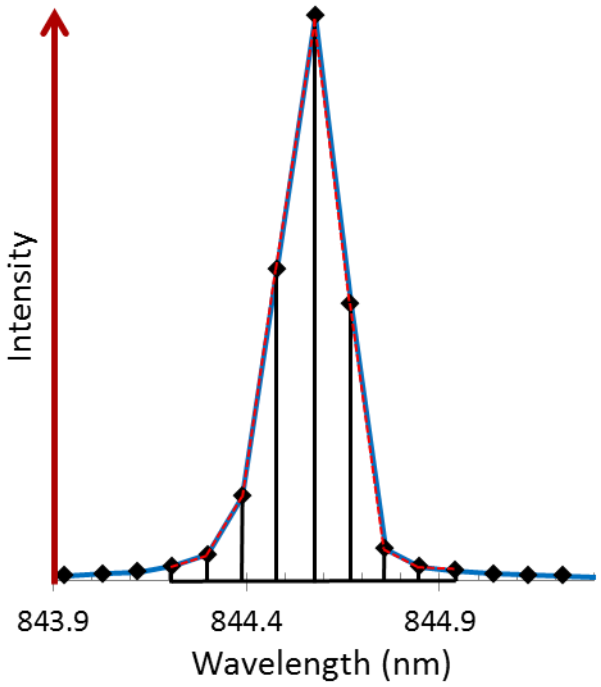

Figure 10-10: Positive area under the curve using a Riemann trapezoidal approximation given by: $A = \sum_{\lambda=200nm}^{\lambda=970nm} \frac{I_1 + I_2}{2}(\lambda_2 - \lambda_1)$

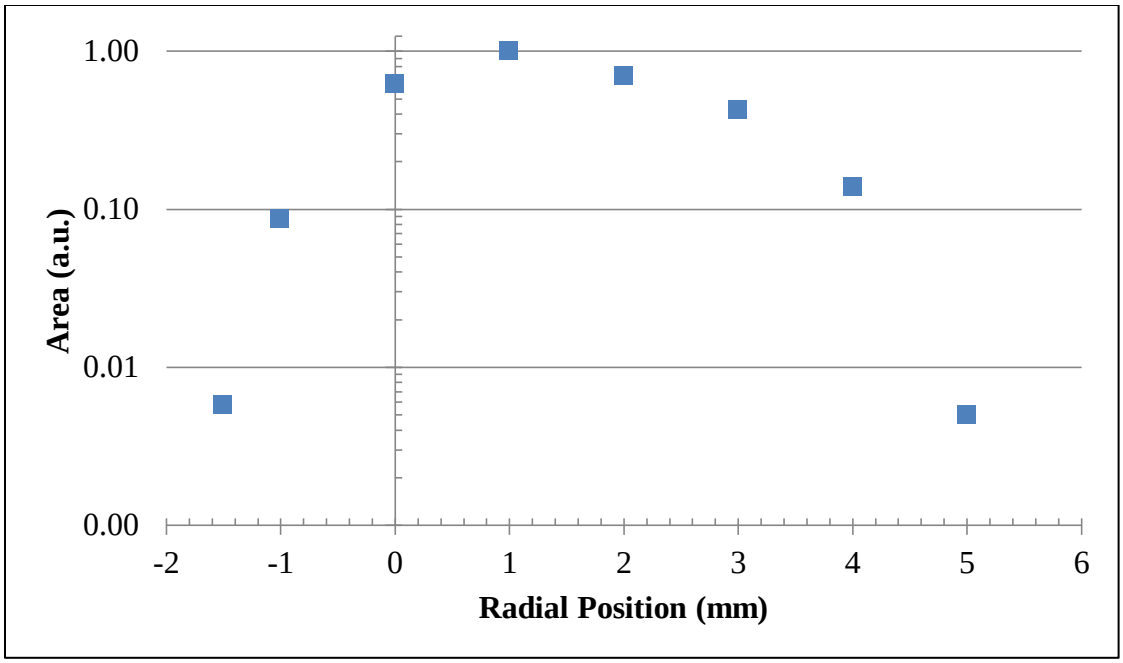

Figure 10-11: Radial intensity area at an axial position of 2 mm shows a slight asymmetric distribution that could be attributed to the vortex fluid flow

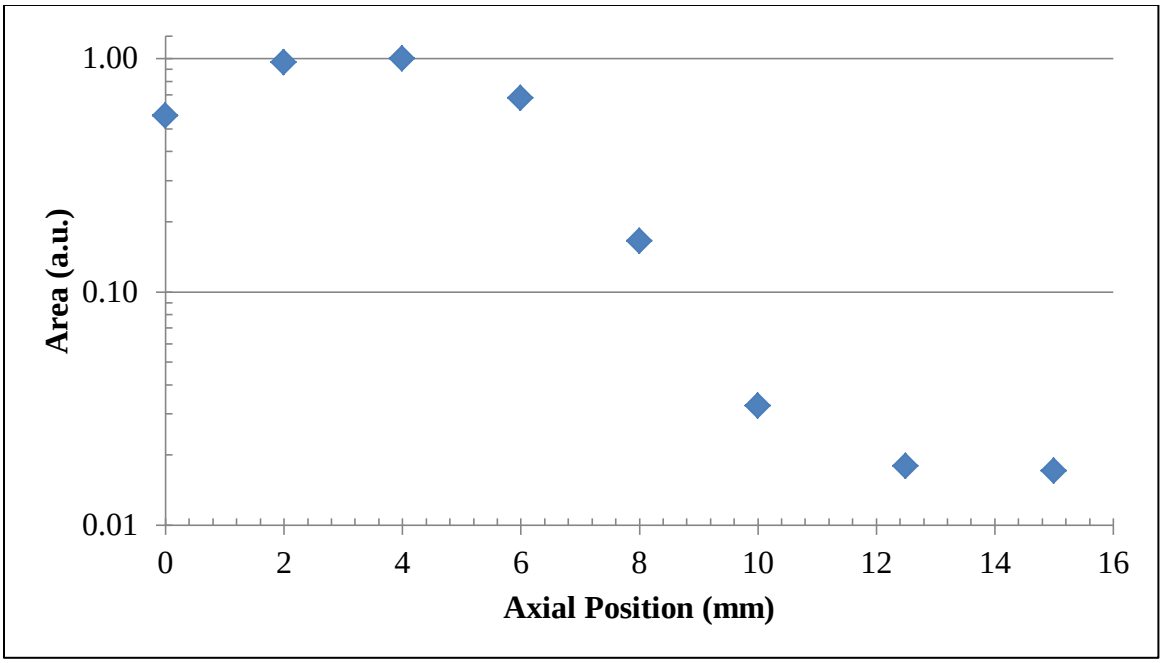

Figure 10-12: Axial intensity area at a radial position of 1 mm that was determined under the experimental conditions to be the most intense location

While the total integrated intensity is useful, it is also worthwhile to consider the complete broadband spectra as shown in Figure 10-13 with each spectrum spaced 4 mm. The normalized spectra show a significant contribution from molecular N_2 and NO-γ species in the 200-400 nm range and the 700-1100 nm range dominated by the atomic O & N species in the spatial region of 0-12 mm. As noted earlier the transition from the high intensity arc region to the lower intensity afterglow region generally begins to occur at the 10-15 mm axial position range and as evident on this graph this region shows a clear demarcation between the well-defined molecular and atomic emission lines and a relatively featureless

broadband continuum. This broadband continuum from 400-800 nm is attributed to the NO_x chemiluminescence emissions.

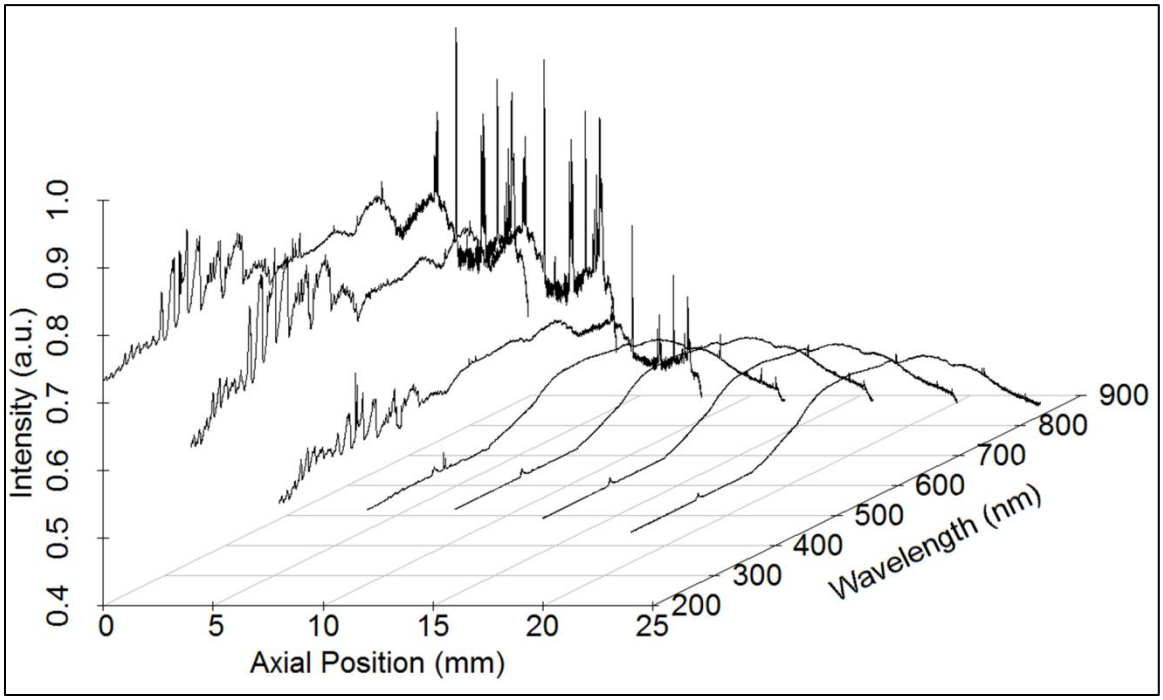

Figure 10-13: The log emission intensity of the spectra along the axial range showing a decrease in the atomic and molecular nitrogen intensities and an increase in the broadband continuum.

10.3 Detailed Spatial Broadband OES

The detailed, higher spatially resolved, OES of the PF5K can be seen in Figure 10-14, Figure 10-15, Figure 10-16, Figure 10-17, Figure 10-18, and Figure 10-19 each corresponding to a radial profile at an axial position of 0, 1, 2, 3, 4, and 5 mm, respectively. Additionally, an axial profile at a radial location of 0 mm can be seen in Figure 10-20. The

radial profiles of the higher spatially resolved spectra, similarly to the spectra obtained in the lower spatial resolution experiments, indicate a slight asymmetric profile about the axial centerline. The higher spatially resolved axial profile also indicates a steadily decreasing intensity with respect to an increasing axial location.

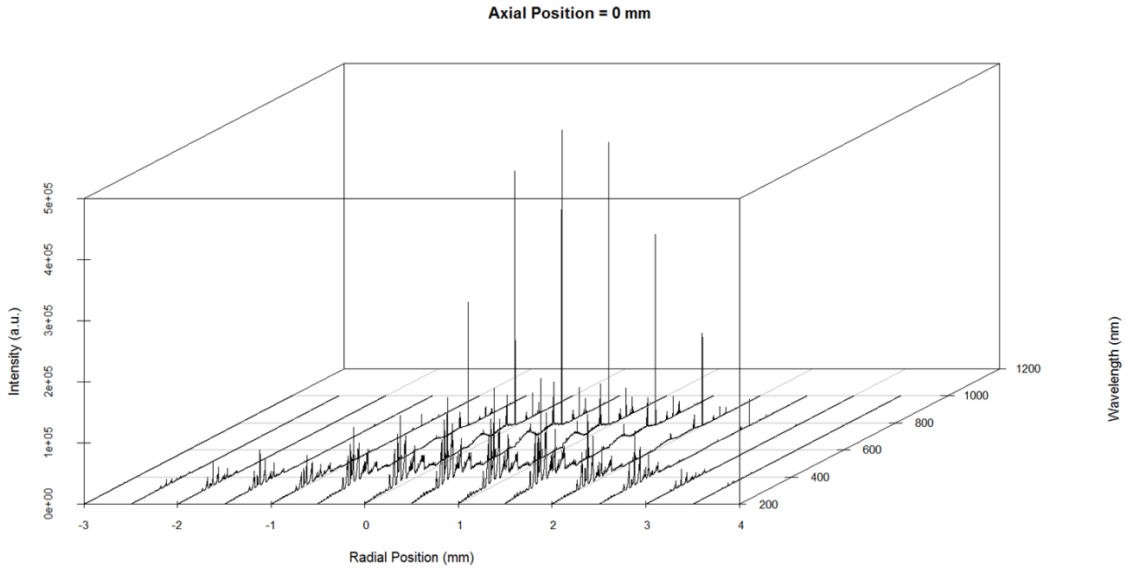

Figure 10-14: Radial OES at an axial position of 0 mm

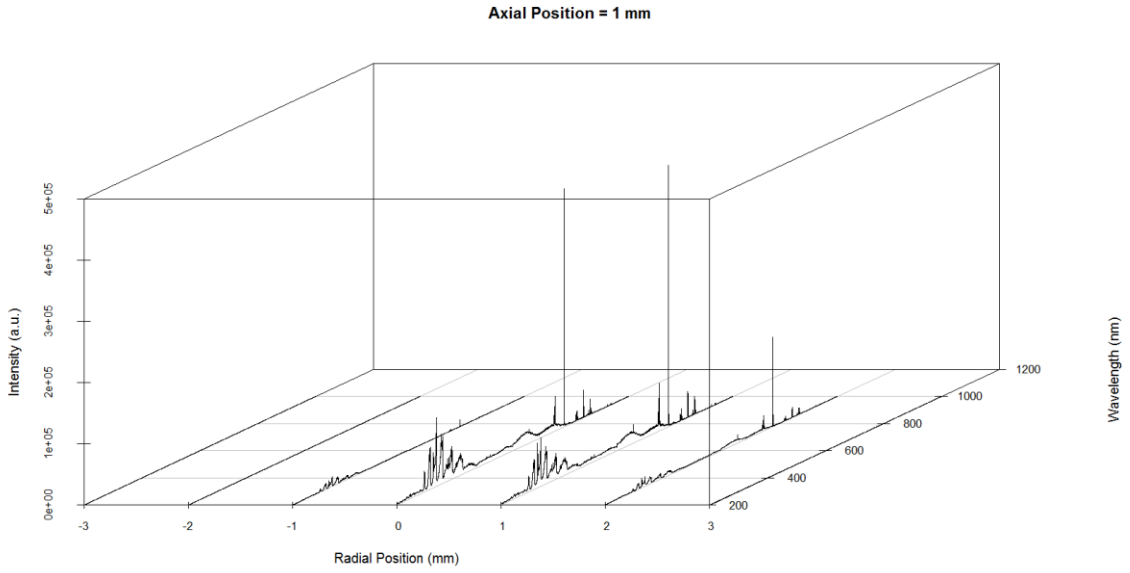

Figure 10-15: Radial OES at an axial position of 1 mm

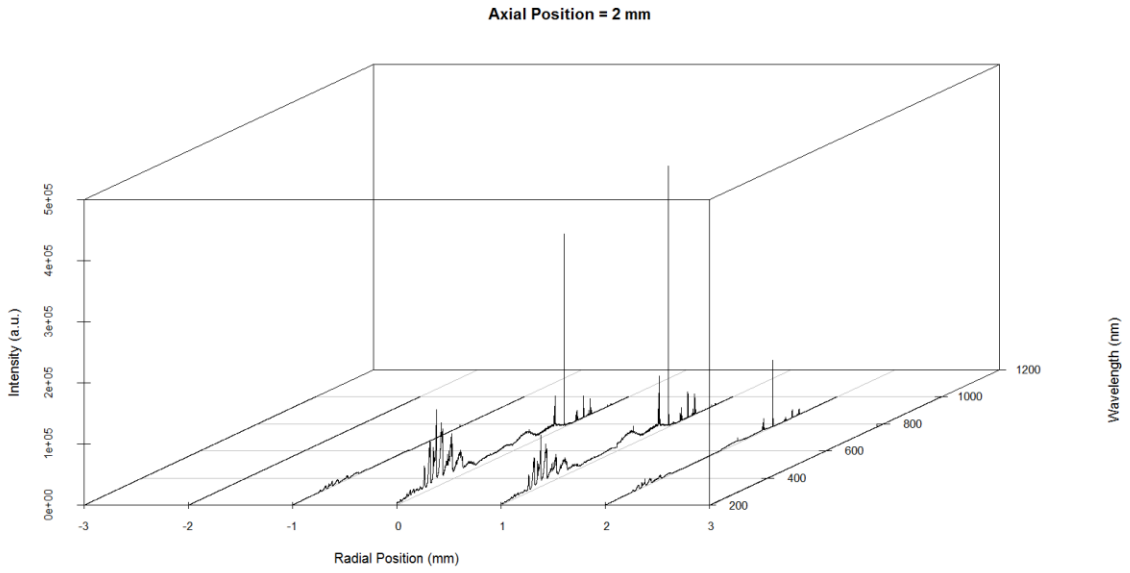

Figure 10-16: Radial OES at an axial position of 2 mm

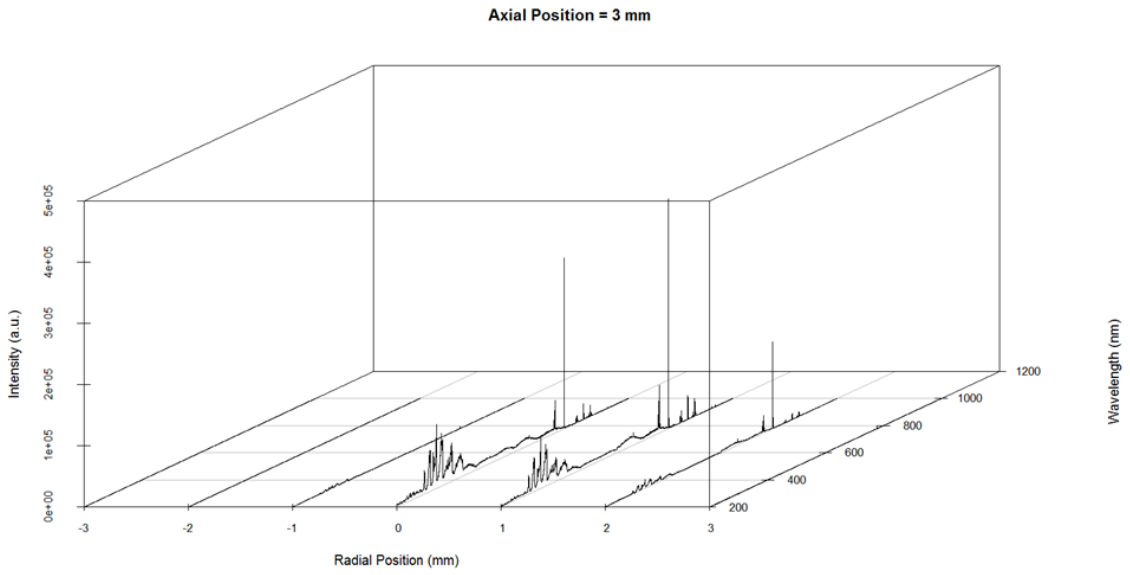

Figure 10-17: Radial OES at an axial position of 3 mm

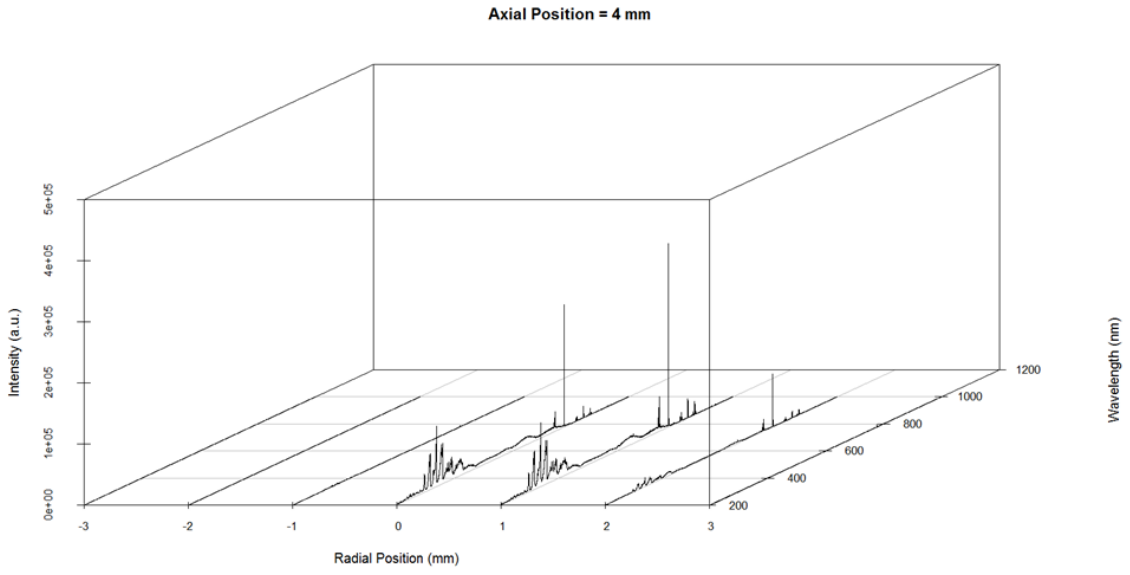

Figure 10-18: Radial OES at an axial position of 4 mm

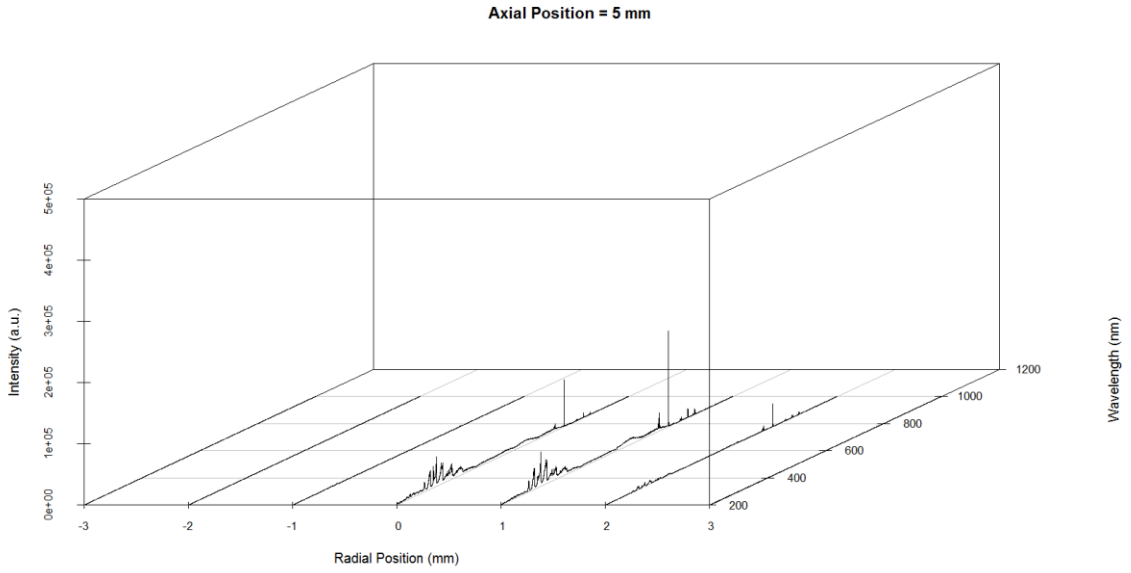

Figure 10-19: Radial OES at an axial position of 5 mm

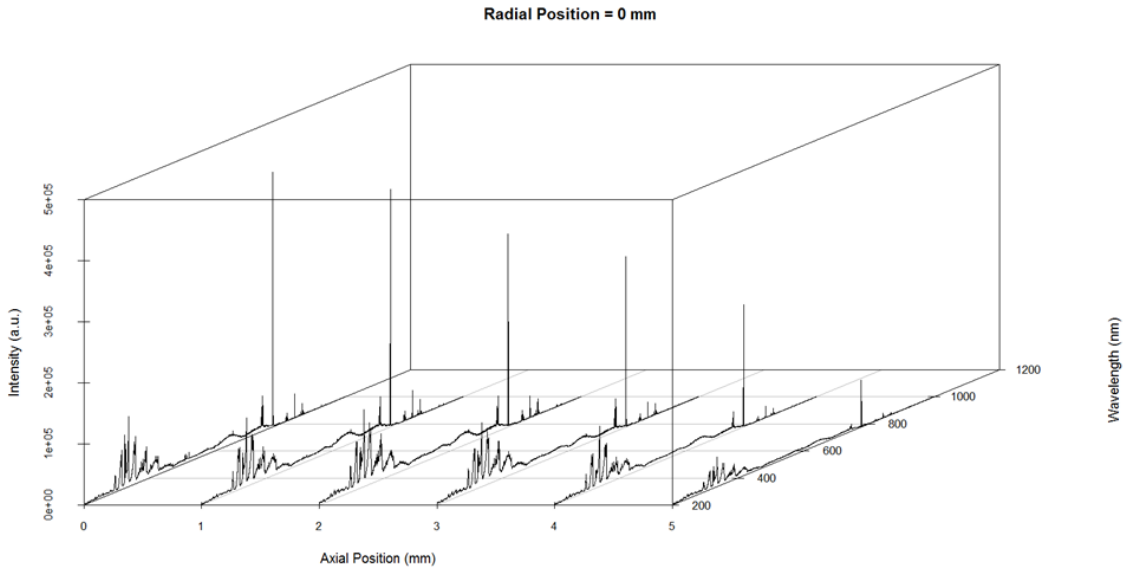

Figure 10-20: Axial OES at a radial position of 0 mm

10.4 Spectroscopic Temperature Calculations

A temperature profile of the plasma torch was calculated based on the Boltzmann line method using the spectroscopic values given in Table 10-1 and is shown in Figure 10-21. These data indicate a maximum temperature of 7,400 K after which it declines steadily with increasing axial position. The range only extends to 10 mm as the Cu I lines were indistinguishable from the background emission past this point. The trio of lines from 510-521 nm provided the strongest linear correlation compared to the other Cu I transitions. It is interesting to note the increase in temperature over the first couple millimeters from the torch nozzle, similar to the increase in total emission intensity, before the decreasing trend dominates. This characterization method could offer a simplistic approach to monitoring the plasma as a feedback for process control during industrial applications given that only a narrow range of ~15 nm needs to be monitored. Additionally, the monitoring of the Cu I lines could be employed to track the rate of electrode erosion.

Table 10-1: Table of spectroscopic values used for Cu I lines. [135,142,146]

λ (nm)	g	A_{ik}	E_i (eV)
324.75	4	1.39E+08	3.819
327.39	2	1.37E+08	3.788
427.34	8	3.45E+07	7.741
464.84	8	3.80E+07	7.741
510.55	4	2.00E+06	3.819
515.32	4	6.00E+07	6.194
521.82	6	7.50E+07	6.195

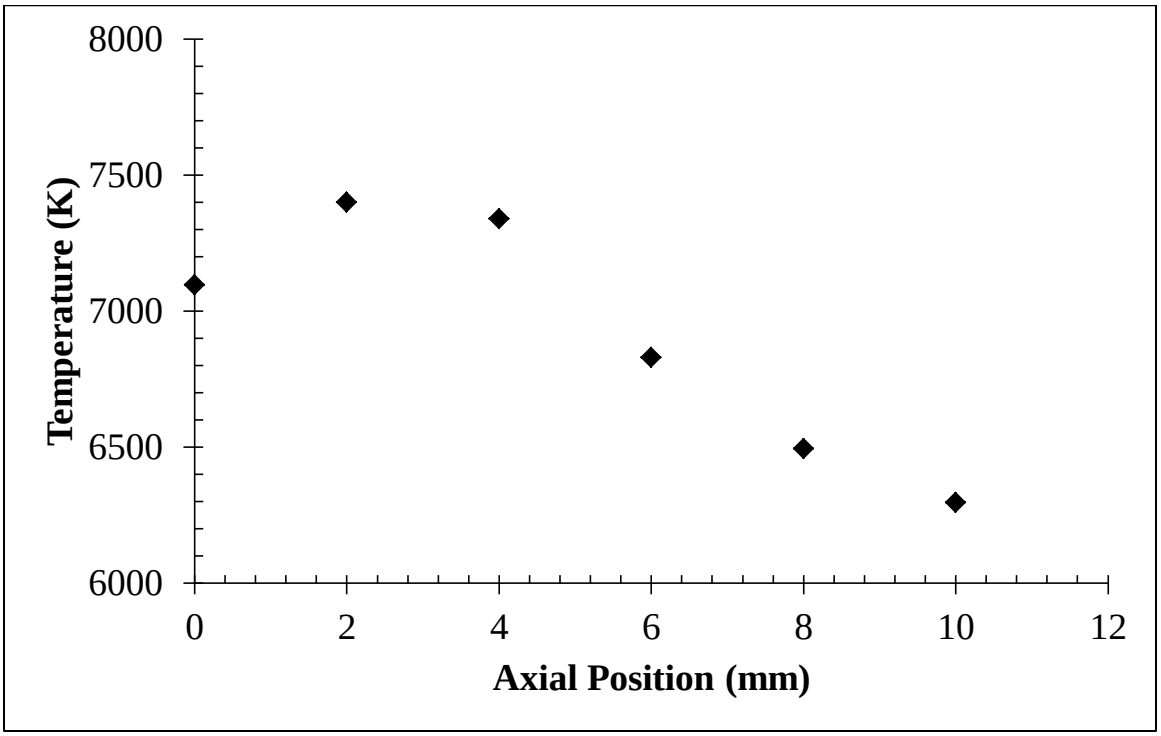

Figure 10-21: Temperature calculated using the Boltzmann line method with Cu I 510.5 nm, 515.3 nm, and 521.8 nm lines.

10.5 *In Situ* OES Characterization

Initial work was completed characterizing the plasma plume as it interacted with the HDPE material and the results are shown in Figure 10-22 and overlaid with the unobstructed plasma emission in Figure 10-23. The main emission lines identified are due to CN, C_2, H I, N I, and O I, there also remain some of the nitrogen vibrational bands. The overlaid spectra indicate a decrease in the NO-γ emission, several of the nitrogen emission bands, and the many of the atomic lines are also reduced. The formation of CN gives credence to the

removal mechanism at least involving the nitrogen species present in the plasma, although further research will be needed to determine if the contribution is due to the molecular or atomic nitrogen constituents. These results also raise a serious issue that if the reaction mechanism is producing CN it could represent a serious safety concern for the operators or anyone nearby the treatment area. Cyanide (CN^-) is a highly toxic chemical that is poisons through histotoxic hypoxia or the inability for cells to take up or utilize oxygen from the bloodstream. Coincidently, the most toxic form of cyanide is the cyanide anion and hydrogen cyanide (HCN) and highly water soluble.[147] Synthesis of hydrogen cyanide has been previously conducted using plasma torches.[148,149]

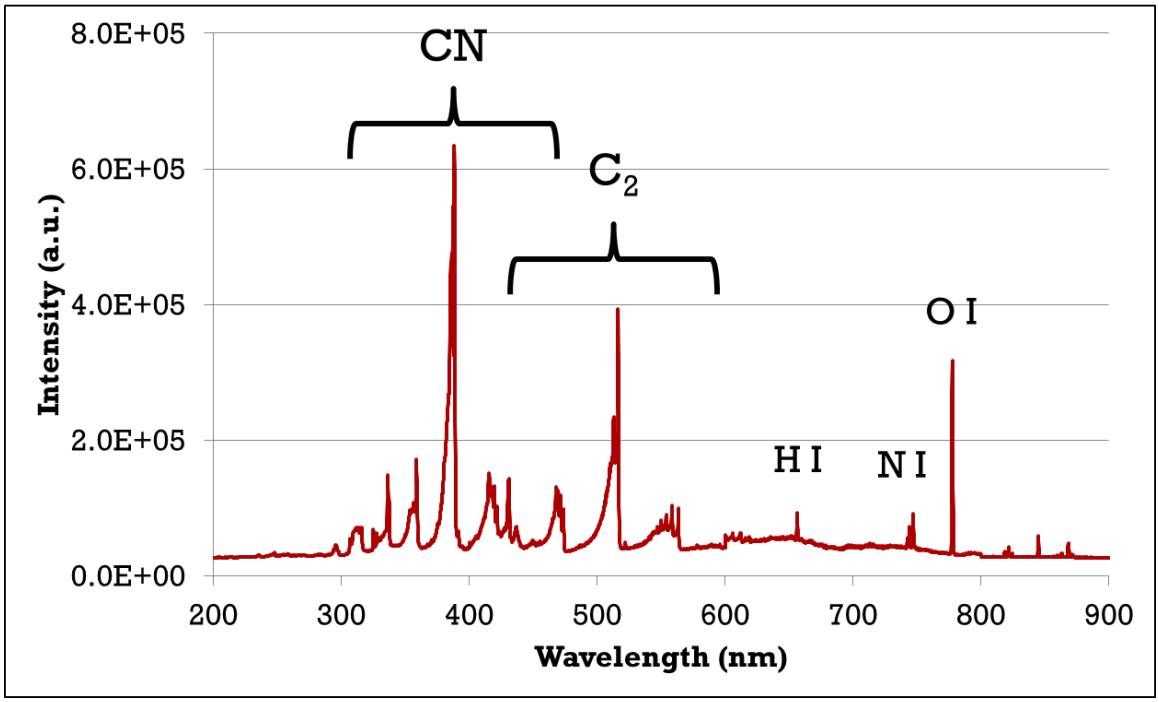

Figure 10-22: Spectrum of the plasma as it interacts with the HDPE sample and the notable emission lines labeled.

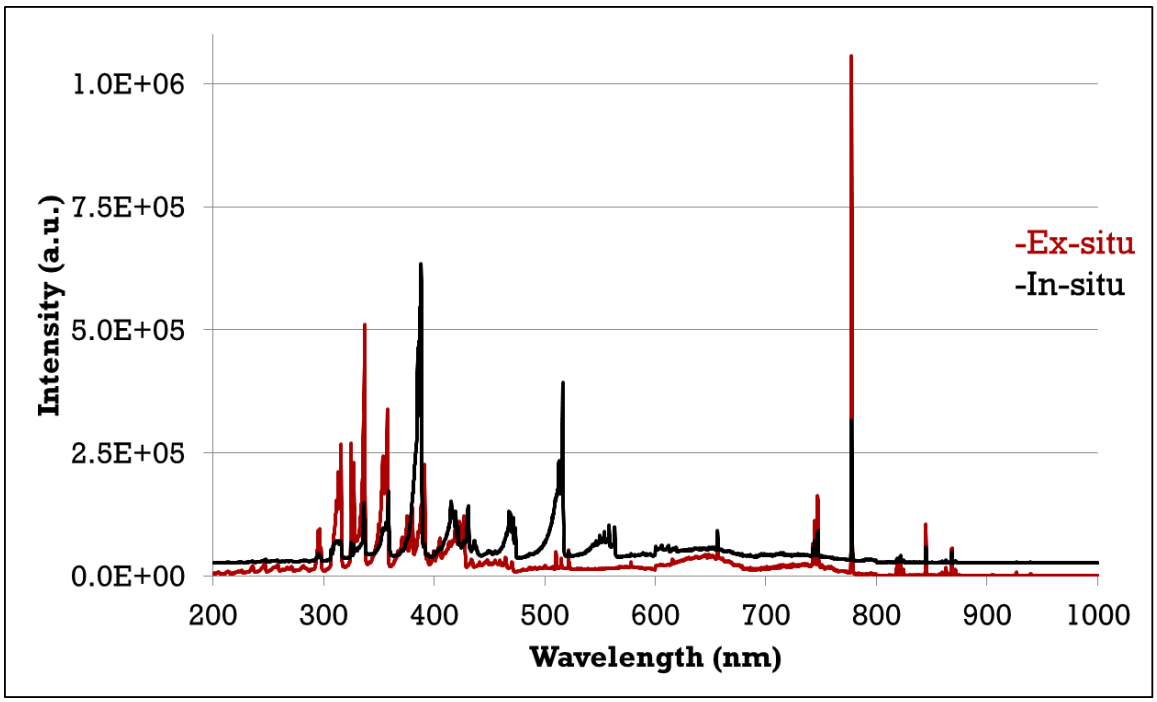

Figure 10-23: Overlaid spectra of the emission from a free flowing unobstructed plasma and from the plasma interacting with the HDPE.

10.6 Thermal Characterization

Several brief experiments investigated the macroscopic thermal component of the plasma torch. One of the characterization experiments looked to quantify the thermal IR emission of the plasma over space and time using the FLIR® video camera by taking real-time movie clips of the torch from plasma ignition to stabilization. While this characterization method might seem straight forward, in practice it was determined early in the project that it was anything but, as there were several issues stemming from the device operating software, controlling and determining the emissivity of the plasma gas and background gas, and distinguishing between the two gases. Even with these limitations, a

still frame from one such clip is shown in Figure 10-24 with several informative points. Firstly, the plasma discharge is significantly hotter than the nozzle and surrounding ambient air. Secondly, the plume is most intense closer to the nozzle and along the axial centerline and appears to be surrounded by a cooler 'shroud' of gas. Thirdly, it was from these thermal imaging experiments that the periodic structures (red color regions) were first noticed. These features were later determined to be shockwaves from an expanding jet. Finally, the thermal imaging can be useful and accurately employed to measure and monitor the thermal emissions from the various torch components and substrates.

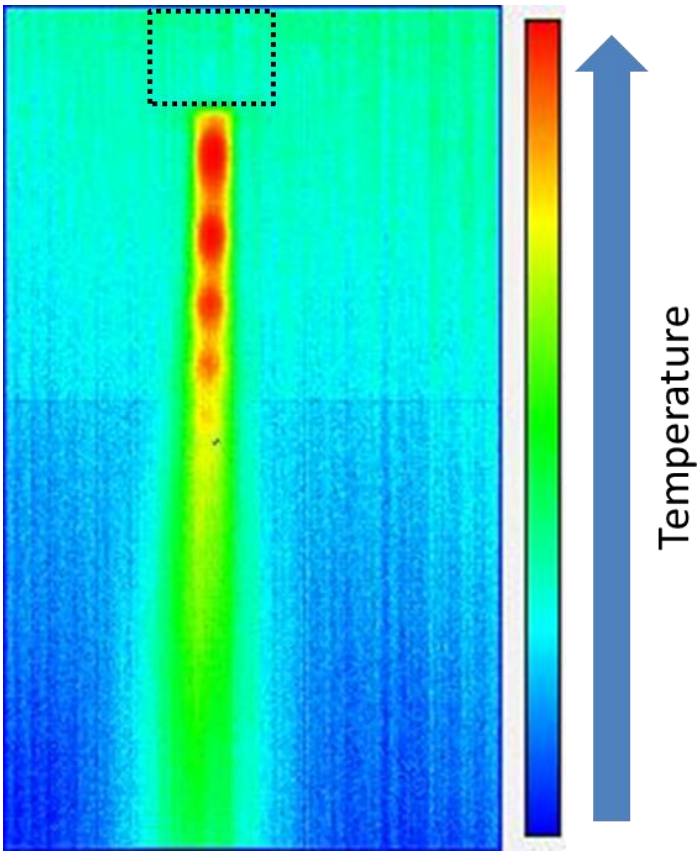

Figure 10-24: FLIR® image of PF5K showing shock waves. The nozzle is outlined and the chromatic temperature scale indicates increasing temperature from blue to red.

Later in the SERDP project a set of experiments were attempted to directly measure the plasma temperature using thermocouples. This was instantly met with a limiting complication that the most intense arc region of the plasma, an axial location where the majority of material removal occurs, is still at a relatively high electrical potential and carries a substantial level of current which directly interferes with the sensitive TC. Thus, direct measurements are limited to locations farther away from the arc region. An experiment was designed to characterize the temperature rise of a TC placed directly within the afterglow of the torch and the results are shown in Figure 10-25 and the time which the plasma is ignited has been normalized for all three measurements to be the same time, approximately 5 seconds. In all three cases there is a rapid increase in temperature as the TC is exposed to the plasma and in under approximately 4 seconds an equilibrated temperature is reached. The maximum temperature is 850 K (597 ^{o}C), 650 K (397 ^{o}C), and 550 K (297 ^{o}C) for the axial positions 20, 30, and 40 mm, respectively. As expected the highest temperature was reached at the closest location to the torch nozzle. These data are also indicative of the overall heating potential of the plasma torch with respect to distance, which is a critical operating parameter to consider if thermally sensitive substrates are treated or dozens of these devices are used in conjunction.

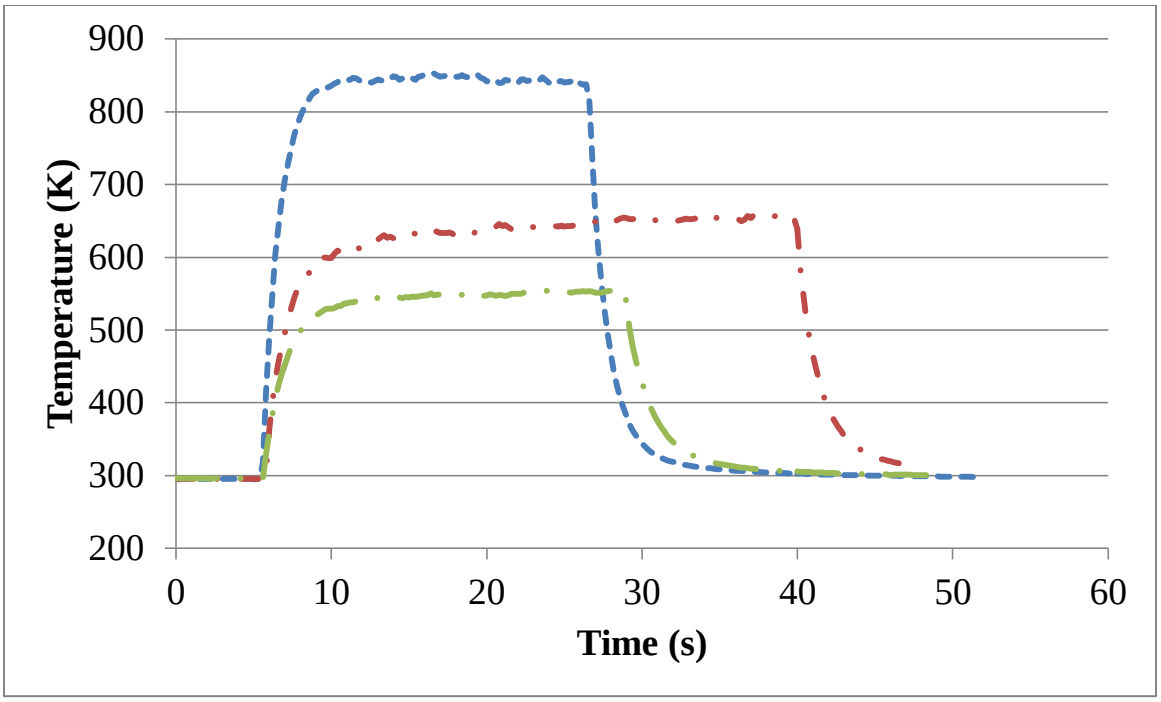

Figure 10-25: Thermocouple measurement of plasma at an axial distance of Z = 20mm **,** Z = 30 mm **, and** Z = 40 mm

As indicated by Figure 10-25 the plasma torch has a considerable amount of thermal energy that can easily be transferred to an object and raises a critical issue of thermal damage with the steel substrates. In order to address this issue, direct thermal measurements on the backside of a ¼" thick sample of DH36 steel were made and are given in Figure 10-26. These thermal measurements clearly indicate the capability of the plasma troch to heat much larger object as well as just TC, and the two pairs of TCs are in close agreement within each pair. As expected the TC directly opposite the torch shows the fastest rate of temperature increase and reaches the highest temperature compared to the other more distant locations. The equilibrated temperatures were selected at a time of 180 seconds and are approximately

530 K (267 ^{o}C), 380 K (107 ^{o}C), and 330 K (57 ^{o}C) for the 0, 25, and 75 mm positions, respectively. The notable issue here is the center point temperature increased over 200 K in roughly 60 seconds and represents a considerable amount of thermal energy being imparted to the substrate. It should be noted that even though this experiment was conducted over a relatively longer period of time with a static torch, as compared to a torch being rastered across the sample, there is the possibility of mechanical failure resulting in a static exposure, the combined thermal output of dozens of torches, and the fact that the measurements were made on the opposing side of the sample that was treated. The surface temperatures in the region under direct plasma treatment would certainly be significantly higher as evident by the presence of a crater and spatter.

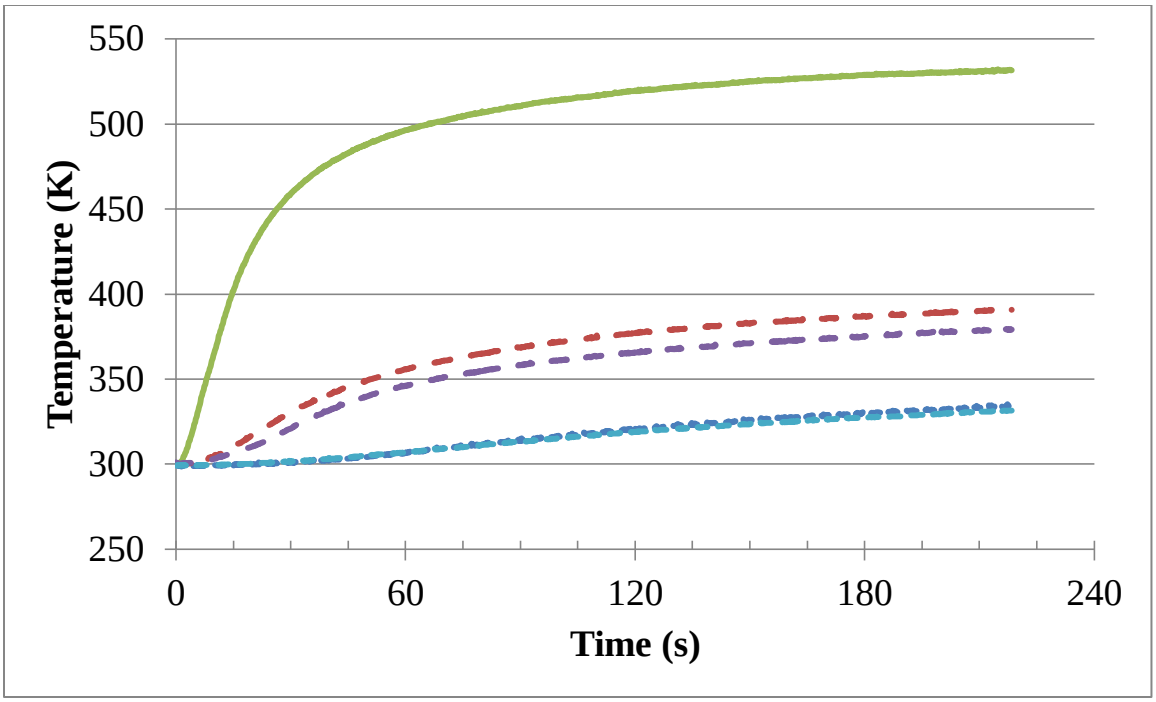

Figure 10-26: TC measurements on the backside of a 1/4" thick DH36 panel with the plasma standoff distance at 2 mm and the X=0 mm location indicates the center of the panel and the other locations are with respect to the center along the length of the panel. The individual locations are denoted as X=-75 mm, X=-25 mm, X=0 mm, X=+25 mm, and X=+75 mm, where each equivalent positive or negative location has the same line style.

10.7 Electrical

As stated previously it was not practical to make electrical measurements on the PF5K so measurements were conducted on the device constructed 'in-house' and powered by the DBD power supply. Typical current and voltage spectra for the described torch are shown in Figure 10-27 depicting a periodic waveform. The I/V waveforms are nearly in phase with each other indicating a resistive type of plasma discharge. From these data, it was calculated

that the RMS power is 598 W and the resistance across the plasma is 2 kΩ. One notable feature is the voltage spike during the initial rise or drop in potential. This feature has been hypothesized as a result of the increased potential needed to begin the gaseous breakdown process for either the primary arc column or one of the secondary arcs. As well, it could simply be an artifact of the power supply capacitor discharging. Further characterization and analysis is needed; however, this work will be left to the manufacture as it surely involves proprietary information.

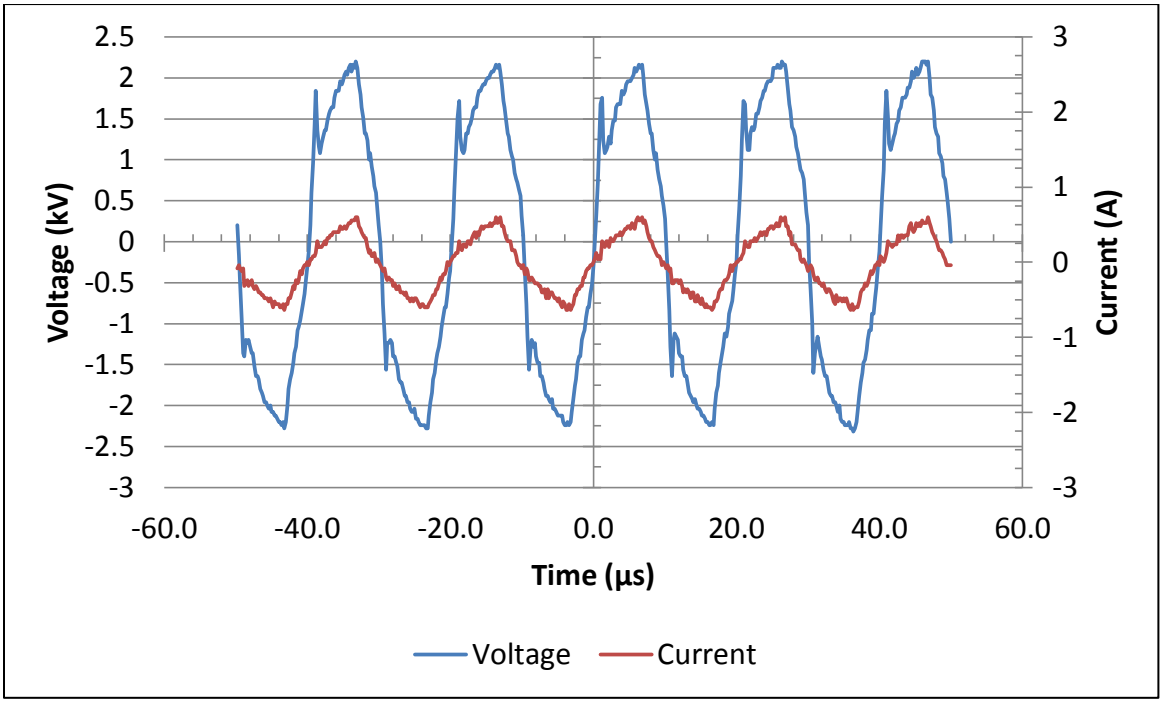

Figure 10-27: I/V characteristics of the IMST-Torch operating at 50 kHz and 50 SLM with a RMS power of 598 W and resistance of 2 kΩ

11 Discussion

The PlasmaFlux™ technology has been proven effective at removing the two US Navy freeboard and antifouling paint systems from steel substrates. The process of scale-up and implementation has several issues that need to be addressed. Firstly, the removal rates need to be comparable to the existing grit blast rates. Extrapolating on mass removal with the assumption that each pass on the 4"x6" sample removed 0.5 g at a velocity of 10 mm/s results in a mass removal rate of 0.18 kg hr^{-1} and if an aircraft carrier has 15,000 kg of paint it would take over 83,000 nozzle*hours to remove all the paint. Compared to 3,000 nozzle*hours for grit blasting it would take an equivalent of 28 plasma devices. The other approach is comparing the effective area removal rates with a grit blasting rate of 270 ft^2hr^{-1} and an estimated 3 ft^2hr^{-1} from AP Solutions would require 90 nozzles to reach an equivalent removal rate to grit blasting. The number of nozzles begins to raise the issue of whether the implementation will remain manual operation as with the current grit blasting or transition to a more automated operation. The issue here is number of nozzles that can be grouped into a single device that is a size and weight that an operator can easily manipulate for an entire 8-hr shift or the number of additional operators that would be required to match the current removal rates. Another issue facing the manual or automated operation is the control of separation distance between the nozzle and surface. The data presented on the removal rates of HDPE with respect to axial distance shows a strong negative dependence wherein at the closer axial positions that are associated with the highest removal rates a small change in position of only 1 mm will result in a >200% reduction in removal rates compared to the axial positions around 10 mm from the nozzle where a ±5 mm change results in only a 20%

change in removal rates. While the closer axial locations might be appealing for higher removal rates, the slightly farther axial locations would likely be better for overall constancy and uniformity in the removal process. Either axial location demonstrates a need for precise control over the separation distance as a manual operator would likely have difficulty maintaining a separation distance of 1 mm or even 1 cm with some as large and heavy as a multi-nozzle plasma device for an 8-hr shift and over such a large treatment area. One possible solution would be to add a mechanical standoff to maintain a proper distance and another would be to have a semi-automated plasma device that has the critical operational parameters such as standoff distance computer controlled and the actual movement controlled remotely by the operator.

The next major issues facing the scale-up issue are the after-effects of the plasma treatment. Firstly, from the thermal data presented in this dissertation a single plasma nozzle is capable of raising the bulk temperature of a ¼“ thick steel sample by several hundred degrees. This heating effect can be lessened by increasing the velocity of the plasma across the sample; however, if there are possibly dozens of such devices treating the surface of a ship there could still be thermal damage induced into the steel hull. To address this, computer modeling could be applied to determine the conditions under which the heat flux would exceed safety levels and have an automatic interlock that would trip whenever any of these conditions were met. The next issue is whether the treated surface is sufficient to recoat with the next paint application. The surface analysis showed that the plasma treated samples were cleaner than the grit blasted samples with respect to surface contaminations. Additionally, the GAXRD indicated that the slight blue-ish discoloration of the surface

following plasma treatment is the presence of a hematite and magnetite iron oxide layer. This layer has been qualitatively proven to be more stable than the freshly grit blasted surface that is prone to flash rusting with several plasma treated sample that have been exposed to the ambient lab air for months with no signs of rust formation. Quantitatively, the surfaces have been proven to be no worse than grit blasted samples through the coating adhesion, alternate immersion, and salt fog tests that were completed to the full time required and in some cases the tests were extended even longer with no adverse effects noticed. Further tests on the residual oxide surface should determine the length of time and other parameters allowing the surface to remain conducive to paint application giving the operators responsible for both pain removal and coating more flexibility. The other problem with the after-effects of the plasma treatment is the production of hazardous and even toxic gases. Even the free flowing plasma that is not treating any material forms a noticeable amount of NO_X which can be an irritant and even lethal. That combined with the presence of the cyanide ion, CN, while treating organic material presents a clear danger to any operators. These toxic gases can be controlled through sufficient exhaust handling; however, active monitoring should be employed to ensure no leaks or accidental buildups occur. Future work to address these after-effect issues need to investigate the amount and composition of the exhaust gases quantitatively using mass spectrometry.

The parametric study was confined to a relatively small controllable range but nonetheless identified a slight increase in removal rates with increasing gas flow and power, and a slight decrease in the removal rates with respect to increasing frequency. While any discussion on why the changes in removal rate occur with the PF5K parameters, amounts to

assumption and speculation; because only the parameter inputs are known and the outputs such as voltage and current are not able to be measured. However, extrapolations can be made using the NCSU lab built plasma torch powered by the DBD power supply since it was possible to connect electrical probes and the operation of the both plasma torches are similar and the power supplies, while different, are assumed to be equivalent in operation. The power was obtained using $P = V_{RMS} I_{RMS}$ by measuring the current and voltage directly at the torch and was analyzed as a function of frequency and gas flow as shown in Figure 11-1. Characterization of the power as a function of gas flow was completed by fixing the frequency at the power supply to 100 kHz and varied the gas flow from 40-140 SLM and power as a function of frequency was determined by fixing the gas flow to 50 SLM and varying the frequency at the power supply from 30-150 kHz.

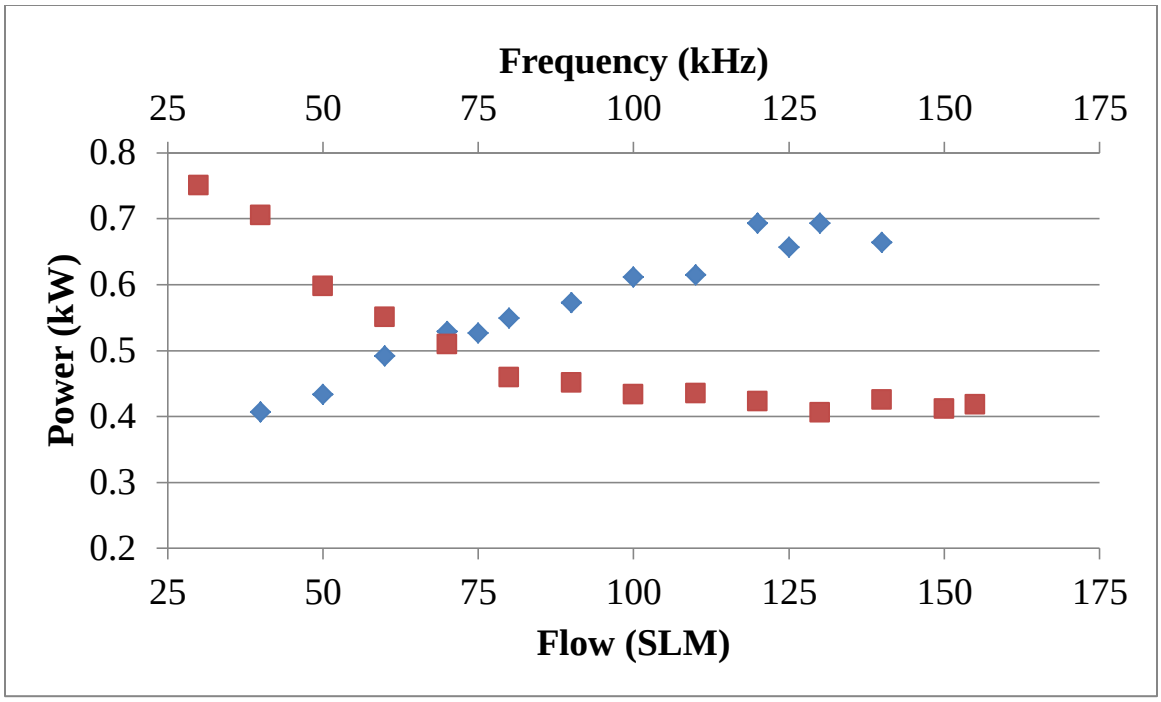

Figure 11-1: The power delivered to the torch as function of flow for a fixed frequency of 100 kHz (◆) corresponding to the bottom axis and as a function of frequency at a fixed flow of 50 SLM (■) corresponding to the top axis.

The parameter ranges were selected based on viable plasma torch operation such that the plasma would exist over the gas flow range and the frequency range was confined to what the power supply could output. From this graph it is apparent that as the gas flow increases there is an increase of 60% in power. The effect of increased gas flow literally pulling more current can be explained by the plasma arc column, which is the conductive pathway that the current follows and is comprised of a certain density of ionized charge carriers that is in some sort of equilibrium between the length and diameter of the arc column and the output of the power supply. As an uptick in the gas flow increases the total number of molecules present

the effective number density of the charge carriers decreases resulting in an increase in the resistance. Following Ohm's Law, $V = IR$, if the power supply is voltage limited or held constant then an increase in resistance will result in a decrease in current and conversely if the power supply is current limited or held constant then an increase in resistance will result in an increase in the voltage. The latter is shown to be the case by comparing the current and voltage waveforms from Figure 11-2, that were obtained at a frequency of 100 kHz and power level of '200 V'. As shown in Figure 11-2 there is little variance in the current over the range of gas flow, whereas the voltage amplitude noticeably increases with respect to increasing gas flow. Comparing this to the uptick in removal rates using the PF5K over the range of gas flows indicates that there is a positive correlation to power.

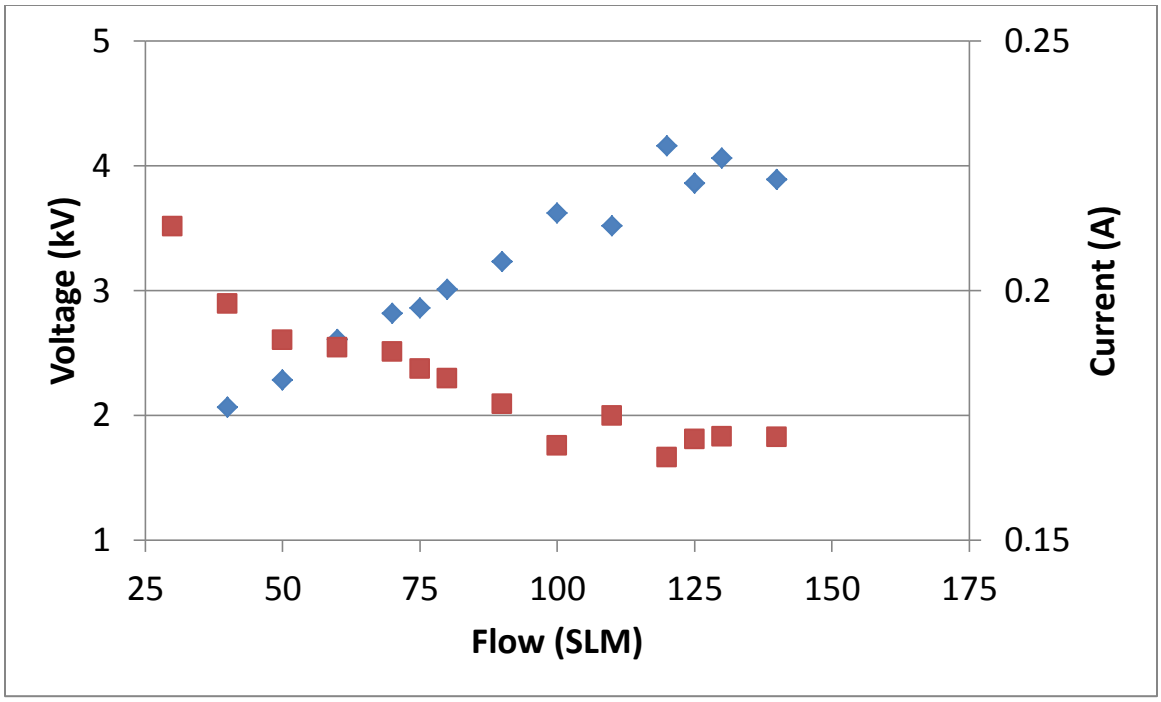

Figure 11-2: The RMS voltage (◆) and current (■) as a function of flow at a set frequency of 100 kHz and power level of '200 V'.

The effect of increasing frequency on current and voltage is shown in Figure 11-3 for a set gas flow of 50 SLM and power level of '200 V'. The current exhibits a rapid decrease from 30-80 kHz followed by a more gradual decrease from 80-155 kHz, whereas the voltage exhibits a fairly steady increase over the entire 30-155 kHz range. Combining this with the relatively stable but still negative relationship between power and frequency over the range 90-110 kHz that the PF5K is able to operate is expressed in the slight negative relationship between the removal rates of the PF5K and frequency.

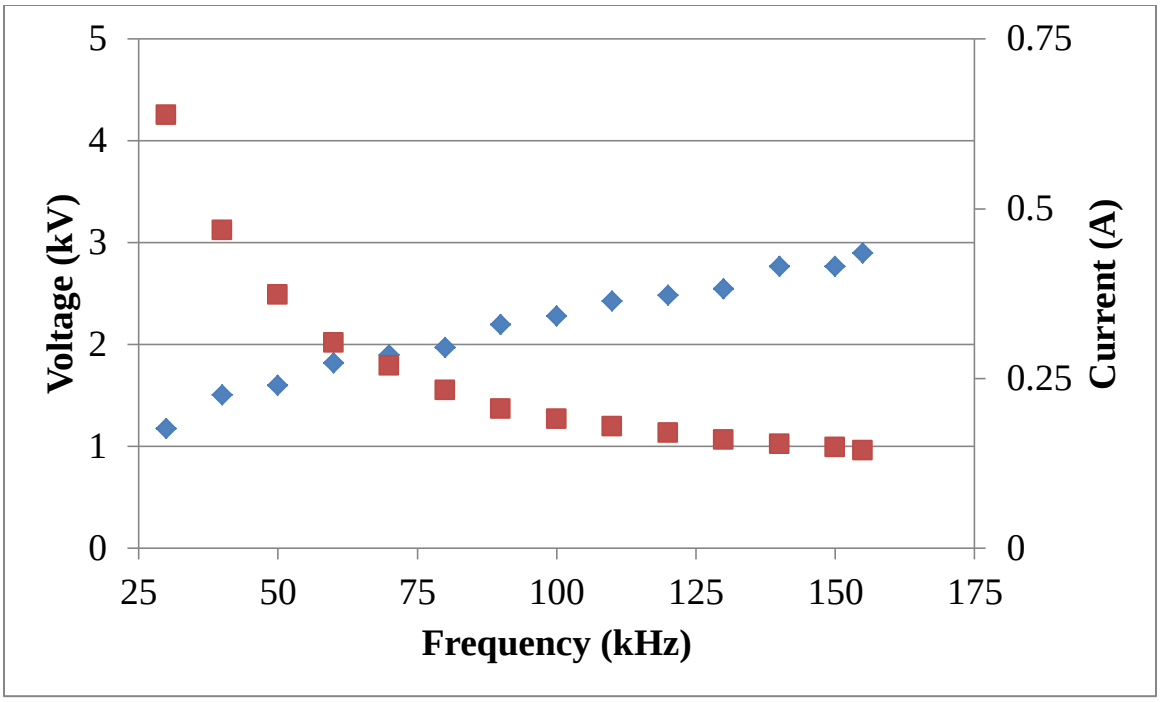

Figure 11-3: The RMS voltage (◆) and current (■) as a function of frequency for a set gas flow of 50 SLM and power level of '250 V'.

As the power transferred to the plasma increases, so follows the removal rates. While that can be stated, it remains unknown what the additional power changes within the plasma to enhance the removal rate. There exist several possibilities to account for the additional power. One possible mechanism is Joule heating, also known as ohmic heating and resistive heating, of the gas, whereby current passing through a resistor dissipates energy as heat. This process could enhance removal by storing more energy in the rotational and vibrational states that comprise the energy reservoirs of molecular nitrogen; also depending on the level of Joule heating there is the possibility for increased ionization. Both of these mechanisms provide more energy, whether it is stored in metastable nitrogen reservoirs or in ionized

species, to react with the target material. Another possibility is that the additional power expands the arc column essentially creating a wider plasma and thus a larger interaction region between the plasma and the target material that would still result in a higher removal rate.

Further experiments should investigate what the additional power changes within the plasma as a method to determine the underlying removal mechanisms. The experiments should be based on a plasma system such as the torch developed by the NCSU L-IMST research group powered by the DBD Power Supply or another system with at least the same range of parameter control or more if possible. Characterization of the plasma parameters should continue by firstly looking at the volume of the plasma both radially and axially as well as the sizes of the primary arc and the afterglow region. Initially this could be done using a digital imaging setup; however, it should then be followed by another round of spatially resolved OES to determine the spatial range of the significant emitting species. The various temperature measurement techniques, such as spectroscopic rotational, vibrational, and Boltzmann calculations as well as direct thermocouple measurements, should also be reevaluated as a function of the various parameters. These results should then be compared to the removal rates obtained under identical operational conditions to identify the variable and the resulting plasma parameter(s) that are responsible for the change in removal rates.

Regarding the OES data and analysis, it is important to keep in mind that much of the emission profiles are qualitative in nature due to the myriad of complex ionization pathways. Another complication with the analysis of emission spectra is the optical thickness of the

plasma. As it pertains to plasma spectroscopy it is a description of how transparent the plasma is to light or other electromagnetic radiation. In the case of emission spectroscopy optical thickness can incorporate self-absorption wherein the photons emitted by the de-excitation of one plasma specie are absorbed by another specie with a similar energy level before the photon escapes the plasma region and is able to be measured. The optically thin plasma has a photon mean free path that is much longer than a characteristic length or the plasma diameter and the self-absorption is negligible. The optically thick plasma has a photon mean free path that is much shorter than a characteristic length or the plasma diameter and the self-absorption is significant.[88] The absorbed photon is not necessarily re-emitted at the same wavelength as in higher pressure plasma there are numerous pathways capable of dissipating part or all of the energy from the absorbed photon. Thus the observed emission intensity of an optically thick plasma would be at a reduced value of the theoretical unobstructed intensity.

The optical thickness can be checked using an experimental setup shown in Figure 11-4. The first step is obtaining an emission spectrum from a free flowing plasma making sure that there are no reflective surfaces behind the plasma region that is being characterized. Then, a mirror is placed behind the plasma such that it reflects the emitted light back through the plasma toward the spectrometer setup and a second spectrum is acquired. A simple comparison of the two intensities should give an indication of the optical thickness. If the emission intensity doubles then the plasma is optically thin, however, if the emission intensity does not increase by an appreciable amount then the plasma is reabsorbing the reflected light emission and is optically thick.

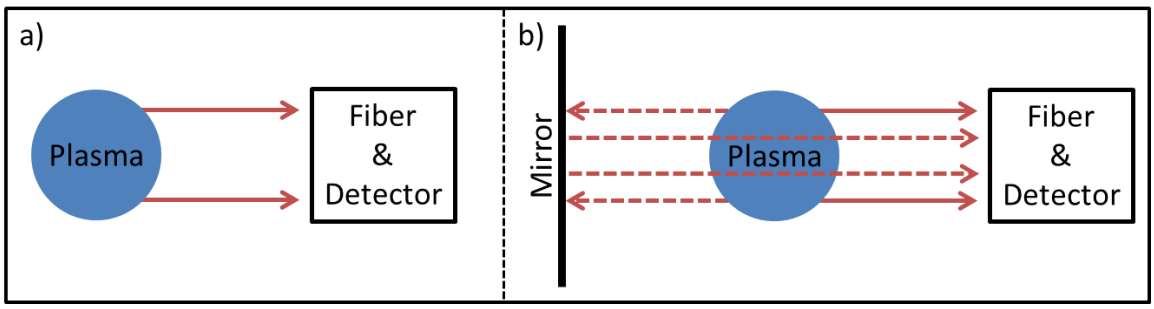

Figure 11-4: Experimental setup to determine optical thickness where panel a) depicts the plasma emission with solid arrows incident on the spectrometer setup and panel b) depicts a mirror behind the plasma and the addition of light emission from the other side of the plasma denoted with dashed arrows that are then reflected toward the spectrometer setup.

The removal mechanisms of the plasma treatment process are part of the main objective of this dissertation. Initially, the commonly held theory postulated that the sole removal mechanism was chemical oxidation of the organic matrix by the atomic oxygen, within the plasma region, according to the following reaction:

$$O + \left[R - CH_2 - R\right] \rightarrow CO_2 + H_2O\,.$$

While this reaction is certainly possible given the species present in the plasma arc, comparison of the removal rates with the emission intensity indicated that there is a strong correlation between the removal rate and the intensity of several different atomic and molecular species, specifically the atomic oxygen and molecular nitrogen. Based on these correlations, a new theory was developed to expand the mechanisms responsible for material removal to provide a more comprehensive theory. Given that the removal rates tracked solidly with emission intensity, the removal mechanism was altered to consider the

possibility of an energy transfer between the excited species within the plasma region and the target material producing volatile products that are capable of leaving the substrate, as described in the generalized reaction:

$$E\left(Plasma\right)+\left[R-CH_2-R\right]\rightarrow \text{Products}.$$

Wherein, the plasma energy could be a variety of energy states such as the rotational, vibrational, and electronic levels of atomic and molecular species as demonstrated by the nitrogen metastable species being commonly referred to as energy reservoirs. The actual removal is thought to occur as the energetic particles are effectively quenched during the interaction with the target material, thereby transferring the stored plasma energy to the bonds between the atoms of the target material. If this transferred energy is greater than or equal to the bond energy, then the bond will dissociate, scissioning the organic matrix into either smaller isolated particles that are removed via gas flow or lower molecular weight fragment that is able to be volatilized.

Experiments that focused on acquiring emission spectra of the plasma-material interaction region were conducted during plasma treatment of HDPE. The intent was not necessarily to provide spatially resolved spectra or detailed information about the interaction region, rather the goal was to identify the presence of species that had been ionized or excited by the plasma. The spectra were analyzed and it was determined that the additional prominent emission features were a result of CN, C_2, and H_2. There are several emissions that arise from CO within the UV-VIS-NIR region that is observable with the spectrometer used in characterizing the experiments; however, no prominent emission features were

identified as CO. This is not to say that there are no CO or CO_2 emissions from the plasma interaction with HDPE, just that the with the spectrometer and peak identification software none were identified. Given the presence of CN, several gas composition experiments were conducted that diluted the normal compressed air feed gas with nitrogen to investigate the removal rate as a function of oxygen. The results presented that in actuality even in the complete absence of oxygen the removal rates remained at approximately 50% of the original values. Incorporating the anoxic material removal and the presence of reaction products in the emission spectra into the removal mechanism provide the following reactions:

$$N + \left[R - CH_2 - R\right] \rightarrow CN + C_2 + H_2$$

$$N_2^* + \left[R - CH_2 - R\right] \rightarrow CN + C_2 + H_2 .$$

Additionally, there could be contributions to the removal rate from free electrons, energetic photons, or reactions involving NO_X and the organic matrix. In summary, the revised removal mechanisms theory includes the likelihood that the contribution from the oxygen species is oxidation and contributes to the overall removal rate and that a substantial amount of the removal is due to the reaction of either atomic or molecular nitrogen with the organic matrix. Supplementary experiments could further identify the products produced from the plasma treatment using higher resolution OES in an attempt to better resolve the peaks and devise a spectrometer setup that is able to analyze the IR region where the majority of the CO and CO_2 emission regions reside. As mentioned before, mass spectroscopy would give a much clearer representation of the gaseous products being produced. Another

approach is to augment the gas composition experiments assuming the plasma torch is able to operate under multiple gas compositions, by diluting N_2 with Ar to determine and isolate the contribution from nitrogen. Other gas compositions that should be addressed are increasing the O_2 concentration in either a N_2 or Ar feed gas to establish if there is an equivalent increase in the removal rate.

12 Conclusion

The plasma torch has proved to be effective at removing the two common paint systems used by the US Navy. The plasma device that was available for characterization (PlasmaFlux 5000) does not have a wide range of controllable parameters and the narrow range had a minimal effect on the removal rate of HDPE. The strongest factor affecting the removal rate remains the distance between the nozzle and substrate. The investigation into the presence of inorganic fillers in the HDPE matrix yielded that the simple presence of inorganic fillers has negligible effect on removal rate. This could be different if binders are used between the matrix and fillers.

Optical emission spectroscopy is a useful non-invasive technique that can be employed to characterize this type of plasma torch. Through the analysis of the spectra it was determined that the torch produces a fairly thermal plasma with a rotational temperature of 8,570 K and a temperature of 7,400 K as determined by Boltzmann method. There is also a significant 'non-thermal' region of the plasma, the afterglow region, producing large amounts of NO_x.

It was observed that the removal rate does not track with the rotational temperature but tracks well with the emission intensity of several molecular and atomic species. From these results the theory that the removal rate was a sole function of chemical oxidation was called into question and it was hypothesized that the removal mechanism is a combination of several different pathways with a considerable contribution coming from the energy reservoir of excited molecular nitrogen species. Altering the gas composition from air to completely

nitrogen does decrease the overall removal rate but, importantly, not to the extent expected if the mechanism was due to only chemical oxidation. Instead the removal rates stayed well within an order of magnitude, more precisely the completely nitrogen plasma remained to within 50% of the removal rates obtained in air. The non-oxidation mechanism theory for removal is supported by the presence of CN, C_2, and H in the optical emission spectra of the torch obtained during plasma treatment of HDPE samples.

It is my conclusion that this type of plasma torch is a reasonable device for the removal of the typical freeboard and antifouling paint stacks used by the US Navy. The conclusion is stated in the context that there are still critical issues that must be resolved before this technology can be implemented as field deployable. Limiting issues include problems with the scalability from a single laboratory device to a more massive device capable of treating an aircraft carrier in a reasonable time frame. The sensitivity of the removal rate with respect to axial position needs to be addressed as a minor change of a couple millimeters can lead to a substantial reduction in removal rate. There are also several safety concerns including the production of hazardous microscopic particulates, synthesis of toxic gaseous by products such as CN and NO_x, the capability of the products forming highly acid solutions with surrounding water or water vapor, and a serious potential hazard of high voltage and high current that could be catastrophic not only to operators near the application but anyone located anywhere along the electrically conductive ship hull and any electronic equipment that is not sufficiently protected. Additionally, there remains a safety issue with respect to the ship coming from the potential of thermal damage to the steel hull.

Future work should focus on not only identifying the previously mentioned concerns but also continue investigating the removal mechanism reaction pathway and kinetics. Other research completed with this plasma torch, though not fully discussed in this dissertation, that warrant consideration include surface activation for enhanced adhesion and chemical bonding, the production of highly acidic solutions through plasma treatment of water, and the dual capability for surface oxidation and reduction of metal oxides.

13 References

1 *About the Semiconductor Industry Association*, <http://www.sia-online.org/about/about-the-semiconductor-industry-association/> (2012).

2 Nae-Man Park, T.-S. K., and Seong-Ju Park. Band gap engineering of amorphous silicon quantum dots for light-emitting diodes. *Applied Physics Letters* **78**, 2575-2577 (2001).

3 C.C. Wu, C. I. W., J.C. Sturm, and A. Kahn. Surface modification of indium tin oxide by plasma treatment: An effective method to improve the efficiency, brightness, and reliability of organic light emitting devices. *Appl. Phys. Lett.* **70**, 1348-1350 (1997).

4 Kenji Yamamoto, A. N., Masashi Yoshimi et. al. A high efficiency thin film silicon solar cell and module. *Solar Energy* **77**, 939-949 (2004).

5 Aberle, A. G. Thin-film solar cells. *Thin Solid Films* **517**, 4706-4710 (2009).

6 Won Seok Choi, J. H., Ilsub Chung, Byungyou Hong. The effect of RF power on tribological properties of the diamond-like carbon films. *Thin Solid Films* **475**, 287-290 (2005).

7 Jiaren Jiang, R. A., Jin Tong. Some special tribological features of DLC coatings deposited on soft substrates. *Wear* **211**, 254-264 (1997).

8 S. Mandl, B. R. Improving the biocompatibility of medical implants with plasma immersion ion implantation. *Surface and Coatings Technology* **156**, 276-283 (2002).

9 Napartovich, A. P. Overview of Atmospheric Pressure Discharges Producing Nonthermal Plasma. *Plasmas and Polymers* **6** (2001).

10 Liu, Y. W. a. C.-j. Plasma Methane Conversion in the Presence of Dimethyl Ether Using Dielectric-Barrier Discharge. *Energy & Fuels* **19**, 877-881 (2005).

11 Shigeru Kado, K. U., Yasushi Sekine, Kaoru Fujimoto. Direct conversion of methane to acetylene or syngas at room temperature using non-equilibrium pulsed discharge. *Fuel* **82**, 1377-1385 (2003).

12 Michael Tendler, P. R., and Guido van Oost. Plasma based waste treatment and energy production. *Plasma Physics and Controlled Fusion* **47**, A219-A230 (2005).

13 Hershcovitch, A. High-pressure arcs as vacuum-atmospher interface and plasma lens for nonvacuum electron beam welding machines, electron beam melting, and nonvacuum ion material modification. *J. Appl. Phys* **78**, 5283-5288 (1995).

14 Ady Hershcovitch, A. T. Air boring and nonvacuum electron beam welding with a plasma window. *Physics of Plasmas* **12** (2005).

15 Hershcovitch, A. Non-vacuum electron beam welding through a plasma window. *Nuclear Instruments and Methods in Physics Research B* **241**, 854-857 (2005).

16 B.T. Pinkoski, I. Z., A. Herscovitch, E.D. Johnson, and D.P. Siddons. X-ray transmission through a plasma window. *Review of Scientific Instruments* **72**, 1677-1679 (2001).

17 Geoff Lloyd, G. F., Syed Jafri, Greg Shultz, Alex Fridman, and Keith Harding. Gas Plasma: Medical Uses and Developments in Wound Care. *Plasma Processes and Polymers* **7**, 194-211 (2009).

18 J.F. Kolb, A. A. H. M., R.O. Price, R.J. Swanson, A. Bowman. Cold atmospheric pressure air plasma jet for medical applications. *Applied Physics Letters* **92**, 241501 (2008).

19 Laroussi, M. Sterilization of Contaminated Matter with an Atmospheric Pressure Plasma. *IEEE Transactions on Plasma Science* **24**, 1188-1191 (1996).

20 Christopher S. Henshilwood, F. d. E., Karen L. van Niekerk, Yvan Coquinot, Zenobia Jacobs, Stein-Erik Lauritzen, Michel Menu, Renata Garcia-Moreno. A 100,000-Year-Old Ochre-Processing Workshop at Blombos Cave, South Africa. *Science* **334**, 219 (2011).

21 McWilliams, A. J. (Norfolk, VA, USA, 2011).

22 Bill Ross, J. B., Chris Fromme. A Semi-Autonomous Robot for Stripping Paint from Large Vessels. *The International Journal of Robotics Research* **22**, 617-626 (2003).

23 Schweitzer, P. A. *Paint and Coatings: Applications and Corrosion Resistance*. (Taylor & Francis Group, LLC, 2006).

24 Thomas J. Rocket, V. R. *The Causes of Boat Hull Blisters* (Washington, D.C., 1987).

25 Wigren, J. Technical Note: Grit Blasting as Surface Preparation Before Plasma Spraying. *Surface and Coatings Technology* **34**, 101-108 (1988).

26 Institution, W. H. O. & Ships, U. S. N. D. B. o. *Marine fouling and its prevention*. Vol. Chapter 9 (George Banta Publishing Co., 1952).

27 Institution, W. H. O. & Ships, U. S. N. D. B. o. *Marine Fouling and Its Prevention*. Vol. Chapter 1 (George Banta Publishing Co., 1952).

28 Biofouling Prevention Coatings. (2009). <http://www.onr.navy.mil/~/media/Files/Fact%20Sheets/Hull-Coatings.ashx>.

29 M.P. Schultz, J. A. B., E.R. Holm, and W.M. Hertel. Economic impact of biofouling on a naval surface ship. *Biofouling* **27**, 87-98 (2011).

30 Jackson, L. Marine Biofouling & Invasive Species: Guidelines for Prevention and Management. (2008).

31 L.D. Chambers, K. R. S., F.C. Walsh, R.J.K Wood. Modern approaches to marine antifouling coatings. *Surface & Coatings Technology* **201**, 3642-3652 (2006).

32 Institution, W. H. O. *Marine fouling and its prevention*. Vol. Chapter 11 (George Banta Publishing Co., 1952).

33 Gabbay, G. B. a. J. Copper, An Ancient Remedy Returning to Fight Microbial, Fungal, and Viral Infections. *Current Chemical Biology* **3**, 272-278 (2009).

34 Kotrikla, A. Environmental management aspects for TBT antifouling wastes from the shipyards. *Journal of Environmental Management* **90**, S77-S85 (2009).

35 Antizar-Ladislao, B. Environmental levels, toxicity and human exposure to tributyltin (TBT)-contaminated marine environment. A review. *Environment International* **34**, 292-308 (2008).

36 Kirill Efimenko, J. F., Maureen E. Callow, James A. Callow, and Jan Genzer. Development and Testing of Hierarchically Wrinkled Coatings for Marine Antifouling. *Applied Materials & Interfaces* **1**, 1031-1040 (2009).

37 in *Detailed Specification: Paint, Epoxy-Polyamide, General Specification For* (2009).

38 in *Performance Specification: Coating Systems, Weather-Resistant, Exterior Use* (2009).

39 in *Performance Specification: Paint System, Anticorrosive and Antifouling, Ship Hull* (2006).

40 B. Djurovic, E. J. M. P., P. Tangestanian, J.K. Spelt. Coating removal from fiber-composites and aluminum using starch media blasting. *Wear* **224**, 22-37 (1999).

41 Joseph Kozol, S. T. a. K. C. The effects of plastic media blasting paint removal on the microstructure of graphite/epoxy composite materials. Report No. NADC-88109-60, (1988).

42 Deng Jianxin, F. Y., Ding Zeliang, Shi Peiwei. Wear behavior of ceramic nozzles in sand blasting treatments. *Journal of the European Ceramic Society* **23**, 323-329 (2003).

43 Datar, S. Vol. Paper 48 (University of New Orleans, 2008).

44 Beth Rosenberg, L. Y., Scott Fulmer. Ergonomics of abrasive blasting: A comparison of high pressure water and steel shot. *Applied Ergonomics* **37**, 659-667 (2006).

45 Alan Echt, K. H. D., and R. Leroy Mickelsen. Automated Abrasive Blasting Equipment for Use on Steel Structures. *Applied Occupational and Environmental Hygiene* **15**, 713-720 (2000).

46 J. R. Martin, A. A. W., & K. E. Lucas. in *Tri-Service Corrosion Conference*.

47 Forbes, D. J. *Characteristics and Treatment of Wastewater Generated during Underwater Hull Cleaning Operations of U.S. Navy Ships* Master of Science in Civil Engineering thesis, University of Maryland College Park, (1996).

48 STAR4D. A Case Study: Ultrahigh Pressure Water Stripping versus Soda Abrasive Blasting for Paint Removal on Military Ground Vehicles. (2003).

49 (ISO), I. O. f. S. in *Part 4: Types of surface and surface preparation* 22 (ISO, Geneve, Switzerland, 1998).

50 Momber, A. Colour-based assessment of atmospheric corrosion products, namely of flash rust, on steel. *Materials and Corrosion* **61**, 1-10 (2010).

51 Henry Leidheiser, J. a. I. C.-N. A Mossbauer Spectroscopic Study of Rust Formed During Simulated Atmospheric Corrosion. *Corrosion Science* **24**, 569-577 (1984).

52 Moavin Islam, W. M., James Tagert, Jim Ellor, and Michael Evans. in *SSPC (Society for Protective Coatings).*

53 Francois Brygo, C. D., F. Le Guern, R. Oltra, A Semerok, J.M. Weulersse. Laser fluence, repetition rate and pulse duration effects on paint ablation. *Applied Surface Science* **252**, 2131-2138 (2006).

54 Walters, C. T. in *Proceeding of SPIE*. 567-575 (High-Power Laser Ablation III).

55 M.J.J. Schmidt, L. L., J.T. Spencer. An investigation into the feasibility and characteristics of using a 2.5 kW high power diode laser for paint stripping. *Journal of Materials Processing Technology* **138**, 109-115 (2003).

56 Baann, T. A. Method and Device for Removing Coatings on a Metal Structure. United States patent US 7,857,914 B2 (2010).

57 Bass, R. Portable Stripping Head Induction Heating System for Stripping Coated and Lined Metal Objects and Surfaces and Methods for Stripping Coated Metal Objects and Surfaces. US patent US 6,700,104 B2 (2004).

58 RockMagnetist. (ed Stoner Wohlfarth Main Loop) (Wikipedia, 2010).

59 F. Douglas Witherspoon, R. W. K., Dennis W. Massey. Pulsed plasma jet plasma removal. USA patent 5,970,993 (1999).

60 Rutledge, B. A. B. S. K. Atmospheric pressure method and apparatus for removal of organic matter with atomic and ionic oxygen. USA patent 5,693,241 (1997).

61 Rutledge, B. A. B. S. K. Process for non-contact removal of organic coatings from the surface of paintings. USA patent 5,560,781 (1996).

62 Selwyn, G. S. Atmospheric-Pressure plasma jet. USA patent 5,961,772 (1999).

63 G.R. Nowling, S. E. B., V. Jankovic, R.F. Hicks. Remote plasma-enhanced chemical vapour deposition of silicon nitride at atmospheric pressure. *Plasma Sources Sci. Technol.* **11**, 97-103 (2002).

64 A. Ladwig, S. B., M. Smith, M. Hester, W. Highland, R. Koch, R. Hicks. Atmospheric plasma deposition of glass coatings on aluminum. *Surface & Coatings Technology* **201**, 6460-6464 (2007).

65 John R. Roth, P. P. T., Chaoyu Liu, Mounir Laroussi, Pauld D. Spence. One atmosphere, uniform glow discharge plasma. USA patent 5,414,324 (1995).

66 John R. Roth, P. P. T., Larry C. Wadsworth, Chaoya Liu, Paul D. Spence. Method and apparatus for glow discharge plasma treatment of polymer materials at atmospheric pressure. USA patent 5,403,453 (1995).

67 Kin Li, M. T. Handheld atmospheric pressure glow discharge plasma source. USA patent 5,977,715 (1999).

68 Kin Li, a. M. T. Surface Modification Using and Atmospheric Pressure Glow Discharge Plasma Source. US patent 5,928,527 (1999).

69 Guo, S. N.-N. a. W.-G. Thermomechanical response of DH-36 structural steel over a wide range of strain rates and temperatures. *Mechanics of Materials* **35**, 1023-1047 (2003).

70 Nemat-Nasser, M. R. A. a. S. Micromechanisms of ductile fracturing of DH-36 steel plates under impulsive loads and influence of polyurea reinforcing. *Int. J. Fract.* **162**, 205-217 (2010).

71 M.A. Legodi, D. d. W. The preparation of magnetite, goethite, hematite and maghemite of pigment quality from mill scale iron waste. *Dyes and Pigments* **74**, 161-168 (2007).

72 R. Naderi, M. M. A., & M.H. Moayed. EIS examination of mill scale on mild steel with polyester-epoxy powder coating. *Progress in Organic Coatings* **50**, 162-165 (2004).

73 Crookes, W. On a Fourth State of Matter. *Proceedings of the Royal Society of London* **30**, 469-472 (1880).

74 Crookes, W. On Radiant Matter. *The Popular Science Monthly*.

75 Langmuir, I. Oscillations in Ionized Gases. *Proceedings of the National Academy of Sciences of the United States of America* **14**, 627-637 (1928).

76 Sir William Slingo, A. B. *Electrical Engineering for Electrical Light Artizans and Students*. (Spottiswoode and Co., 1891).

77 Edison, T. A. Electric-Lamp. USA patent 223,898 (1880).

78 Edison, T. A. Fluorescent Electric Lamp. USA patent 865,367 (1896).

79 Batishchev, O. V. Minihelicon Plasma Thruster. *IEEE Transactions on Plasma Science* **37**, 1563-1571 (2009).

80 Kazutake Taniguchi, T. F., Hiroyuki Yoshiki, & Yasuhiro Horiike. Generation of Integrated Atmospheric-Pressure Microplasmas. *Japanese Journal of Applied Physics* **42**, 6584-6589 (2003).

81 Laroussi, M. Nonthermal Decontamination of Biological Media by Atmospheric-Pressure Plasmas: Review, Analysis, and Prospects. *IEEE Transactions on Plasma Science* **30**, 1409-1415 (2002).

82 Kennedy, A. F. a. L. A. *Plasma Physics and Engineering*. (Taylor & Francis Group, 2011).

83 Penning, M. J. D. F. M. The Mechanism of Electrical Discharges in Gases of Low Pressure. *Reviews of Modern Physics* **12**, 87-174 (1940).

84 Raether, H. *Electron Avalanches and Breakdown in Gases*. (Butterworth Inc., 1964).

85 Loeb, L. B. *Electrical Coronas: Their Basic Physical Mechanisms*. (University of California Press, 1965).

86 Craggs, J. M. M. a. J. D. *Electrical Breakdown of Gases*. (John Wiley & Sons, Ltd., 1978).

87 Somerville, J. M. *The Electrical Arc*. (John Wiley & Sons Inc., 1959).

88 Hoyaux, M. F. *Arc Physics*. (Springer-Verlag, 1968).

89 Kennedy, A. F. a. L. A. *Plasma Physics and Engineering*. (Taylor & Francis Group, 2001).

90 Milan Hrabovsky, M. K., Vladimir Kopecky, and Viktor Sember. Processes and Properties of Electric Arc Stabilized by Water Vortex. *IEEE Transactions on Plasma Science* **25**, 833-839 (1997).

91 Kobayashi, Y. A. a. A. Application of a gas tunnel to high-energy-density plasma beams. *J. Appl. Phys.* **59**, 3039-3044 (1986).

92 F.X. Lu, G. F. Z., J.G. Sun, Y.L. Fu, W.Z. Tang, J.J. Wang, G.H. Li, J.M. Zang, C.H. Pan, C.X. Tang, T.L. Lo, and Y.G. Zhang. A new type of DC arc plasma torch for low cost large area diamond deposition. *Diamond and Related Materials* **7**, 737-741 (1998).

93 (ed Nozzle de Laval diagram.svg) (Wikipedia, 2008).

94 B.E. Djakov, R. E., D. Oliver. Supersonic Jets with Periodic Structure due to Arc plasma Expansion into a Low pressure ambient. *Contrib. Plasma Phys.* **37**, 57-76 (1997).

95 M. Gindrat, J.-L. D., Ch. Hollenstein, A. Refke, G. Barbezat. Characterization of supersonic low pressure plasma jets with electrostatic probes. *Plasma Sources Sci. Technol.* **13**, 484-492 (2004).

96 Jong-Uk Kim, Y. J. K. Investigation on the Flow Field Characteristics of a Highly Underexpanded Pulsed Plasma Jet. *KSME International Journal* **15**, 1691-1698 (2001).

97 P.L. Eggins, D. A. J. Laser-Doppler velocity measurements in an under-expanded free jet. *J. Phys. D: Appl. Phys* **7**, 1894-1906 (1974).

98 Mahmoud Rajabian, D. V. G., Serge Vacquie. Measurements of Temperature and Electron Number Density in a dc Argon-Nitrogen PlasmaTorch-Supersonic Operation. *Plasma Chemistry and Plasma Processing* **24**, 285-305 (2004).

99 Gage, R. M. Arc Torch and Process. USA patent 2,806,124 (1957).

100 Smith, E. Development of a plasma energy pyrolysis system (PEPS) to treat complex military waste streams. *Federal Facilities Environmental Journal* **Spring**, 51-67 (1999).

101 Oost, G. V. Pyrolysis of waste using a hybrid argon-water stabilized torch. *Vacuum* **80**, 1132-1137 (2006).

102 Gomez, E. Thermal plasma technology for the treatment of wastes: A critical review. *Journal of Hazardous Materials* **161**, 614-626 (2009).

103 Heberlein, J. Thermal plasma waste treatment. *J. Phys. D: Appl. Phys.* **41**, 053001 (2008).

104 Pfender, E. Fundamental studies associated with the plasma spray process. *Surface and Coatings Technology* **34**, 1-14 (1988).

105 Lasher, M. Safe disposal of pyrotechnic ordnance using a plasma treatment system. *Waste Management* **20**, 425-433 (2000).

106 Counts, D. A. Thermal plasma waste remediation technology: historical perspective and current trends. *Naval Research Laboratory* (1999).

107 Mayne, P. W. Plasma magmavication of soils by nontransferred arc. *Journal of Geotechnical and Geoenvironmental Engineering*, 387 (2000).

108 Boulos, M. I. RF induction plasma spraying: state-of-the-art review. *Journal of Thermal Spray Technology* **1**, 33-40 (1992).

109 Kuo, S. P. Fan-shaped microwave plasma for mail decontamination. *Plasma Sources Sci. Technol.* **16**, 581-586 (2007).

110 Tyler, G. AA or ICP - Which do you choose? , (1991).

111 Reed, T. B. Growth of Refractory Crystals Using the Induction Plasma Torch. *Journal of Applied Physics* **32**, 2534 (1961).

112 Boer, P. W. J. M. B. a. F. J. d. An Assessment of the Inductively Coupled High-frequency Plasma for Simultaneous Multi-element Analysis. *Proc. Anal Div. Chem.Soc* **12**, 140-152 (1975).

113 Kniseley, V. A. F. R. N. Inductively Coupled Plasma - Optical Emission Spectroscopy. *Analytical Chemistry* **46**, 1110-1120 (1974).

114 French, D. J. D. J. B. An improved interface for inductively coupled plasma-mass spectrometry (ICP-MS). *Spectrochimica Acta* **41B**, 197-204 (1986).

115 Kazutake Taniguchi, T. F., Kiroyuki Yoshiki, and Yasuhiro Horiike. Generation of Integrated Atmospheric-Pressure Microplasmas. *Jpn. J. Appl. Phys.* **42**, 6584-6589 (2003).

116 Tomoyuki Kikuchi, Y. H., and Hajime Shirai. RF microplasma jet at atmospheric pressure: characterization and application to thin film processing. *J. Phys. D: Appl. Phys.* **37**, 1537-1543 (2004).

117 Shinji Ibuka, F. F., Ryo Mikami, Koichi Yasuoka, and Shozo Ishii. Battery-Driven Portable High Voltage Pulse Generator for Microplasma Applications. *IEEE Pulsed Power Conference Publication*, 1356-1359 (2005).

118 J.A. Perez-Martinez, R. P.-E., R. Lopez-Callejas, A. Mercado-Cabrera, R.A. Valencia, S.R. Barocio, J.S. Benitez-Read, and J.O. Pacheco-Sotelo. An RF microplasma facility development for medical applications. *Surface & Coatings Technology* **201**, 5684-5687 (2007).

119 Popa, S. D. Vibrational distributions in a flowing nitrogen glow discharge. *J. Phys. D: Appl. Phys.* **29**, 411-415 (1996).

120 Fukuchi, T. Detection of Metastable Excited Molecules in an Atmospheric Pressure Nitrogen Discharge by Raman Scattering. *Electronics and Communications in Japan* **93** (2010).

121 Gui-Bing Zhao, X. H., Morris D. Arhyle, and Maciej Radosz. N Atom Radicals and N2 Found to be Responsible for Nitrogen Oxides Conversion in Nonthermal Nitrogen Plasma. *Ind. Eng. Chem. Res* **43**, 5077-5088 (2004).

122 Laux, C. O. in *Dissertation* (Department of Mechanical Engineering at Stanford University, 1993).

123 Sergey Y. Savinov, H. L., Hyung Keun Song, and Byung-Ki Na. The Effect of Vibrational Excitation of Molecules on Plasmachemical Reactions Involving Methane and Nitrogen. *Plasma Chemistry and Plasma Processing* **23**, 159-173 (2003).

124 Kaufman, F. The Air Afterglow and Its Use in the Study of Some Reactions of Atomic Oxygen. *Proc. R. Soc. Lond. A* **247**, 123-139 (1958).

125 Roodebush, W. H. The Reaction Between Nitric Oxide and Atomic Oxygen. *Chem. Rev.* **17**, 409-412 (1935).

126 Boris F. Gordiets, C. M. F., Vasco L. Guerra, Jorge M. A. H Loureiro, Jacimar Nahorny, Daniel Pagon, Michel Touzeau, and Marinette Vialle. Kinetic Model of a Low-Pressure N2-O2 Flowing Glow Discharge. *IEEE Transactions on Plasma Science* **23**, 750 (1995).

127 Oda, R. O. a. T. Measurement of vibrationally excited O2(v=6) in the afterglow of pulsed positive corona discharge. *Plasma Sources Science and Technology* **18** (2009).

128 Zhdanok, V. V. N. a. S. A. Afterglows in Nonequilibrium Reactive Plasma Flows Near Atmospheric Pressure. *Physica Scripta* **T63**, 295-296 (1996).

129 G.D. Stancu, F. K., D.A. Lacoste, and C.O. Laux. Atmospheric pressure plasma diagnostics by OES, CRDS and TALIF. *J. Phys. D: Appl. Phys* **43** (2010).

130 E.E. Gulcicek, J. P. D., and S.O. Vaughan. Absolute Differential and Integral Electron Excitation Cross Sections for Atomic Oxygen. *Journal of Geophysical Research* **93**, 5885-5889 (1988).

131 Cosby, P. C. Electron impact dissociation of nitrogen. *The Journal of Chemical Physics* **98**, 9544-9553 (1993).

132 C.W. Walter, P. C. C., and H. Helm. N(4So), N(2Do), and N(2Po) yields in predissociation of excited singlet states of N2. *The Journal of Chemical Physics* **99**, 3553-3561 (1993).

133 R.P. Vaudo, Z. Y., J.W. Cook Jr., and J.F. Schetzina. Atomic-nitrogen production in a radio-frequency plasma source. *Optics Letters* **18**, 1843-1845 (1993).

134 B. Nemet, L. K. Time-resolved optical emission spectrometry of Q-switched Nd:YAG laser-induced plasma from copper targets in air at atmospheric pressure. *Spectrochimica Acta Part B* **50**, 1869-1888 (1995).

135 M.S. Cresser, T. S. W. Some interference studies in atomic fluorescence spectroscopy with a continuum source. *Spectrochimica Acta* **25B**, 61-68 (1970).

136 Marr, G. V. *Plasma Spectroscopy*. (Elsevier Publishing Company Ltd., 1968).

137 Lochte-Holtgreven, W. *Plasma Diagnostics*. (American Institute of Physics, 1995).

138 Xuetie Zhou, Y. L., Junde Wang, Zhonghua Huang. The Temperature Measurement of the Electrothermal-Chemical Launcher Plasma by Atomic Emission Spectroscopy. *IEEE Transactions on Plasma Science* **29**, 360-364 (2001).

139 J-L. Meunier, N. D.-S. Erosion rate evaluation of plasma torch electrodes from measurements of the emitted metal vapor radiation. *J. Phys. D: Appl. Phys.* **27**, 2522-2525 (1994).

140 Isaac Reif, V. A. F., Richard N. Kniseley. Spectroscopic flame temperature measurements and their physical significance-I. Theoretical concepts-A critical review. *Spectrochimica Acta* **28B**, 105-128 (1973).

141 Commons, W.

142 Ralchenko, Y., Kramida, A.E., Reader, J., and NIST ASD Team. in *NIST Atomic Spectra Database (ver. 4.1.0)* (2012).

143 Company, A. D. *GX-K series and GF-K series High resolution industrial balance Instruction Manual*. (A&D Company, Limited).

144 *Polymers Center of Excellence*, <http://www.polymers-center.org/index.htm> (2012).

145 C.O. Laux, R. J. G., C.H. Kruger, F. Roux, F. Michaud, S.P. Davis. Rotational temperature measurements in air and nitrogen plasmas using the first negative system of N_2^+. *Journal of Quantitative Spectroscopy & Radiative Transfer* **68**, 473-482 (2001).

146 B. Nemet, L. K. Time-resolved optical emission spectrometry of Q-switched Nd:Yag laser-induced plasmas from copper targets in air at atmophseric pressure. *Spectrochimica Acta Part B* **50**, 1869-1888 (1995).

147 ICMI. *Cyanide Chemistry*, <http://www.cyanidecode.org/cyanide_chemistry.php> (2012).

148 Bronfin, B. R. Hydrogen Cyanide Synthesis in a Thermal Radiofrequency Induction Plasma. *Advances in Chemistry* **In Chemical Reactions in Electrical Discharges**, 423-439 (1969).

149 Freeman, M. P. Reactive Species Titration; Further Quantitative Studies. *Advances in Chemistry* **In Chemical Reactions in Electrical Discharges**, 406-422 (1969).

Appendix

Appendix: 1

Preliminary HDPE Removal Data

Table 0-1: Data set acquired on 6/15/2011. PF5K parameters were 100 kHz, 250 V, and 100 SLM air and the plasma treatment parameters were 10 passes at 150 mm/s for an exposure time of 0.677 seconds per pass for a width of 101.6 mm (4").

#	Z (mm)	m_1 (g)	m_2 (g)	dm (g)	g/pass	g/second	mg/sec
2	2	95.475	94.877	0.598	0.060	0.088287	88.2874
3	4	93.203	92.816	0.387	0.039	0.057136	57.13583
4	6	93.510	93.267	0.243	0.024	0.035876	35.87598
5	8	96.034	95.779	0.255	0.026	0.037648	37.64764
6	10	94.350	94.164	0.186	0.019	0.027461	27.46063
7	12	93.826	93.657	0.169	0.017	0.024951	24.95079
8	14	94.831	94.712	0.119	0.012	0.017569	17.5689
9	16	95.353	95.238	0.115	0.011	0.016978	16.97835
10	18	96.390	96.307	0.083	0.008	0.012254	12.25394
11	20	94.723	94.698	0.025	0.003	0.003691	3.690945
13	4	92.825	92.447	0.378	0.038	0.055807	55.80709
14	6	93.276	92.964	0.312	0.031	0.046063	46.06299
15	8	95.785	95.567	0.218	0.022	0.032185	32.18504
16	10	94.171	93.969	0.202	0.020	0.029823	29.82283
17	12	93.663	93.493	0.170	0.017	0.025098	25.09843
18	14	94.716	94.573	0.143	0.014	0.021112	21.1122
19	16	95.241	95.151	0.090	0.009	0.013287	13.2874
20	18	96.303	96.244	0.059	0.006	0.008711	8.71063
21	20	94.703	94.691	0.012	0.001	0.001772	1.771654

Table 0-2: Data set acquired on 6/17/2011. PF5K parameters were 100 kHz, 250 V, and 100 SLM air and the plasma treatment parameters were 150 mm/s for an exposure time of 0.677 seconds per pass for a width of 101.6 mm (4") with the number of passes per sample as indicated in column 4.

#	Z (mm)	V (mm/s)	Passes	m_1 (g)	m_2 (g)	dm (g)	g/pass	g/s	mg/s
9	20	150	50	94.923	94.652	0.271	0.00542	0.003671	3.671147
13	20	150	50	94.667	94.289	0.378	0.00756	0.005121	5.12064
10	22	150	50	94.293	94.148	0.145	0.0029	0.001964	1.964267
14	22	150	50	94.163	93.893	0.27	0.0054	0.003658	3.6576
11	25	150	50	95.043	95.003	0.04	0.0008	0.000542	0.541867
15	25	150	50	95.018	94.935	0.083	0.00166	0.001124	1.124373
12	30	150	100	93.218	93.19	0.028	0.00028	0.00019	0.189653
16	30	150	100	93.219	93.162	0.057	0.00057	0.000386	0.38608

Table 0-3: This tabulated data set is a combination of the data obtained on 6/15/2011 and 6/17/2011, if multiple Z data points existed the averaged value was taken.

Z	mg/s
2	88.287
4	56.471
6	40.969
8	34.916
10	28.642
12	25.025
14	19.341
16	15.133
18	10.482
20	4.043
22	2.811
25	0.833
30	0.288

Appendix: 2

Parametric HDPE Plasma Removal Data

Table 0-4: This is the tabulated data set for the HDPE parametric plasma removal experiments. The header row from left to right: '#' is the order that the samples were treated and the according sample ID: YYYYMMDD-#, 'Z (mm)' is the separation distance between the torch and sample in millimeters, for each set of conditions a total of three samples were treated identified as A, B, & C where the next six columns are the initial and final masses indicated by the subscript 1 & 2 respectively e.g.: 'A-m_1 (g)' is the initial mass of the sample directly prior to treatment measured in grams, 'A-m_2 (g)' is the final mass of the sample measured in grams directly after treatment, the next three columns refer to the change in mass for each sample and the final column on the right is the median of the three mass differences. For this set each '#' represents a unique subset of parameters set at the PF5K power supply: frequency, power, and flow with a total of 4 'Z' positions of 10, 12, 14, and 16 mm.

#	Z	A-m_1	A-m_2	B-m_1	B-m_2	C-m_1	C-m_2	dm-	dm-	dm-	med-dm
1	10	14.118	14.075	14.010	13.968	14.129	14.086	0.043	0.042	0.043	0.043
1	12	14.049	14.006	14.025	13.988	14.135	14.097	0.043	0.037	0.038	0.038
1	14	14.027	13.989	14.012	13.976	14.021	13.986	0.038	0.036	0.035	0.036
1	16	14.021	13.991	14.032	14.005	14.027	14.004	0.030	0.027	0.023	0.027
2	10	14.098	14.056	14.094	14.055	14.029	13.994	0.042	0.039	0.035	0.039
2	12	14.027	13.989	14.040	14.001	14.025	13.988	0.038	0.039	0.037	0.038
2	14	14.018	13.984	14.017	13.986	14.199	14.165	0.034	0.031	0.034	0.034
2	16	14.134	14.108	14.020	13.994	14.014	13.991	0.026	0.026	0.023	0.026
3	10	14.010	13.965	14.046	13.999	14.026	13.980	0.045	0.047	0.046	0.046
3	12	14.022	13.975	14.064	14.015	14.024	13.975	0.047	0.049	0.049	0.049
3	14	14.027	13.985	14.021	13.981	14.020	13.982	0.042	0.040	0.038	0.040
3	16	14.036	14.006	14.095	14.068	14.074	14.049	0.030	0.027	0.025	0.027
4	10	14.037	13.987	14.069	14.020	14.038	13.987	0.050	0.049	0.051	0.050
4	12	14.030	13.979	14.070	14.021	14.033	13.986	0.051	0.049	0.047	0.049
4	14	14.029	13.986	14.021	13.980	14.020	13.983	0.043	0.041	0.037	0.041
4	16	14.047	14.011	14.175	14.139	14.057	14.025	0.036	0.036	0.032	0.036
5	10	14.043	13.990	14.031	13.982	14.020	13.972	0.053	0.049	0.048	0.049
5	12	14.037	13.983	14.029	13.976	14.021	13.971	0.054	0.053	0.050	0.053
5	14	14.019	13.972	14.022	13.979	14.090	14.048	0.047	0.043	0.042	0.043
5	16	14.057	14.017	14.018	13.984	14.019	13.985	0.040	0.034	0.034	0.034

#	Z	A-m_1	A-m_2	B-m_1	B-m_2	C-m_1	C-m_2	dm-	dm-	dm-	med-dm
6	10	14.019	13.970	14.042	13.992	14.035	13.987	0.049	0.050	0.048	0.049
6	12	14.162	14.107	14.026	13.977	14.014	13.965	0.055	0.049	0.049	0.049
6	14	14.008	13.962	14.019	13.974	14.019	13.975	0.046	0.045	0.044	0.045
6	16	14.011	13.976	14.018	13.982	14.013	13.978	0.035	0.036	0.035	0.035
7	10	14.016	13.973	14.017	13.977	13.994	13.955	0.043	0.040	0.039	0.040
7	12	13.992	13.952	13.995	13.955	14.003	13.967	0.040	0.040	0.036	0.040
7	14	14.027	13.993	14.109	14.076	13.985	13.956	0.034	0.033	0.029	0.033
7	16	14.009	13.985	13.995	13.972	13.999	13.977	0.024	0.023	0.022	0.023
8	10	14.018	13.970	14.015	13.968	14.036	13.990	0.048	0.047	0.046	0.047
8	12	13.996	13.950	13.989	13.944	13.788	13.742	0.046	0.045	0.046	0.046
8	14	13.997	13.957	14.066	14.025	13.998	13.963	0.040	0.041	0.035	0.040
8	16	13.988	13.956	13.993	13.960	13.995	13.966	0.032	0.033	0.029	0.032
9	10	13.784	13.729	14.006	13.954	14.013	13.962	0.055	0.052	0.051	0.052
9	12	14.019	13.969	14.012	13.965	14.012	13.963	0.050	0.047	0.049	0.049
9	14	13.990	13.946	13.993	13.952	13.788	13.749	0.044	0.041	0.039	0.041
9	16	14.006	13.972	13.995	13.962	14.003	13.973	0.034	0.033	0.030	0.033
10	10	14.007	13.963	14.004	13.960	14.011	13.968	0.044	0.044	0.043	0.044
10	12	14.009	13.963	14.018	13.975	14.019	13.977	0.046	0.043	0.042	0.043
10	14	14.006	13.967	14.020	13.983	13.814	13.777	0.039	0.037	0.037	0.037
10	16	14.023	13.995	14.013	13.986	14.014	13.987	0.028	0.027	0.027	0.027
11	10	14.013	13.975	14.028	13.991	14.005	13.970	0.038	0.037	0.035	0.037
11	12	14.008	13.971	14.019	13.982	13.990	13.957	0.037	0.037	0.033	0.037
11	14	13.997	13.968	13.998	13.967	14.001	13.974	0.029	0.031	0.027	0.029
11	16	14.009	13.987	14.000	13.982	14.007	13.988	0.022	0.018	0.019	0.019
12	10	14.057	14.016	14.001	13.961	14.015	13.977	0.041	0.040	0.038	0.040
12	12	14.029	13.987	14.006	13.968	14.025	13.987	0.042	0.038	0.038	0.038
12	14	14.012	13.978	14.007	13.972	14.010	13.977	0.034	0.035	0.033	0.034
12	16	13.999	13.976	13.993	13.971	13.997	13.975	0.023	0.022	0.022	0.022
13	10	14.126	14.073	14.013	13.962	14.009	13.959	0.053	0.051	0.050	0.051
13	12	14.027	13.980	13.992	13.948	13.996	13.949	0.047	0.044	0.047	0.047
13	14	13.986	13.940	14.040	13.996	14.019	13.978	0.046	0.044	0.041	0.044
13	16	13.997	13.961	14.014	13.980	14.026	13.994	0.036	0.034	0.032	0.034
14	10	14.004	13.948	14.004	13.950	13.989	13.936	0.056	0.054	0.053	0.054
14	12	13.992	13.937	14.001	13.945	14.045	13.993	0.055	0.056	0.052	0.055
14	14	13.988	13.937	14.019	13.970	14.012	13.963	0.051	0.049	0.049	0.049
14	16	13.999	13.959	14.001	13.961	14.015	13.975	0.040	0.040	0.040	0.040
15	10	14.078	14.039	14.009	13.970	14.022	13.985	0.039	0.039	0.037	0.039
15	12	14.027	13.990	13.991	13.953	14.010	13.974	0.037	0.038	0.036	0.037
15	14	14.003	13.975	14.019	13.991	13.998	13.970	0.028	0.028	0.028	0.028
15	16	14.023	13.999	14.013	13.989	14.003	13.981	0.024	0.024	0.022	0.024

#	Z	A-m_1	A-m_2	B-m_1	B-m_2	C-m_1	C-m_2	dm-	dm-	dm-	med-dm
16	10	13.991	13.951	13.998	13.958	13.998	13.958	0.040	0.040	0.040	0.040
16	12	14.007	13.968	14.011	13.971	14.004	13.965	0.039	0.040	0.039	0.039
16	14	14.015	13.980	14.010	13.977	14.010	13.979	0.035	0.033	0.031	0.033
16	16	14.004	13.978	13.996	13.970	13.996	13.973	0.026	0.026	0.023	0.026
17	10	13.992	13.942	14.040	13.990	14.013	13.964	0.050	0.050	0.049	0.050
17	12	14.008	13.961	13.998	13.950	14.007	13.961	0.047	0.048	0.046	0.047
17	14	13.996	13.954	14.007	13.967	14.010	13.971	0.042	0.040	0.039	0.040
17	16	14.019	13.987	14.002	13.970	14.009	13.975	0.032	0.032	0.034	0.032
18	10	14.017	13.964	13.993	13.939	13.986	13.938	0.053	0.054	0.048	0.053
18	12	14.004	13.952	14.035	13.982	13.990	13.941	0.052	0.053	0.049	0.052
18	14	14.005	13.956	14.006	13.958	13.997	13.953	0.049	0.048	0.044	0.048
18	16	13.989	13.954	14.004	13.968	13.992	13.958	0.035	0.036	0.034	0.035
19	10	13.989	13.952	13.990	13.950	14.002	13.960	0.037	0.040	0.042	0.040
19	12	13.992	13.954	14.018	13.981	14.004	13.970	0.038	0.037	0.034	0.037
19	14	14.008	13.977	13.990	13.960	13.997	13.969	0.031	0.030	0.028	0.030
19	16	14.000	13.976	14.005	13.981	13.990	13.967	0.024	0.024	0.023	0.024
20	10	14.003	13.945	13.989	13.935	13.998	13.942	0.058	0.054	0.056	0.056
20	12	14.025	13.970	13.996	13.945	13.998	13.945	0.055	0.051	0.053	0.053
20	14	14.008	13.959	13.995	13.947	14.002	13.954	0.049	0.048	0.048	0.048
20	16	14.082	14.041	14.002	13.961	13.997	13.961	0.041	0.041	0.036	0.041
21	10	13.990	13.945	14.017	13.971	14.007	13.962	0.045	0.046	0.045	0.045
21	12	14.003	13.961	13.997	13.956	13.996	13.955	0.042	0.041	0.041	0.041
21	14	14.009	13.973	14.011	13.975	13.997	13.963	0.036	0.036	0.034	0.036
21	16	13.998	13.973	13.996	13.968	13.992	13.967	0.025	0.028	0.025	0.025
22	10	14.013	13.972	14.006	13.964	14.006	13.965	0.041	0.042	0.041	0.041
22	12	14.003	13.963	13.997	13.957	13.995	13.957	0.040	0.040	0.038	0.040
22	14	13.997	13.958	14.007	13.970	14.012	13.979	0.039	0.037	0.033	0.037
22	16	14.019	13.991	14.019	13.995	14.025	14.001	0.028	0.024	0.024	0.024
23	10	14.021	13.975	14.015	13.971	14.022	13.978	0.046	0.044	0.044	0.044
23	12	14.011	13.969	14.009	13.966	13.989	13.950	0.042	0.043	0.039	0.042
23	14	13.997	13.960	14.022	13.984	14.012	13.976	0.037	0.038	0.036	0.037
23	16	14.015	13.987	14.029	14.003	14.024	13.997	0.028	0.026	0.027	0.027
24	10	14.015	13.964	14.024	13.973	14.017	13.967	0.051	0.051	0.050	0.051
24	12	14.042	13.993	14.024	13.975	14.023	13.976	0.049	0.049	0.047	0.049
24	14	14.048	14.004	14.013	13.973	14.024	13.985	0.044	0.040	0.039	0.040
24	16	14.017	13.983	14.022	13.989	14.023	13.988	0.034	0.033	0.035	0.034
25	10	14.013	13.961	14.024	13.976	14.031	13.982	0.052	0.048	0.049	0.049
25	12	14.014	13.969	14.009	13.964	14.019	13.970	0.045	0.045	0.049	0.045
25	14	14.008	13.965	14.151	14.111	14.044	14.002	0.043	0.040	0.042	0.042
25	16	14.080	14.045	14.040	14.006	14.042	14.007	0.035	0.034	0.035	0.035

#	Z	A-m_1	A-m_2	B-m_1	B-m_2	C-m_1	C-m_2	dm-	dm-	dm-	med-dm
26	10	14.009	13.965	14.020	13.977	14.006	13.961	0.044	0.043	0.045	0.044
26	12	14.009	13.961	14.013	13.965	14.055	14.013	0.048	0.048	0.042	0.048
26	14	14.014	13.976	14.012	13.975	14.021	13.983	0.038	0.037	0.038	0.038
26	16	14.016	13.985	14.013	13.982	14.013	13.984	0.031	0.031	0.029	0.031
27	10	14.023	13.967	14.017	13.962	14.011	13.961	0.056	0.055	0.050	0.055
27	12	14.017	13.961	14.025	13.970	14.016	13.963	0.056	0.055	0.053	0.055
27	14	14.007	13.955	14.012	13.965	14.012	13.965	0.052	0.047	0.047	0.047
27	16	14.010	13.966	14.014	13.970	14.009	13.969	0.044	0.044	0.040	0.044

Table 0-5: This is the tabulated data set and DOE for the HDPE parametric plasma removal experiments. The header row from left to right indicates the sample number '#', the height 'Z', and the given parameters of frequency, power, and flow controlled at the PF5K power supply, and the resultant mass removal rate as calculated before using the measured sample width.

#	Z	Frequency	Power	Flow	mg/s
1	10	95	225	100	17.238
1	12	95	225	100	15.234
1	14	95	225	100	14.432
1	16	95	225	100	10.824
2	10	100	225	125	15.634
2	12	100	225	125	15.234
2	14	100	225	125	13.630
2	16	100	225	125	10.423
3	10	95	250	90	18.441
3	12	95	250	90	19.643
3	14	95	250	90	16.035
3	16	95	250	90	10.824
4	10	100	250	100	20.044
4	12	100	250	100	19.643
4	14	100	250	100	16.436
4	16	100	250	100	14.432
5	10	95	250	125	19.643
5	12	95	250	125	21.247
5	14	95	250	125	17.238
5	16	95	250	125	13.630
6	10	95	250	100	19.643

#	Z	Frequency	Power	Flow	mg/s
6	12	95	250	100	19.643
6	14	95	250	100	18.040
6	16	95	250	100	14.031
7	10	110	225	100	16.035
7	12	110	225	100	16.035
7	14	110	225	100	13.229
7	16	110	225	100	9.220
8	10	110	250	100	18.841
8	12	110	250	100	18.441
8	14	110	250	100	16.035
8	16	110	250	100	12.828
9	10	110	275	125	20.846
9	12	110	275	125	19.643
9	14	110	275	125	16.436
9	16	110	275	125	13.229
10	10	100	250	90	17.639
10	12	100	250	90	17.238
10	14	100	250	90	14.833
10	16	100	250	90	10.824
11	10	110	225	90	14.833
11	12	110	225	90	14.833
11	14	110	225	90	11.626
11	16	110	225	90	7.617
12	10	95	225	90	16.035
12	12	95	225	90	15.234
12	14	95	225	90	13.630
12	16	95	225	90	8.819
13	10	100	275	100	20.445
13	12	100	275	100	18.841
13	14	100	275	100	17.639
13	16	100	275	100	13.630
14	10	95	275	100	21.648
14	12	95	275	100	22.049
14	14	95	275	100	19.643
14	16	95	275	100	16.035
15	10	100	225	90	15.634
15	12	100	225	90	14.833
15	14	100	225	90	11.225
15	16	100	225	90	9.621
16	10	100	225	100	16.035

#	Z	Frequency	Power	Flow	mg/s
16	12	100	225	100	15.634
16	14	100	225	100	13.229
16	16	100	225	100	10.423
17	10	110	275	100	20.044
17	12	110	275	100	18.841
17	14	110	275	100	16.035
17	16	110	275	100	12.828
18	10	95	275	90	21.247
18	12	95	275	90	20.846
18	14	95	275	90	19.242
18	16	95	275	90	14.031
19	10	110	225	125	16.035
19	12	110	225	125	14.833
19	14	110	225	125	12.026
19	16	110	225	125	9.621
20	10	100	275	125	22.449
20	12	100	275	125	21.247
20	14	100	275	125	19.242
20	16	100	275	125	16.436
21	10	110	250	90	18.040
21	12	110	250	90	16.436
21	14	110	250	90	14.432
21	16	110	250	90	10.022
22	10	95	225	125	16.436
22	12	95	225	125	16.035
22	14	95	225	125	14.833
22	16	95	225	125	9.621
23	10	110	275	90	17.639
23	12	110	275	90	16.837
23	14	110	275	90	14.833
23	16	110	275	90	10.824
24	10	100	275	90	20.445
24	12	100	275	90	19.643
24	14	100	275	90	16.035
24	16	100	275	90	13.630
25	10	100	250	125	19.643
25	12	100	250	125	18.040
25	14	100	250	125	16.837
25	16	100	250	125	14.031
26	10	110	250	125	17.639

#	Z	Frequency	Power	Flow	mg/s
26	12	110	250	125	19.242
26	14	110	250	125	15.234
26	16	110	250	125	12.427
27	10	95	275	125	22.049
27	12	95	275	125	22.049
27	14	95	275	125	18.841
27	16	95	275	125	17.639

Appendix: 3

HDPE-TiO_2 Loading Plasma Removal Data

Table 0-6: This table contains the DOE and original data from the HDPE-TiO_2 Loading experiments. The header row from left to right: '#' is the order that the samples were treated and the according sample ID: YYYYMMDD-#, 'HDPE %' is the loading level of the sample in weight percent HDPE, 'Z (mm)' is the separation distance between the torch and sample in millimeters, for each set of conditions a total of three samples were treated identified as A, B, & C where the next six columns are the initial and final masses indicated by the subscript 1 & 2 respectively e.g.: 'A-m_1 (g)' is the initial mass of the sample directly prior to treatment measured in grams, 'A-m_2 (g)' is the final mass of the sample measured in grams directly after treatment, the next three columns refer to the change in mass for each of the samples and the final column on the right is the median of the three mass differences.

#	HDPE %	Z (mm)	A-m_1 (g)	A-m_2 (g)	B-m_1 (g)	B-m_2 (g)	C-m_1 (g)	C-m_2 (g)	dm-A (g)	dm-B (g)	dm-C (g)	med-dm(g)
1	70	2	18.206	17.972	18.236	18.008	18.234	18.009	0.234	0.228	0.225	0.228
2	50	16	22.583	22.553	22.597	22.565	22.624	22.595	0.030	0.032	0.029	0.030
3	80	12	16.489	16.435	16.488	16.435	16.510	16.458	0.054	0.053	0.052	0.053
4	50	8	22.600	22.524	22.585	22.510	22.587	22.513	0.076	0.075	0.074	0.075
5	60	16	20.240	20.208	20.307	20.274	20.308	20.274	0.032	0.033	0.034	0.033
6	60	14	20.273	20.229	20.371	20.329	20.334	20.293	0.044	0.042	0.041	0.042
7	80	6	16.489	16.405	16.511	16.429	16.520	16.436	0.084	0.082	0.084	0.084
8	100	4	14.018	13.931	14.019	13.933	14.024	13.937	0.087	0.086	0.087	0.087
9	70	10	18.247	18.191	18.173	18.117	18.236	18.181	0.056	0.056	0.055	0.056
10	50	24	22.604	22.599	22.598	22.593	22.614	22.608	0.005	0.005	0.006	0.005
11	50	6	22.607	22.516	22.614	22.528	22.612	22.524	0.091	0.086	0.088	0.088
12	100	22	14.022	14.011	14.022	14.012	14.030	14.017	0.011	0.010	0.013	0.011
13	90	6	15.211	15.124	15.225	15.137	15.206	15.121	0.087	0.088	0.085	0.087
14	80	22	16.521	16.515	16.503	16.494	16.488	16.480	0.006	0.009	0.008	0.008
15	60	24	20.411	20.406	20.353	20.348	20.210	20.206	0.005	0.005	0.004	0.005
16	80	20	16.511	16.498	16.483	16.469	16.516	16.501	0.013	0.014	0.015	0.014
17	80	10	16.510	16.452	16.501	16.443	16.503	16.446	0.058	0.058	0.057	0.058
18	90	20	15.195	15.180	15.197	15.180	15.184	15.168	0.015	0.017	0.016	0.016
19	40	4	25.780	25.658	25.819	25.700	25.777	25.661	0.122	0.119	0.116	0.119
20	90	2	15.211	15.011	15.224	15.023	15.187	14.982	0.200	0.201	0.205	0.201

#	HDPE %	Z (mm)	A-m_1 (g)	A-m_2 (g)	B-m_1 (g)	B-m_2 (g)	C-m_1 (g)	C-m_2 (g)	dm-A (g)	dm-B (g)	dm-C (g)	med-dm(g)
21	50	14	22.605	22.562	22.612	22.570	22.605	22.566	0.043	0.042	0.039	0.042
22	80	24	16.493	16.489	16.506	16.500	16.487	16.481	0.004	0.006	0.006	0.006
23	60	4	20.234	20.139	20.213	20.118	20.210	20.115	0.095	0.095	0.095	0.095
24	100	8	14.017	13.944	14.024	13.949	14.027	13.956	0.073	0.075	0.071	0.073
25	70	22	18.236	18.228	18.237	18.231	18.221	18.211	0.008	0.006	0.010	0.008
26	90	10	15.201	15.137	15.214	15.155	15.213	15.152	0.064	0.059	0.061	0.061
27	80	4	16.481	16.396	16.495	16.410	16.513	16.428	0.085	0.085	0.085	0.085
28	40	14	25.860	25.815	25.853	25.812	25.862	25.817	0.045	0.041	0.045	0.045
29	90	18	15.230	15.203	15.207	15.183	15.247	15.220	0.027	0.024	0.027	0.027
30	90	16	15.195	15.158	15.213	15.176	15.210	15.172	0.037	0.037	0.038	0.037
31	100	16	14.019	13.978	14.031	13.990	14.022	13.982	0.041	0.041	0.040	0.041
32	60	22	20.234	20.225	20.323	20.315	20.317	20.308	0.009	0.008	0.009	0.009
33	40	18	25.879	25.858	25.674	25.655	25.576	25.556	0.021	0.019	0.020	0.020
34	100	18	14.017	13.988	14.009	13.980	14.005	13.977	0.029	0.029	0.028	0.029
35	70	24	18.258	18.255	18.218	18.213	18.250	18.246	0.003	0.005	0.004	0.004
36	60	6	20.268	20.175	20.259	20.165	20.275	20.182	0.093	0.094	0.093	0.093
37	70	18	18.239	18.217	18.222	18.198	18.218	18.195	0.022	0.024	0.023	0.023
38	70	14	18.225	18.177	18.220	18.174	18.234	18.187	0.048	0.046	0.047	0.047
39	70	16	18.236	18.202	18.212	18.179	18.244	18.212	0.034	0.033	0.032	0.033
40	50	4	22.600	22.498	22.632	22.530	22.557	22.456	0.102	0.102	0.101	0.102
41	70	6	18.236	18.146	18.231	18.144	18.235	18.146	0.090	0.087	0.089	0.089
42	40	10	25.761	25.695	25.831	25.766	25.779	25.714	0.066	0.065	0.065	0.065
43	100	2	14.020	13.796	14.025	13.799	14.021	13.772	0.224	0.226	0.249	0.226
44	40	16	25.804	25.772	25.784	25.750	25.777	25.747	0.032	0.034	0.030	0.032
45	60	12	20.261	20.210	20.218	20.167	20.274	20.222	0.051	0.051	0.052	0.051
46	90	4	15.220	15.135	15.227	15.139	15.187	15.103	0.085	0.088	0.084	0.085
47	50	10	22.630	22.568	22.539	22.477	22.605	22.546	0.062	0.062	0.059	0.062
48	90	14	15.203	15.151	15.205	15.155	15.198	15.150	0.052	0.050	0.048	0.050
49	60	20	20.252	20.241	20.298	20.282	20.285	20.271	0.011	0.016	0.014	0.014
50	100	10	14.017	13.953	14.020	13.959	14.017	13.955	0.064	0.061	0.062	0.062
51	80	8	16.517	16.446	16.501	16.429	16.525	16.453	0.071	0.072	0.072	0.072
52	60	8	20.324	20.250	20.261	20.188	20.282	20.209	0.074	0.073	0.073	0.073
53	100	20	14.031	14.012	14.008	13.990	14.029	14.010	0.019	0.018	0.019	0.019
54	100	6	14.009	13.915	14.003	13.914	14.006	13.919	0.094	0.089	0.087	0.089
55	60	18	20.265	20.244	20.275	20.254	20.279	20.258	0.021	0.021	0.021	0.021
56	70	8	18.209	18.143	18.233	18.166	18.214	18.146	0.066	0.067	0.068	0.067
57	50	20	22.603	22.593	22.561	22.548	22.567	22.558	0.010	0.013	0.009	0.010
58	40	24	25.777	25.772	25.778	25.776	25.844	25.840	0.005	0.002	0.004	0.004
59	90	24	15.184	15.180	15.197	15.192	15.219	15.216	0.004	0.005	0.003	0.004

#	HDPE %	Z (mm)	A-m_1 (g)	A-m_2 (g)	B-m_1 (g)	B-m_2 (g)	C-m_1 (g)	C-m_2 (g)	dm-A (g)	dm-B (g)	dm-C (g)	med-dm(g)
60	80	2	16.494	16.298	16.537	16.347	16.507	16.303	0.196	0.190	0.204	0.196
61	60	2	20.276	20.064	20.242	20.030	20.293	20.095	0.212	0.212	0.198	0.212
62	100	24	14.021	14.016	14.011	14.005	14.017	14.011	0.005	0.006	0.006	0.006
63	90	12	15.202	15.149	15.207	15.157	15.195	15.142	0.053	0.050	0.053	0.053
64	40	12	25.796	25.741	25.790	25.728	25.805	25.752	0.055	0.062	0.053	0.055
65	40	22	25.779	25.773	25.804	25.798	25.822	25.818	0.006	0.006	0.004	0.006
66	60	10	20.171	20.115	20.278	20.222	20.317	20.261	0.056	0.056	0.056	0.056
67	70	12	18.237	18.191	18.243	18.194	18.265	18.216	0.046	0.049	0.049	0.049
68	70	4	18.215	18.122	18.185	18.090	18.212	18.118	0.093	0.095	0.094	0.094
69	50	18	22.580	22.559	22.592	22.577	22.552	22.534	0.021	0.015	0.018	0.018
70	40	2	25.833	25.580	25.791	25.539	25.835	25.606	0.253	0.252	0.229	0.252
71	80	16	16.521	16.491	16.511	16.481	16.498	16.465	0.030	0.030	0.033	0.030
72	40	8	25.808	25.731	25.796	25.720	25.804	25.729	0.077	0.076	0.075	0.076
73	50	12	22.576	22.527	22.506	22.456	22.543	22.493	0.049	0.050	0.050	0.050
74	40	20	25.832	25.824	25.795	25.787	25.786	25.777	0.008	0.008	0.009	0.008
75	100	14	14.018	13.969	14.016	13.969	14.014	13.966	0.049	0.047	0.048	0.048
76	80	14	16.484	16.443	16.525	16.481	16.502	16.459	0.041	0.044	0.043	0.043
77	80	18	16.509	16.490	16.516	16.496	16.538	16.517	0.019	0.020	0.021	0.020
78	70	20	18.211	18.200	18.215	18.202	18.233	18.222	0.011	0.013	0.011	0.011
79	50	22	22.610	22.606	22.605	22.602	22.602	22.600	0.004	0.003	0.002	0.003
80	90	8	15.197	15.131	15.223	15.155	15.220	15.152	0.066	0.068	0.068	0.068
81	40	6	25.773	25.685	25.825	25.739	25.777	25.691	0.088	0.086	0.086	0.086
82	100	12	14.028	13.974	14.020	13.965	14.016	13.960	0.054	0.055	0.056	0.055
83	90	22	15.187	15.176	15.222	15.212	15.213	15.205	0.011	0.010	0.008	0.010
84	50	2	22.620	22.410	22.597	22.378	22.621	22.407	0.210	0.219	0.214	0.214

Table 0-7: This is the tabulated data set of the mass removal rate in mg/s, the header row from left to right as follows: Z (mm) is the separation distance between the torch nozzle and the sample surface; the remaining columns are HDPE % starting with 'pure' HDPE and moving towards the most loaded. The removal rates are calculated based on a torch velocity of 200 mm/s, for 10 passes, and the median measured width of 5 samples for each loading.

Z	100%	90%	80%	70%	60%	50%	40%
2	90.599	80.320	78.212	90.909	84.412	85.174	100.279
4	34.877	33.966	33.919	37.480	37.826	40.597	47.354
6	35.678	34.765	33.520	35.486	37.030	35.025	34.222
8	29.264	27.173	28.731	26.715	29.066	29.851	30.243
10	24.855	24.376	23.144	22.329	22.297	24.677	25.865
12	22.049	21.179	21.149	19.537	20.307	19.900	21.886
14	19.242	19.980	17.159	18.740	16.723	16.716	17.907
16	16.436	14.785	11.971	13.158	13.140	11.940	12.734
18	11.626	10.789	7.981	9.171	8.362	7.164	7.959
20	7.617	6.394	5.587	4.386	5.574	3.980	3.183
22	4.410	3.996	3.192	3.190	3.584	1.194	2.388
24	2.405	1.598	2.394	1.595	1.991	1.990	1.592

Table 0-8: This is the tabulated data set for the volume removal in mm^3/s, the header row from left to right as follows: Z (mm) is the separation distance between the torch nozzle and the sample surface; the remaining columns are HDPE % starting with 'pure' HDPE and moving towards the most loaded. The removal rates are calculated based on a torch velocity of 200 mm/s, for 10 passes, and the median measured width, length, and thickness of 5 samples for each loading and the median initial mass of the 36 samples for each loading used in the experiment.

Z	100%	90%	80%	70%	60%	50%	40%
2	98.437	81.321	72.935	77.089	64.869	58.457	60.311
4	37.894	34.389	31.630	31.782	29.069	27.863	28.480
6	38.765	35.199	31.258	30.092	28.457	24.038	20.582
8	31.796	27.511	26.792	22.653	22.337	20.487	18.189
10	27.005	24.679	21.583	18.934	17.135	16.936	15.557
12	23.956	21.443	19.722	16.567	15.605	13.658	13.163
14	20.907	20.229	16.001	15.891	12.851	11.473	10.770
16	17.858	14.969	11.164	11.158	10.098	8.195	7.659
18	12.631	10.924	7.442	7.777	6.426	4.917	4.787
20	8.276	6.473	5.210	3.719	4.284	2.732	1.915
22	4.791	4.046	2.977	2.705	2.754	0.819	1.436
24	2.613	1.618	2.233	1.352	1.530	1.366	0.957

Appendix: 4

Volumetric Measurements of HDPE Loaded Samples

Table 0-9: The full set of volume measurements for the various HDPE loadings.

HDPE %	#	Width (mm)	Length (mm)	Thickness (mm)
100	1	49.94	74.84	4.08
	2	49.95	74.74	4.08
	3	49.88	74.83	4.07
	4	49.88	74.83	4.09
	5	49.89	74.73	4.12
90	1	50.06	75.06	4.09
	2	50.05	75.01	4.15
	3	50.05	74.99	4.11
	4	50.08	75.03	4.09
	5	50.04	75.95	4.1
80	1	50.1	75.08	4.08
	2	50.12	75.12	4.1
	3	50.12	75.1	4.09
	4	50.1	75.09	4.08
	5	50.12	75.06	4.11
70	1	50.15	75.22	4.1
	2	50.16	75.2	4.11
	3	50.16	75.17	4.09
	4	50.19	75.18	4.09
	5	50.17	75.18	4.1
60	1	50.25	75.33	4.12
	2	50.23	75.22	4.13
	3	50.23	75.31	4.12
	4	50.21	75.29	4.12
	5	50.23	75.22	4.14

50	1	50.26	75.3	4.1
	2	50.26	75.29	4.1
	3	50.25	75.33	4.09
	4	50.22	75.26	4.1
	5	50.25	75.26	4.1
40	1	50.25	75.29	4.1
	2	50.26	75.31	4.1
	3	50.26	75.26	4.1
	4	50.25	75.28	4.1
	5	50.26	75.32	4.1

Table 0-10: This is the tabulated data set for the median of the 5 volumetric measurements for each HDPE-TiO_2 loading set as given by the width, length and thickness with the volume calculated from these values and the mass 'm' calculated from the median of the 36 samples of each loading used in the HDPE-TiO_2 Loading Plasma Removal experiment and the resulting density in mg/mm^3 was calculated using the previous values.

HDPE %	Width (mm)	Length (mm)	Thickness (mm)	Volume (mm^3)	Mass (mg)	Density (mg/$mm^{3)}$
100	49.89	74.83	4.08	15232	14019	0.92038
90	50.05	75.03	4.10	15397	15207	0.98769
80	50.12	75.09	4.09	15393	16507	1.07235
70	50.16	75.18	4.10	15461	18233	1.17927
60	50.23	75.29	4.12	15581	20275	1.30126
50	50.25	75.29	4.10	15512	22601	1.45704
40	50.26	75.29	4.10	15515	25796	1.66268

Appendix: 5

Additional Characterization

Plasma Acid and Calorimeter

The treatment of water for the purpose of determining the thermal output of the PF1K torch and the subsequent acidification of the treated water can be seen in Figure 0-1 and Figure 0-2 respectively. From Figure 0-1 it can be seen that the longer the water is treated the higher the measured temperature becomes as would be expected, and the median thermal power output of the PF1K can be calculated at 528 W with a standard deviation of 35 W and refined to 564 W with a standard deviation of 18 W when only considering the runs when the mass loss is less than 1%. Additionally the pH of the water decreases drastically as shown in Figure 0-2 with a starting neutral pH of 7 and quickly reaching a pH of 4 in only 5 seconds and rapidly approaches a pH of 2 as the treatment time increases to 2 minutes. The energy and power were calculated using $Q = m * c * \Delta T$ where Q is the energy in Joules, m is the mass in grams, c is specific heat capacity in J/gK which for water is 4.1813 J/gK, and ΔT is the change in temperature in K as per the following example using the initial water mass of 250 g with a temperature increase of 10 K results in approximately 10.5 kJ which if it is over a treatment time of 20 seconds gives a power of 500.25 Watts.

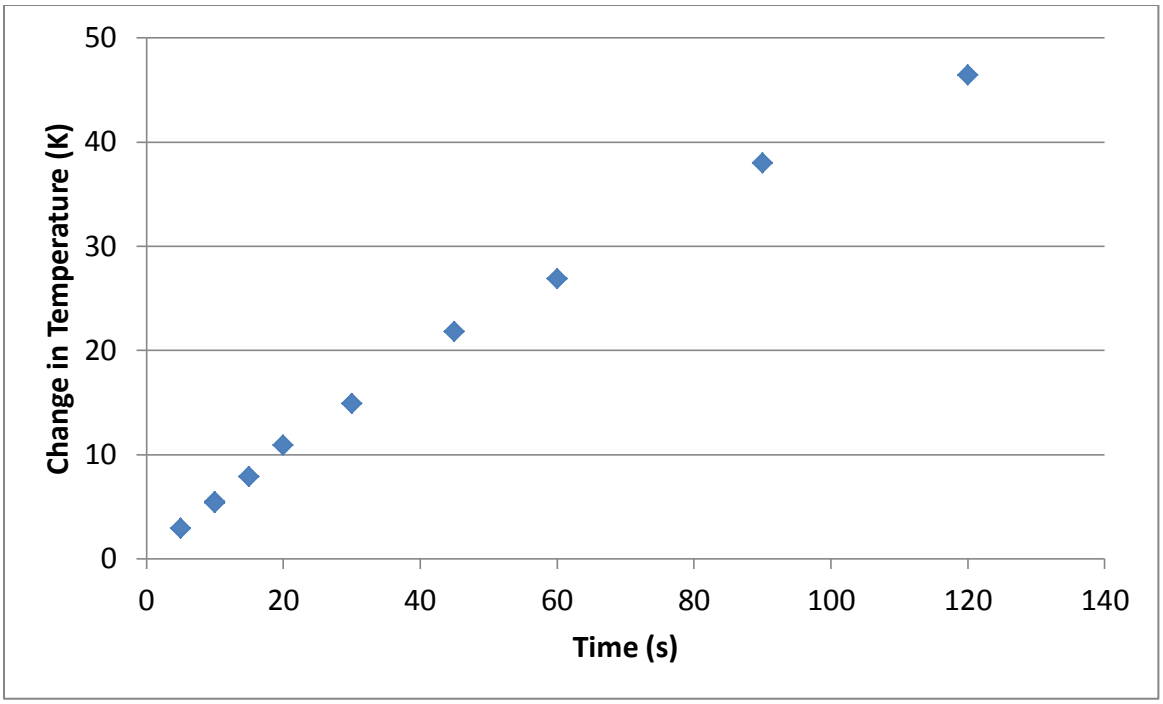

Figure 0-1: Change in water temperature as a function of plasma treatment time

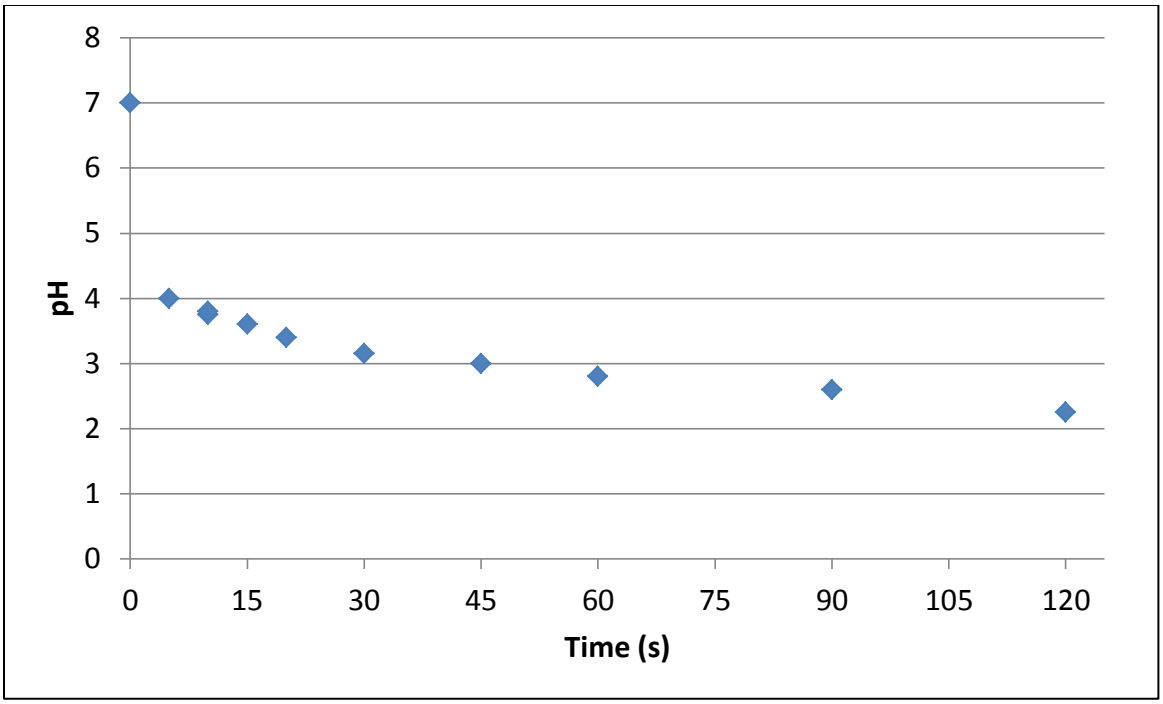

Figure 0-2: The pH of DI water as a function of time using the PF1K

Table 0-11: Data for the plasma acid and calorimeter experiment with the run number, treatment time, initial and final mass of water, initial and final water temperatures, the measured pH, the change in temperature in Kelvin, the energy transferred to the water in Joules, and the calculated power in Watts

Run #	t (s)	m_1 (g)	m_2 (g)	T_1 (^{o}C)	T_2	pH	dT	E (J)	Watts
1	5	250.1	247.9	20.8	23.7	4	2.9	3005.04	601.01
2	10	250.2	249.2	21	26.5	3.75	5.5	5729.11	572.91
3	10	250	249.1	21.4	26.8	3.8	5.4	5622.69	562.27
4	15	250	248.1	21.4	29.3	3.6	7.9	8192.76	546.18
5	20	250	247.6	21.3	32.2	3.4	10.9	11281.15	564.06
6	30	250	246.2	20.5	35.4	3.15	14.9	15333.83	511.13
7	45	250.4	247.1	22	43.8	3	21.8	22516.74	500.37
8	60	250	244	21	47.9	2.8	26.9	27435.85	457.26
9	90	250	240.2	21.5	59.5	2.6	38	38153.37	423.93
10	120	250	234.5	21.1	67.5	2.25	46.4	45481.74	379.01

Coating Thickness

Representative coating thickness measurements were made of the freeboard and antifouling 4”x6” and 2’x3’ panels. The 4”x6” panels were measured in a manner as shown in Figure 0-3 and 2’x3’ panels were measured in a manner as shown in Figure 0-4.

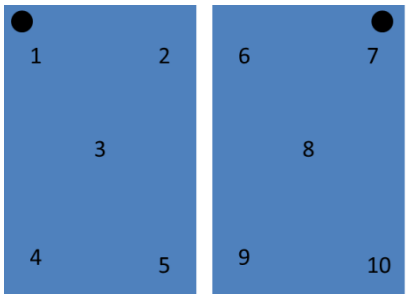

Figure 0-3: Numbering and location scheme for thickness measurements of 4"x3" panels

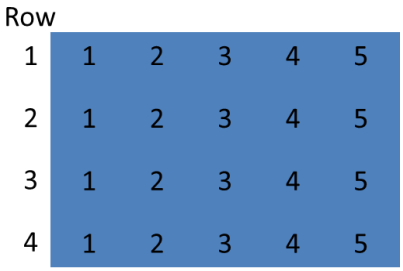

Figure 0-4: Numbering and location scheme for thickness measurements of 2'x3' panels

Five panels were used for the antifouling and freeboard 4”x6” panels and one panel was used for each of the antifouling and freeboard 2’x3’ panels. The tabulated data are shown in Table 0-12 and Table 0-13 for the freeboard and antifouling 4”x6” panels and in

Table 0-14 and Table 0-15 for the freeboard and antifouling 2'x3' panels respectively. For this experiment the convention used is the side with the hole in the upper left corner as the front and the side with the hole in the upper right corner as the back. The results show that for the FB 4"x6" panels the average thickness is 19.06 mils and 18.35 mils for the front and back respectively with an overall average thickness of 18.71 mils. The AF 4"x6" panels have an average thickness of 20.54 mils and 20.64 mils for the front and back respectively with an overall average thickness of 20.59 mils. The FB 2'x3' panel has an average thickness of 6.54 mils and the AF 2'x3' panel has an average of 23.52 mils.

Table 0-12: Coating thickness in mils for freeboard 4"x6" panels

Position	# 1	# 2	# 3	# 4	# 5
1	23.60	25.05	21.30	18.15	20.15
2	19.70	20.90	20.20	15.60	18.30
3	21.65	20.35	18.50	17.70	17.10
4	19.80	20.10	17.55	16.70	18.45
5	17.25	17.80	18.60	14.74	17.20
6	22.45	19.45	17.60	17.85	22.10
7	20.15	19.70	17.50	17.30	22.10
8	19.58	14.10	17.40	16.70	23.70
9	18.90	14.98	16.45	13.76	21.35
10	19.05	16.00	16.85	14.14	19.65

Table 0-13:Coating thickness in mils for antifouling 4"x6" panels

Position	# 1	# 2	# 3	# 4	# 5
1	20.25	20.45	20.10	21.20	18.50
2	19.20	20.55	19.15	21.90	18.80
3	20.60	22.40	19.80	22.90	21.15
4	20.50	20.40	20.60	19.85	19.75
5	21.90	21.90	20.45	20.80	20.35
6	23.60	18.10	24.95	20.55	21.65
7	21.75	19.65	24.00	21.15	21.95

8	25.20	19.90	22.80	21.75	21.50
9	25.05	19.90	23.10	21.60	19.80
10	22.55	18.50	22.75	19.00	20.50

Table 0-14:Coating thickness in mils for freeboard 2'x3' panels

Position	# 1	# 2	# 3	# 4
1	6.78	7.52	6.52	5.08
2	7.32	7.42	6.92	5.04
3	6.86	7.50	7.50	6.86
4	6.68	7.62	6.56	6.06
5	5.71	5.55	5.31	6.06

Table 0-15:Coating thickness in mils for antifouling 2'x3' panel

Position	# 1	# 2	# 3	# 4
1	18.55	17.70	20.25	24.20
2	23.95	23.70	23.55	27.85
3	21.75	21.65	26.80	31.10
4	25.95	19.45	20.70	21.25
5	27.00	27.95	24.85	22.15

Pneumatic Slide Speed Verification

To verify the speed of the pneumatic slide it was operated at 50 psi with the tank regulator valve at the same position as the actual testing. For an accurate width 20 measurements were made with a digital caliper at the exact location the switch roller traversed with data shown in Table 0-16 for a median width of 49.945 mm with a standard deviation of 0.0945 mm or 0.19%. Additionally 20 measurements were made of the velocity, the time values of the switch that correspond to the passing of the HDPE sample are given in Table 0-17 with a median time of 0.10595 s with a standard deviation of 0.00497 s or 5.69%

for a calculated velocity of 471.4 mm/s with a possible range from 450-495 mm/s. A representation of the signal output recorded by the DATAQ DI-710-UHS is given in Figure 0-5 showing the narrow pulse due to the passage of the HDPE sample and the wider pulse originating from the manual relocation of the carriage and an enlarged view of the narrow pulse is shown in Figure 0-6 noting the very sharp demarcations between the open and closed states of the switch often being limited to two data points, one open and one closed over a period of 0.0005 s.

Table 0-16: Width values for 100% HDPE sample used in speed verification

#	W (mm)
1	49.57
2	49.93
3	49.97
4	49.9
5	49.76
6	49.94
7	49.98
8	49.98
9	49.99
10	49.97
11	49.96
12	49.95
13	49.99
14	49.9
15	49.92
16	49.94
17	49.95
18	49.98
19	49.92
20	49.93
Median	**49.945**

Table 0-17: Time values for the duration of the switch lever being depressed while passing over the sample

#	T_i	T_f	Δt (s)	V (mm/s)
1	9.4772	9.5915	0.1143	436.9641
2	**19.914**	**20.02**	0.1060	471.1792
3	**29.3324**	**29.4384**	0.1060	471.1792
4	**36.8555**	**36.9668**	0.1113	448.7421
5	**46.8407**	**46.9418**	0.1011	494.0158
6	**54.9646**	**55.0589**	0.0943	529.6394
7	**62.3525**	**62.4546**	0.1021	489.1773
8	**71.2245**	**71.3319**	0.1074	465.0372
9	**77.4166**	**77.5221**	0.1055	473.4123
10	**83.0516**	**83.1653**	0.1137	439.27
11	**88.1976**	**88.3035**	0.1059	471.6242
12	**93.048**	**93.1535**	0.1055	473.4123
13	**99.2566**	**99.3679**	0.1113	448.7421
14	**104.9898**	**105.0904**	0.1006	496.4712
15	**111.0341**	**111.1318**	0.0977	511.2078
16	**117.3764**	**117.4819**	0.1055	473.4123
17	**123.8407**	**123.9428**	0.1021	489.1773
18	**130.0498**	**130.1558**	0.1060	471.1792
19	**135.8073**	**135.9137**	0.1064	469.4079
20	**142.2497**	**142.3601**	0.1104	452.4004

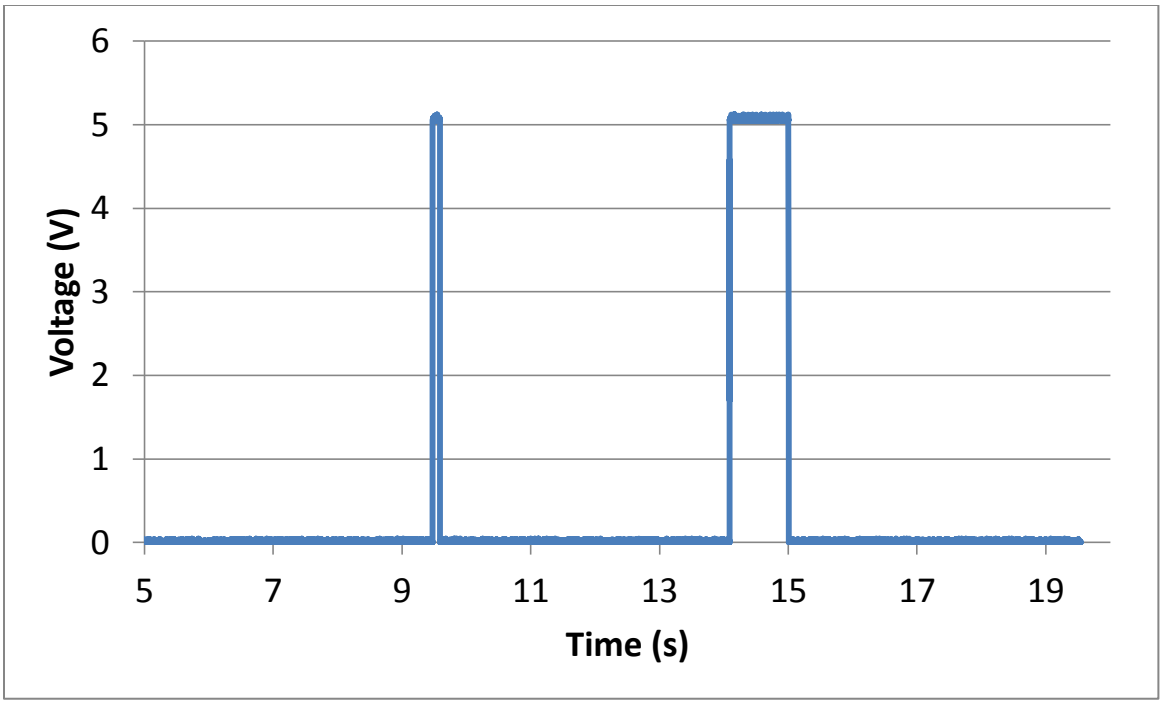

Figure 0-5: Typical signal output for the speed verification. The narrow pulse is when the switch was activated by the HDPE sample and the second wider pulse is related to manually moving the carriage back to the starting location.

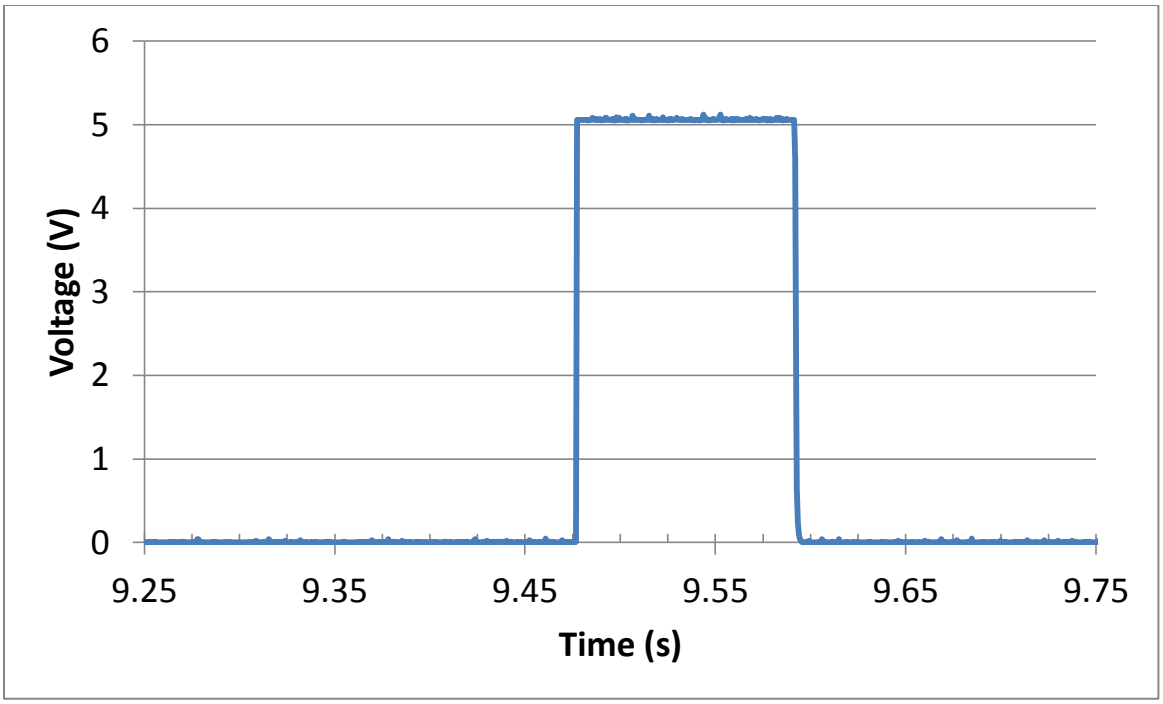

Figure 0-6: Enlarged view of the voltage pulse related to the speed of the carriage.